NATURAL RESOURCES

GEOLOGIC MAP OF THE VIOLET PRAIRIE 7.5-MINUTE QUADRANGLE, THURSTON AND LEWIS COUNTIES, WASHINGTON

by Michael Polenz, Brian A. Ostrom, Todd R. Lau, Andrew J. Sadowski, Angela L. Blanks-Bennett, Recep Cakir, Jeffrey H. Tepper, Gabriel Legoretta Paulín, Elizabeth Nesbitt, and S. Andrew DuFrane

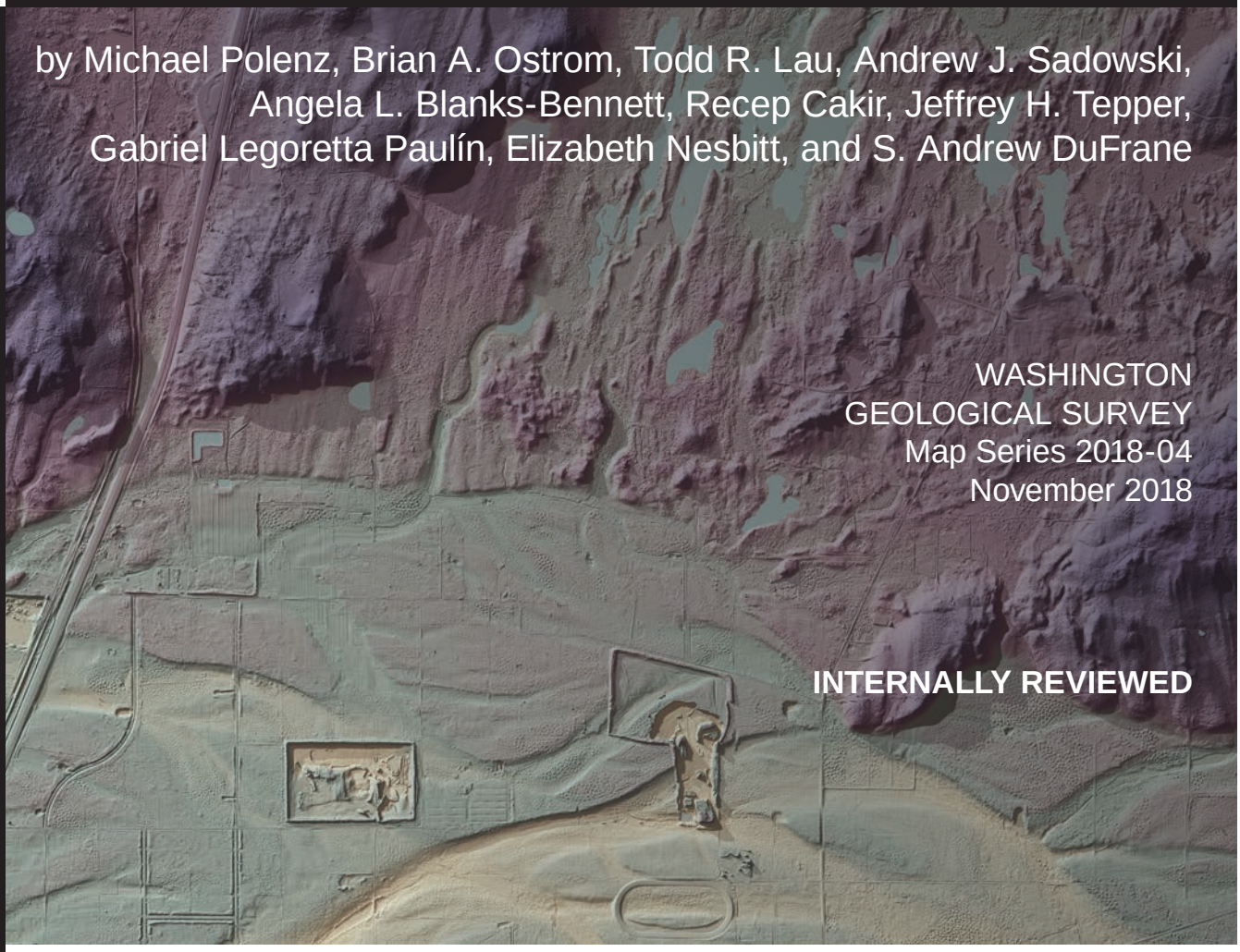

WASHINGTON
GEOLOGICAL SURVEY
Map Series 2018-04
November 2018

INTERNALLY REVIEWED

WASHINGTON STATE DEPARTMENT OF
NATURAL RESOURCES
WASHINGTON GEOLOGICAL SURVEY

GEOLOGIC MAP OF THE VIOLET PRAIRIE 7.5-MINUTE QUADRANGLE, THURSTON AND LEWIS COUNTIES, WASHINGTON

by Michael Polenz, Brian A. Ostrom, Todd R. Lau, Andrew J. Sadowski, Angela L. Blanks-Bennett, Recep Cakir, Jeffrey H. Tepper, Gabriel Legorreta Paulín, Elizabeth Nesbitt, and S. Andrew DuFrane

WASHINGTON
GEOLOGICAL SURVEY
Map Series 2018-04
November 2018

This geologic map was funded in part by the USGS National Cooperative Geologic Mapping Program, award no. G17AC00262

This publication has been subject to an iterative technical review process by at least one Survey geologist who is not an author. This publication has also been subject to an iterative review process with Survey editors and cartographers.

WASHINGTON STATE DEPARTMENT OF
NATURAL RESOURCES
WASHINGTON GEOLOGICAL SURVEY

DISCLAIMER

Neither the State of Washington, nor any agency thereof, nor any of their employees, makes any warranty, express or implied, or assumes any legal liability or responsibility for the accuracy, completeness, or usefulness of any information, apparatus, product, or process disclosed, or represents that its use would not infringe privately owned rights. Reference herein to any specific commercial product, process, or service by trade name, trademark, manufacturer, or otherwise, does not necessarily constitute or imply its endorsement, recommendation, or favoring by the State of Washington or any agency thereof. The views and opinions of authors expressed herein do not necessarily state or reflect those of the State of Washington or any agency thereof.

INDEMNIFICATION

Research supported by the U.S. Geological Survey, National Cooperative Geologic Mapping Program, under USGS award number G17AC00262. The views and conclusions contained in this document are those of the authors and should not be interpreted as necessarily representing the official policies, either expressed or implied, of the U.S. Government.

WASHINGTON STATE DEPARTMENT OF NATURAL RESOURCES

Hilary S. Franz—*Commissioner of Public Lands*

WASHINGTON GEOLOGICAL SURVEY

David K. Norman—*State Geologist*
John P. Bromley—*Assistant State Geologist*

Washington State Department of Natural Resources
Washington Geological Survey

Mailing Address:
MS 47007
Olympia, WA 98504-7007

Street Address:
Natural Resources Bldg, Rm 148
1111 Washington St SE
Olympia, WA 98501

Phone: 360-902-1450
Fax: 360-902-1785
Email: geology@dnr.wa.gov
Website: http://www.dnr.wa.gov/geology

Publications and Maps:
www.dnr.wa.gov/programs-and-services/geology/publications-and-data/publications-and-maps

Washington Geology Library Searchable Catalog:
www.dnr.wa.gov/programs-and-services/geology/washington-geology-library

Suggested Citation: Polenz, Michael; Ostrom, B. A.; Lau, T. R.; Sadowski, A. J.; Blanks-Bennett, A. L.; Cakir, Recep; Tepper, J. H.; Legoretta Paulín, Gabriel; Nesbitt, Elizabeth; DuFrane, S. A., 2018, Geologic map of the Violet Prairie 7.5-minute quadrangle, Thurston and Lewis Counties, Washington: Washington Geological Survey Map Series 2018-04, 1 sheet, scale 1:24,000, 41 p. text. [http://www.dnr.wa.gov/publications/ger_ms2018-04_geol_map_violet_prairie_24k.zip]

© 2018 Washington Geological Survey
Published in the United States of America

Contents

Introduction 1
Geologic Overview 2
    Bedrock 2
    Surficial Deposits 2
    Tectonic Framework 3
Methods 3
    Geologic Mapping 3
    Geophysical Surveys 3
    Geochronology and Paleontology 4
    Geochemistry 4
    Sedimentary Provenance of Quaternary Units 4
    Quaternary Geochronology 4
Description of Map Units 5
    Quaternary Unconsolidated Deposits 5
    Tertiary Volcanic and Sedimentary Bedrock 13
Ages of Deposits and Paleoenvironmental Interpretations 17
    Cenozoic Volcanic and Sedimentary Bedrock 17
    Quaternary Units 21
    Geochemistry 25
Structures in the Map Area 27
    Faults 27
    Folds 29
    Structural Implications of Landslides in the Map Area 31
Acknowledgments 31
References 31
Appendix A. New Radiocarbon Age Estimates 37
Appendix B. New U-Pb Age Estimates 38

FIGURES

Figure 1. Relative abundances of lithologies in clast counts.....5
Figure 2. Clast weathering whisker plots 6
Figure 3. Lidar-derived hillshade images of Grand Mound, Violet, and Rock Prairies.....8
Figure 4. Lidar-based image of Mima mounds and relict outwash channels in Rock Prairie.....10
Figure 5. Diamicton in gravel mine at photo site P2.....11
Figure 6. Diamicton (unit Qgic?) and outwash (unit Qgog).....11
Figure 7. Combined zircon age peaks from U-Pb analysis of five detrital and two tuff samples.....14
Figure 8. Well section for the Bannse No. 1 oil exploration well 16
Figure 9. Carbonaceous Skookumchuck Formation 18
Figure 10. Map of faults, folds, and major named coal beds.....22
Figure 11. Lidar-based image of a large landslide in the Skookumchuck Formation.....25
Figure 12. Geochemical data.....26
Figure 13. Lidar-based image of large landslide with anomalous scarps 29
Figure 14. Stereonet diagrams for bedding planes at and near site GD29.....30
Figure B1A. Concordia plot for ages from five zircons at the young end of the age spectrum from age site GD3 40
Figure B1B. Younger zircon age peaks for age site GD3.....40
Figure B1C. Older zircon age peaks for age site GD3. 40
Figure B2A. Concordia plot for ages from the youngest three zircons at the young end of the age spectrum for age site GD4.....40
Figure B2B. Younger zircon age peaks for age site GD4.....40
Figure B2C. Older zircon age peaks for age site GD4. 40

TABLES

Table A1. Radiocarbon ages 37
Table B1. U-Pb data 39

MAP SHEET

Geologic Map of the Violet Prairie 7.5-minute Quadrangle,
Thurston and Lewis Counties, Washington

Figure M1. Regional geologic map of the Violet Prairie quadrangle and surrounding areas
Figure M2. Aeromagnetic map of the Violet Prairie quadrangle and vicinity
Figure M3. Complete Bouguer gravity anomaly map of the Violet Prairie quadrangle and vicinity.

Geologic Map of the Violet Prairie 7.5-minute Quadrangle, Thurston and Lewis Counties, Washington

by Michael Polenz[1], Brian A. Ostrom[1], Todd R. Lau[1], Andrew J. Sadowski[1], Angela L. Blanks-Bennett[1], Recep Cakir[1], Jeffrey H. Tepper[2], Gabriel Legorreta Paulín[3], Elizabeth Nesbitt[4], S. Andrew DuFrane[5]

[1] Washington Geological Survey
MS 47007
Olympia, WA
98504-7007

[2] Geology Department
University of Puget Sound
1500 N Warner
Tacoma, WA 98416

[3] Instituto de Geografía
Universidad Nacional Autónoma de México
Ciudad Universitaria, Del Coyoacán
cp 04510, México, D.F.

[4] The Burke Museum of Natural History and Culture
University of Washington
Box 353010
Seattle, WA 98195

[5] University of Alberta
Department of Earth and Atmospheric Sciences
1-26 Earth Sciences Building
Edmonton, Alberta, Canada T6G 2E3

ABSTRACT

The Violet Prairie quadrangle straddles Thurston and Lewis counties along western Washington's economically vital I-5 corridor. This 1:24,000-scale geologic map aims to identify hazards and improve geologic understanding for private and public resource management and planning. A synthesis of new and existing geologic information provides fresh insight into the glacial deposits, bedrock units, and structural geology of the study area. Glacial deposits of Vashon age and at least one pre-Vashon ice incursion into the quadrangle are likely northern-sourced, but may include some Cascades-sourced, pre-Vashon deposits. Outwash provides ample gravel resources and highly productive but easily polluted aquifers. Field- and lidar-informed mapping suggests that some landslides may be seismically triggered. Lidar also improved mapping of mima mounds and confirmed that they are found only on outwash surfaces. New radiocarbon ages indicate that despite ample outwash, most surficial sediments in the Skookumchuck River valley are late Holocene alluvium. Seven new U-Pb analyses from the upper McIntosh, lower Skookumchuck, and lower and middle Lincoln Creek Formations provide improved benchmarks for ages, sediment sources, and biostratigraphic correlations throughout southwest Washington of: (1) the Eocene McIntosh and Skookumchuck Formations, (2) the Eocene–Oligocene Lincoln Creek Formation, (3) the Miocene Wilkes Formation, and (4) the Pleistocene Logan Hill Formation. New geochemical data suggest that all volcanic rocks in the quadrangle are Northcraft Formation. The data also suggest geochemical distinctions between sedimentary rock units, but more work is needed to attribute these to either unit distinctions or depositional environment distinctions. Mapped faults are reinterpreted as northeast-dipping dextral-reverse.

INTRODUCTION

The Violet Prairie 7.5-minute quadrangle is located in southern Thurston and northern Lewis Counties, Washington, about 20 mi south of Olympia. The map area is approximately bounded on the west by Interstate 5, on the east by the towns of Tenino and Bucoda, and on the south by the city of Centralia. Elevations range from 160 ft in the Chehalis River valley near the southwest map corner to 700 ft at Lemon Hill near the northeast map corner. The northern half of the map area is drained by Scatter Creek, which flows westward from Tenino, via Sunnydale. The creek is flanked by broad glacial outwash terraces in Rock, Violet, and Grand Mound Prairies. Forested hills dominate the southern half of the quadrangle and are drained by west-flowing Prairie Creek, south-flowing Coffee Creek, the Skookumchuck River, and Hanaford Creek. All streams in the map area ultimately drain to the Chehalis River, which flows north just west of the quadrangle.

Lowland areas within the quadrangle are primarily used for agriculture and residential development. Most hills are private timberlands. Several open pit mines produce gravel from glacial deposits in Grand Mound, Violet, Rock, Waunch, and Fords Prairies. Coal mining from the Skookumchuck Formation in and near the map area began with the arrival of settlers in the 1850s and peaked in the early 20th century. The coal was used mostly for domestic heating and railroad operations (Snavely and others, 1958). In 1971, the Centralia open-pit coal mine began operating just east of the quadrangle and worked five coal beds to produce a lifetime average of 4.3 million tons per year, burned on-site to produce electricity (Schasse, 2001). The

operation was a major economic driver for Lewis County until mining ceased in 2006.

This geologic mapping is part of a multi-year effort to map bedrock, surficial, and structural geology across the southern Puget Lowland and west into the Willapa Hills, with particular emphasis toward improved characterization of crustal faults and deformation in and near the Doty–Willapa Hills area. The purpose of this map is to provide private and public decision-makers information to help assess and manage geologic resources, hazards, and groundwater, and to facilitate geotechnical engineering, development, and research. Geologic hazards in the area include: (1) earthquakes (from regional-scale subduction events and more local earthquakes in the shallow crust and subducting slab), (2) landslides (both shallow and deep-seated), and (3) floods.

GEOLOGIC OVERVIEW

Bedrock

Early to middle Eocene Crescent Formation and (or) mantle rocks are thought to form a strongly magnetic, dense basement tens of kilometers thick beneath the map area (Finn, 1990; Trehu and others, 1994; Gao and others, 2011; Schmandt and Humphreys, 2011). Crescent Formation is not exposed in the map area but is widely exposed farther west and northwest in the Willapa Hills and Black Hills, respectively (Pease and Hoover, 1957; Globerman, 1981; Wells, 1982; Logan, 1987; Walsh and others, 1987; Wells and Sawlan, 2014; Polenz and others, 2017). The Crescent Formation is part of the Siletzia terrane, a large igneous province of submarine to subaerial, tholeiitic to calc-alkaline basalt (Glassley, 1974; Irving, 1979; Babcock and others, 1992, 1994; Wells and others, 2014; Phillips and others, 2017). Siletzia was extruded near the margin of North America between 56 and 48.4 Ma and accreted to North America approximately 53 to 50 Ma (Wells and others, 2014; Eddy and others, 2017).

The oldest exposed rocks in the quadrangle are mapped as middle Eocene, marine McIntosh Formation, which Snavely and others (1958, 1959) correlated with Cowlitz Formation (Weaver, 1937; Wells, 1981). Weaver's Cowlitz Formation includes rocks previously mapped by Culver (1919) as "Eocene Puget Series (coal bearing)" of southwestern Washington. Wells (1981) further identified the McIntosh Formation as equivalent to Henricksen's (1956) Stillwater Creek member of the lower Cowlitz Formation. Snavely and others (1958) inferred a paleoshoreline east of the Violet Prairie quadrangle during deposition of the marine McIntosh Formation, with coeval deposition of terrestrial sediment farther east (Snavely and others, 1951).

Whereas Snavely and others (1959) had excluded volcanic rocks from their formal definition of the McIntosh Formation, Snavely and others (1958) mapped a volcanic McIntosh Formation member in the Black Hills in and near the northern part of the Rochester quadrangle. Snavely's coauthor Rau later indicated that all volcanic rocks (and sedimentary interbeds) in the Black Hills are Crescent Formation (oral commun. to Tim Walsh, 1987; consistent with Rau, 2004, record no. 119). That interpretation is also supported by geochemical traits in Black Hills basalt (Polenz and others, 2017), and Polenz and others (2017) presented a 47.3 Ma U-Pb age on siltstone from above Crescent Formation basalt in the southern Black Hills as a basal age for the McIntosh Formation (as formally defined by Snavely and others, 1959). However, an older, lower McIntosh Formation member was informally mapped elsewhere in southwest Washington (Pease and Hoover, 1957; Wagner, 1967; Armentrout, 1987; Walsh and others, 1987; Wells, 1989; Wells and Sawlan, 2014).

McIntosh Formation deposition was followed by deposition of the middle to upper Eocene, locally coal-bearing, deltaic, terrestrial to shallow marine Skookumchuck Formation (Snavely and others, 1958). Deposition of the mostly terrestrial Skookumchuck Formation in the Violet Prairie quadrangle indicates that by late Eocene time, the paleoshoreline had migrated west into and beyond the Violet Prairie quadrangle (Snavely and others, 1958; Buckovic, 1979; Flores and Johnson, 1995).

Both the McIntosh and Skookumchuck formations adjoin and in places likely interfinger with Eocene andesitic to basaltic volcanic and volcaniclastic rocks of the Northcraft Formation (Snavely and others, 1951, 1958; Buckovic, 1979; Rau, 1981; Schasse, 1987; Flores and Johnson, 1995; Logan and others, 2009). Northcraft Formation rocks entered the map area from a terrestrial volcanic center east of the map area and thin westward into a progressively more marine Eocene paleoenvironment (Snavely and others, 1958; Buckovic, 1979; Flores and Johnson, 1995).

Weaver (1912, 1937) introduced the name Lincoln Formation for rocks exposed along the Chehalis River, north of Galvin. He later identified the type section as outcrops along the Chehalis River from Centralia to Porter, WA, and in hills southwest of the river (Weaver, 1944). Snavely and others (1958) describe the "Lincoln Formation (of Weaver)" as basaltic marine sandstone in a lower member of the formation and tuffaceous marine sandstone and siltstone in an upper member. Combined, the two members were thought to form approximately 2,000 ft of section. Beikman and others (1967) established biostratigraphic age controls for the unit and changed the name to Lincoln Creek Formation. Deposition of this unit in the map area indicates that the Eocene delta was followed by a return to marine basin conditions during Oligocene–late Eocene time.

The Miocene Wilkes Formation overlies Lincoln Creek Formation along an angular unconformity. The unit appears to correspond to a "Tertiary nonmarine unit" that Snavely and others (1958) mapped in parts of the southern half of the Centralia–Chehalis district, although they did not show either unit in the Violet Prairie quadrangle.

Surficial Deposits

The maximum southern extent of multiple glacial advances of the Cordilleran ice sheet lies within the Violet Prairie quadrangle. The most recent ice advance during the Vashon Stade of the Fraser glaciation culminated near Scatter Creek (Bretz, 1911, 1913; Lea, 1984; Logan and others, 2009), approximately 15.7 ka (Polenz and others, 2015). Drift from this ice advance mostly conceals Eocene sedimentary and volcanic bedrock north of Scatter Creek. Older drift locally extends slightly farther south and is distinguished from Vashon drift by more advanced weathering (Noble and Wallace 1966; Lea, 1984). Lea (1984) suggested that the two recognizable ice advances into the map area are the Vashon and Double Bluff glaciations, corresponding

to marine oxygen isotope stages (MIS[1]) 2 and 6, respectively. The Scatter Creek corridor was a major pathway for Vashon meltwater (Bretz, 1913; Walsh and Logan, 2005; Logan and others, 2009) resulting in a relatively flat valley with multiple glacial outwash terrace sets. The development of mima mounds, which are widespread on these terraces, remains enigmatic despite decades of debate (Bretz, 1913; Dalquest and Scheffer, 1942; Newcomb, 1952; Ritchie, 1953; Washburn, 1988; Berg, 1990; Pringle and Goldstein, 2002; Logan and Walsh, 2009; Horwath Burnham and Johnson, 2012; Gabet and others, 2014). Farther south, the Skookumchuck River, flanked by narrower outwash terraces, flows southwest from Bucoda to Centralia, between hills of Eocene sedimentary rocks. This valley was a drainage pathway for proglacial meltwater (Bretz, 1911, 1913; Lea, 1984). Landslides are common south of the ice limit (Lea, 1984).

Tectonic Framework

The Violet Prairie quadrangle lies within the forearc of the seismically active Cascadia subduction zone, which produces great earthquakes in southwest Washington on average every 500 years (Clague, 1997), perhaps more often (Goldfinger and others, 2016). The most recent Cascadia subduction zone earthquake measured an estimated M8.7 to 9.2 on January 26, 1700 (Satake and others, 2003). Oblique subduction of the Juan de Fuca plate beneath the North American plate has resulted in structural complexity within the Cascadia forearc (Wells and others, 1998; Lewis and others, 2003; Johnson and others, 2004; McCaffrey and others, 2007, 2013). Approximately 4.4–6 mm/ yr of on-going north-south shortening between western Oregon and the relatively stable Coast Mountains of British Columbia have been interpreted as an expression of clockwise rotation (Johnson and others, 2004; McCaffrey and others, 2013; Wells and McCaffrey, 2013). The shortening resulted in a series of basins and uplifts bounded by active, mostly east-west-striking reverse faults and folds, mostly recognized in the Puget Lowland north of the map area (Clowes and others, 1987; Johnson and others, 1996, 2004; Wang, 1996; Pratt and others 1997; Wells and others, 2017; Bowman and Czajkowski, 2016).

The Violet Prairie quadrangle and surrounding areas are intersected by multiple northwest-striking faults and fault-parallel folds (Snavely and others, 1958; Schasse, 1987; Walsh and others, 1987). Their relationship to the west-striking Doty–Salzer Creek fault system south of the map area remains uncertain (Sadowski and others, 2018). Paleomagnetic rotation suggests that long-term rates of rotation of crustal blocks in the Cascadia forearc resemble ongoing rotation rates inferred by GPS data (McCaffrey and others, 2007; Wells and McCaffrey, 2013). The GPS data presented by McCaffrey and others (2007) also indicate that the rates of rotation in the Washington forearc basin at the longitude of the map area are markedly smaller than those farther west in the Willapa Hills and Olympic Mountains. In models of McCaffrey and others (2007; 2013), the Doty–Salzer Creek fault system appears to coincide with a boundary between separately rotating crustal blocks. Wells and others (2017) presented arguments for possible linkage of crustal faults near the map area to segmentation of activity on the Cascadia subduction zone. If real, these linkages further suggest that at least the Doty–Salzer Creek fault system (Sadowski and others, 2018), 4 mi south of the map area, may be active.

METHODS

Geologic Mapping

We identified units from field observations made between July 1 and November 2, 2017. We collected field data and constructed preliminary field-based maps using ArcMap and ArcCollector. We measured orientations of bedding, joints, and shears where outcrops suggested more than random cracks or nontectonic brecciation (such as from landslides). Most outcrops were small, and no measured features could be traced beyond individual outcrops. We used thin-section analysis, well and boring records, geotechnical reports, geophysical data, prior geologic mapping and studies, aerial orthophotos, and geomorphic features identified from lidar to refine the mapping. We reviewed more than 1,120 water well logs and boring records (Jeschke and others, 2016; Snavely and others, 1958; WGS unpublished records) in and within ~1 mi of the Violet Prairie quadrangle. We could confidently locate 222 and used 12 of those in the development of Cross Section A–A′. We used a lidar-based digital elevation model (DEM) with a 2-m grid resolution to estimate site elevations and derive hillshade images, contours, and other products. Edge mismatches with the adjacent Maytown quadrangle (Logan and others, 2009) are intentional and based on differences in classification or interpretation. We used the geologic time scale of the United States Geological Survey (USGS) Geologic Names Committee (2010). Where that scale lacked Epoch subdivisions, we referred to Walker and Geissman (2009). Topographic lineaments and structural measurements were compared to max spot clusters[2], other anomalies, and lineaments in several aeromagnetic images generated by Richard Blakely (USGS, written commun., 2016, 2017).

Geophysical Surveys

MAGNETICS

Multiple, customized aeromagnetic images for the map area and vicinity (Richard Blakely, USGS, written commun., 2016, 2017)

[1] MIS: global marine oxygen isotope stage curve, where even-numbered stages are used as a proxy for timing and intensity of global glacial periods (Morrison, 1991). For discussion of corresponding Cordilleran ice sheet advances into the Puget Lowland, see Booth and others (2004), Troost and Booth (2008), Polenz and others (2013, 2015), and Troost (2016). For timing of the MIS 2 ice advance into the map area at the southern limit of the Vashon glaciation, we refer to Polenz and others' (2015) fig. 3 and discussion, although the southern tip of their fig. 3 should have been extended south of Olympia to the Vashon ice limit south of Scatter Creek.

[2] Locations of anomalously large aeromagnetic field strength gradients, objectively identified by curvature analysis, which assumes that contacts are vertical and remanent magnetization is unimportant (Richard Blakely, USGS, written commun., 2013). See Blakely and others (2004) for a description of aeromagnetic max-spots methodology.

were complemented by ground magnetic surveys conducted using two portable magnetometers; a G-859 Cesium Vapor Magnetometer for survey lines and a G-857 Proton Procession (manufactured by Geometrics Inc.) for base station measurements. For magnetic measurements north of the boundary between the Violet Prairie and Centralia quadrangles, the base station was located at 46.77675°N, 123.06137°W. For magnetic measurements south of the Violet Prairie–Centralia quadrangle boundary the base station was located at 46.67537°N, 122.93258°W.

Ground magnetic data were preprocessed using Geometrics MagMap2000TM software for de-spiking and correcting diurnal variations measured at the base station. We used Geosoft's Oasis Montaj® software to apply a band-pass filter to further eliminate local spikes in the data. The result is a map that images anomalies produced by near-surface magnetic rocks. Model geometry (depth) and material properties (magnetic susceptibilities) were constrained from local borehole information and previous studies (Finn, 1990; Telford and others, 1990).

GRAVITY

We used a LaCoste Romberg Model G-908 gravimeter to develop gravity survey profiles with a 0.25 km station spacing and gravity readings in areas where aeromagnetic data, previous studies, or field observations suggested structural significance. Gravity data are referenced to base station Chehalis B (46.394169°N, 122.580970°W)(Nilsen, 1976). Gravity readings were imported into Oasis Montaj® software, where tidal, drift, latitude, free air, Bouguer anomaly, curvature (Bullard B), and terrain corrections were performed. Crustal density was set to 2.67 g/cm^3. Terrain corrections were calculated from a regional terrain correction grid constructed using 10 m DEM and local lidar DEM, using an outer distance of 50 km and an inner correction distance of 100 m (328 ft). Regional gravity data (Bowman, 2013) were combined with data from this study to create a Complete Bouguer Anomaly grid. Block model densities were constrained using previous regional studies (Finn, 1990) or globally averaged values (Telford and others, 1990). Geophysical cross section models were calculated with the 2D GM-SYS Modeling software (Geosoft, Inc.) using both magnetic and Complete Bouger anomaly data as constraints.

Geochronology and Paleontology

Ellington and Associates, Inc. (Houston, TX, a division of ALS Global) prepared samples for microfossil analysis using a 140-mesh sieve (105 micron openings). Elizabeth Nesbitt and Ruth Martin (both at the Burke Museum, University of Washington) analyzed the macro- and microfossil content of the samples (Table DS1A). The sample sites are shown on the map with the prefix GD, numbered consecutively from north to south. Samples outside the map area are assigned higher numbers than any inside the quadrangle and are shown on Figure M1.

Geochemistry

Minor and trace element analyses were performed on 33 samples of volcanic and sedimentary bedrock, drift and weathering products of bedrock and drift. ALS (geochemistry laboratory in North Vancouver, BC, Canada) performed major and trace element analysis by ICP-AES (major elements), ICP-MS (trace elements), and combustion oven (loss on ignition). Geochemistry samples are shown on the map with the prefix G, numbered consecutively from north to south. Samples outside the map area are assigned higher numbers than any inside the quadrangle and are shown on Figure M1.

Clay mineral analysis by XRD was performed by WGS staff using a Rigaku MiniFlex 600 XRD device on samples of sedimentary rock and northern-sourced pre-Vashon till. Because these analyses provided no discriminating insights for the Violet Prairie quadrangle but did suggest useful distinctions for the Centralia quadrangle, they are presented by Sadowski and others (2018) in the context of that quadrangle.

Sedimentary Provenance of Quaternary Units

We used weathering data from clast counts (Table DS3) and petrographic review of matrix content to estimate relative sample ages. Unlike Porter (1975), Colman and Pierce (1981), and Lea (1984), we did not limit clast counts to basaltic rocks because assessments of clast weathering in recent studies of nearby areas showed little difference in weathering signals between basaltic rocks alone and all rock types combined (Polenz and others, 2016; 2017). We used clast counts (Table DS3), petrographic review of matrix content, sedimentary attributes (such as bedding style, grain size, and textural changes), and field relations to infer provenance of Quaternary sediment exposures and help determine their depositional setting (glacial, nonglacial, or undivided). Pebble clast lithologies were tabulated to explore lithologic trends indicative of provenance (Fig. 1). Two clast counts from pebbly lenses in Skookumchuck Formation sedimentary rock were added to explore if clast counts may be useful for associating weathered deposits of unknown affiliation with either bedrock or unlithified sediment units. Clast count sites are shown on the map as sites with the prefix C, numbered consecutively from north to south. Samples outside the map area are assigned higher numbers than any inside the quadrangle and are shown on Figure M1.

Quaternary Geochronology

WEATHERING

Relative ages of Quaternary units were assessed using clast weathering and thin-section petrographic assessment of matrix weathering. The results are tabulated in Table DS3 and graphically summarized in Figure 2.

RADIOCARBON ANALYSIS

Conventional "radiocarbon plus" analyses were performed by Beta Analytic (Miami, FL) on wood that had been embedded in floodplain sediment at two locations along the banks of the Skookumchuck River. These samples were placed in zip-lock bags on-site (air tight and saturated) and oven-dried at the WGS lab a few days later.

PALEOMAGNETIC ANALYSIS

Paleomagnetic samples were collected from five exposures of Skookumchuck Formation to assess the rotation of sedimentary

bedrock since deposition. Samples were analyzed by Bernard Housen and William Callebert (Western Washington University).

DESCRIPTION OF MAP UNITS

Quaternary Unconsolidated Deposits

POSTGLACIAL DEPOSITS

Postglacial deposits in glaciated parts of the map area are in most cases readily identified by their lack of compaction. However, there are exceptions, and in unglaciated parts of the map area glacial/postglacial distinctions are difficult and commonly meaningless. These issues and variations are discussed in more detail below (see *Ages of Deposits and Paleoenvironmental Interpretations*).

Holocene Nonglacial Deposits

af **Artificial fill**—Cobbles, pebbles, sand, silt, clay, and boulders, in varied amounts and mostly of northern-sourced lithologies. Used to raise roadbeds and other infrastructure throughout the map area.

ml **Modified land**— Rubble of northern-sourced cobbles, pebbles, sand and boulders in varied amounts and lithologies; locally derived but redistributed to modify topography; excludes roads and some pits where underlying units can be readily identified, fill areas appear minor, excavation exposes the same unit as the surrounding surface, or exposure of underlying units was deemed likely to be permanent.

Qp **Peat**—Organic and organic-rich sediment; includes peat, gyttja, muck, silt, clay, and sand, in varied amounts; typically in closed depressions; mapped in wetland areas and distinctly flat-bottomed depressions; also mapped on the basis of evaluation of infrared and color aerial photos and (or) spectral analysis of Landsat data. Most peat deposits are inferred from evidence of a wetland setting and the thickness of most peat deposits is unassessed. Patchy peat is widespread in the northern portion of the map area where stagnant ice left many closed depressions. Broader wetlands span some of the valley floors farther south because proglacial outwash dammed tributary valleys of the Skookumchuck River and Scatter Creek (Lea, 1984).

Qls **Landslide deposits**—Sand, silt, clay, cobbles, pebbles, diamicton, and boulders of sandstone, siltstone, and conglomerate, in varied amounts; weathering varied; clasts angular to rounded; unsorted; generally loose, jumbled and unstratified, but locally retaining primary bedding and compaction; derived from units upslope (or underfoot in some landslide toes). Unit thickness varies throughout the map area and is mostly unassessed. Mapped mostly from lidar, informed considerably by interpretations of the WGS landslide hazards group, and only where identified confidently and extensive enough to show at map scale. Landforms that to varied degrees suggest landslides also abound elsewhere in the map area, especially south of the Vashon ice limit.

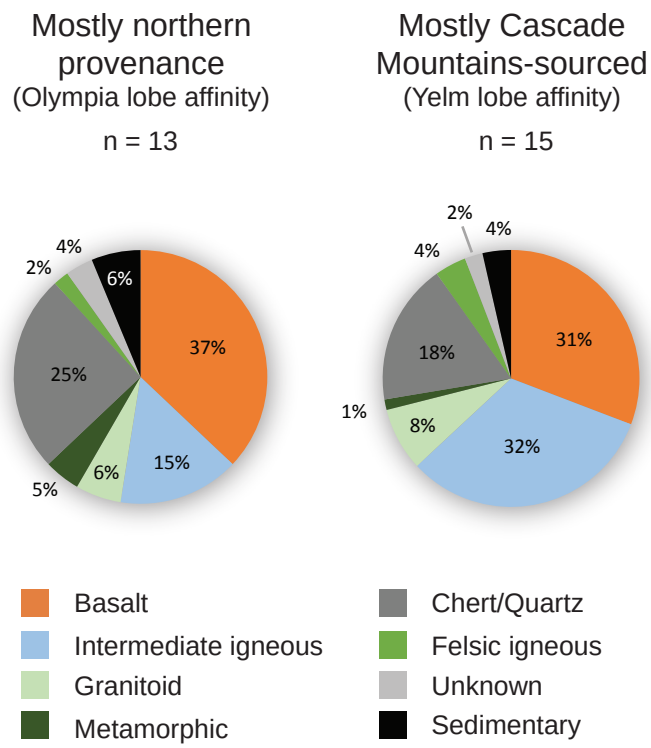

Figure 1. Relative abundances of lithologies in clast counts of 50 randomly sampled clasts from each of 28 samples of Quaternary sediment in or near the map area (Table DS3). Field-based assessments of either northern or possible Cascade Mountains provenance samples yielded clast distributions that, on average, appear separable by percentages of basalt, intermediate igneous rocks, quartz and chert. Principal component analysis indicates that the trends are weak, with more overlap than distinctions, and that the best single discriminant is a greater content of quartz and chert in northern-sourced clast assemblages. Field relations suggest that virtually all samples are mixed, having to varied degrees incorporated rocks of both northern and Cascade Mountains provenances.

The extent of these landforms is in many instances morphologically vague, and where field-verified, other attributes commonly associated with slope movement, such as stressed vegetation or disrupted drainage, were found to be absent or ambiguous. Such landforms cover a large part of the map area but the presence of corresponding landslide deposits is uncertain. They are identified by the "mass wasting" overlay pattern (see geologic symbols on Map Sheet). Some landslides are unmapped because slopes or streams have dispersed their deposits. Absence of a mapped landslide does not imply stability or absence of hazard.

Pleistocene to Holocene Nonglacial Deposits

Qa, Qoa **Alluvium**—Pebbles, cobbles, sand, silt, clay, peat, and boulders in varied amounts along stream channels and on flood plains; mapped as unit Qoa where active channels no longer contribute to the deposit; clasts and matrix generally light tannish gray to dark brown, mostly depending on the amount and source of silt, clay, and organic matter; fresh to lightly weathered except where streams have proximally absorbed older deposits, locally resulting in bimodal weathering; not compacted and not cemented; particles mostly well rounded and moderately to well sorted; clast lithologies

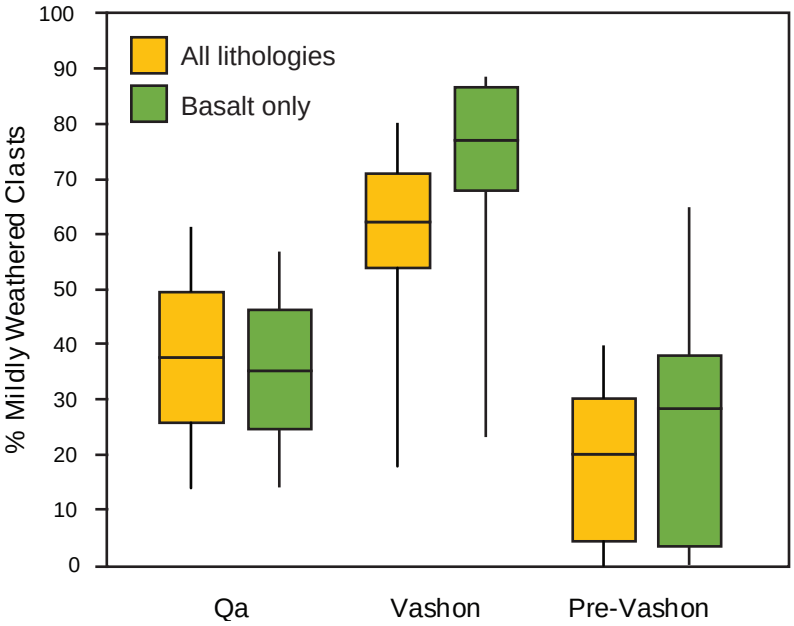

Figure 2. Clast weathering whisker plots. Range of clast weathering for unit Qa and Vashon and pre-Vashon glacial deposits. Glacial deposits were classified as Vashon or pre-Vashon based on multiple criteria. Clast count samples were tentatively field-classified as Vashon or pre-Vashon. Age classifications were either confirmed or re-evaluated after completion of the clast counts and, for selected samples, petrographic examination of the matrix. The classifications of Vashon or pre-Vashon age displayed here integrate clast weathering, matrix weathering, outcrop stratigraphy, geographic location, field relations, and site conditions (for example, if sampled from a subsurface boring at a depth that we expect to be generally waterlogged, we would expect a less weathered clast assemblage than if the sample had been subjected to frequent wetting and drying). All clast counts are included in this diagram, except for C4 and C26, which are from pebbly lenses in Skookumchuck Formation. Limiting clast weathering assessment to basalts did little to change the overall weathering signals.

vary depending on upvalley source materials. Due to the presence of glacial or proglacial deposits in the northern part of the map area and in the valley of the Skookumchuck River, deposits there tend to have more polymict clast assemblages than streams farther south, where the Skookumchuck Formation (and to some degree the Lincoln Creek and Wilkes formations) supplies almost exclusively sandstone, siltstone, claystone, and shale clasts. Geomorphic terrace relationships combined with two radiocarbon analyses on wood from terrace deposits exposed along the banks of the Skookumchuck River provide clear evidence that most of the Skookumchuck River valley floor consists of late Holocene deposits (although many of the clasts may be reworked from glacial outwash). An age sample from site GD1 was wood embedded in a red, 1-ft-thick sand lens with abundant fragments of charcoal and flattened wood in floodplain sediment. Sample GD2 was cut out of a 1.5 to 2 ft-thick log protruding from flood plain sediment at water level. The sample captured approximately 60 outermost growth rings. No bark was observed, and the sample may therefore represent interior growth rings from a formerly thicker log. Both radiocarbon samples were exposed at water level along the active Skookumchuck River channel and yielded late Holocene ages that indicate the Skookumchuck River is actively moving sediment (channel bed load and flood plain sand and silt) across the full width of the valley floor.

Qaf
Qoaf

Alluvial fan—Sand, silt, clay, pebbles, and cobbles in varied amounts; gray to brown; loose; subangular to rounded; moderately to poorly sorted; stratified to unstratified; derived largely from sedimentary bedrock. Most instances of the unit are inferred from a distinctive, concentrically convex, lobate landform where streams emerge from a confining valley. Morphology in most cases suggests a minimum thickness of 10 to 20 ft. Deposition at the base of hillslopes is commonly sudden, hazardous, and associated with significant storm events. Unit Qoaf 400 ft west of geochemistry site G8 north of Violet Prairie includes an inferred, queried alluvial fan deposit that was mapped because a concentrically convex landform here is morphologically distinctive, but the upslope valley lacks morphologic evidence of a fluvial channel and, based on lidar data, instead forms a smoothed, gentle trough. The alluvial fan deposit here may be largely relict (unaffected by on-going sedimentation) and pre-Vashon in age. Unit Qoaf is mapped in three other locations where the source valley no longer contains an active channel or the channel has incised too deeply to deposit new material onto the fan surface. Unit Qoaf in these instances was identified as relict landforms in western tributaries of Coffee Creek based on geomorphic cross-cutting relations (secs. 17–18, 20, and 27, T15N R2W).

PLEISTOCENE GLACIAL DEPOSITS

Vashon Drift of the Fraser Glaciation

Qgo

Vashon recessional outwash, undivided—Pebbles, cobbles, sand, silt, and clay in varied amounts; mostly light gray where fresh, ranging to dark gray; pale brown to tan and light orange where weathered (or only surficially iron stained); lightly weathered, with most weathering rinds less than 2 mm thick (Table DS3); loose but may locally be lightly cemented; clasts well rounded to subrounded and moderately to well sorted in gravel facies. Matrix-rich gravel, sand and finer facies were not observed in the map area but provided for in unit description because sandy and silty facies are in places present in ice-proximal deposits of the same unit outside the map area; unbedded to bedded. The undivided unit Qgo is mapped in only two polygons, both north of Grand Mound Prairie, where the outwash surfaces are truncated on their upstream end by ice

contact deposits of unit Qgic, suggesting that the outwash in this part of the map area is proximally derived from Puget Lobe ice that occupied the adjacent areas mapped as unit Qgic (Figs. 3A and B). Mima mounds (Fig. 4; map overlay) on the larger, eastern patch of unit Qgo (Fig. 3B) locally suggest an excessively drained gravel deposit texturally similar to the broader prairies with mima mounds farther south. However, much of the undivided unit Qgo lacks mima mounds, and we did not observe enough of the outwash in unit Qgo to determine if it is consistently gravel-dominated (a characteristic we generally associate with unit Qgog). Olympia lobe-derived deposits generally contain more basalt, quartz and chert, and fewer intermediate igneous clasts than deposits farther east, which tend to include more Cascade Mountains-sourced rocks, although these trends are weak in the map area (Fig. 1). Divided into:

Qgog **Vashon recessional outwash, gravel**—Pebble- to cobble gravel, locally bouldery, clast-supported, with most exposures containing a sparse to moderately voluminous matrix of coarse sand; mostly pale or medium gray where fresh, ranging to dark gray; pale brown to tan and light orange where weathered (or only surficially iron stained); lightly weathered, with most weathering rinds less than 2 mm thick (Table DS3); loose but may locally be lightly cemented, with some exposures revealing localized, <2 mm-thick crusts of quartz precipitate on the bottom of some clasts; clasts well rounded to subrounded; moderately to well sorted. Clast lithologies are polymict and for deposits in Rock, Violet, and Grand Mound prairies seem to be mostly derived from the Yelm ice lobe, whereas lithologies of deposits in the Skookumchuck River valley suggest association with the Olympia ice lobe (Fig. 1). Exposures vary from unbedded to distinctly bedded, but most are only faintly bedded. Some exposures contain localized interbeds or lenses of sand, but the only observed sand package of any note was in a gravel pit at clast count sites C5, C6, and C7 (Grand Mound Prairie), where 4 ft of planar-bedded, gray sand was exposed at the base of the exposure, about 15 ft below the surface.

Well records suggest a typical unit thickness of about 40 to 100 ft in Rock, Violet, and Grand Mound prairies and in the Skookumchuck River valley, but this includes an unknown amount of Vashon advance outwash and similar pre-Vashon outwash. In Rock, Violet, and Grand Mound prairies the unit also includes diamicton, which was observed within <20 ft of the surface in a gravel pit in Rock Prairie (Figs. 5 and 6; eastern gravel pit in Fig. 3A). The diamicton is distinguished from adjacent and overlying outwash gravel by a lack of bedding and a more abundant and less sorted matrix. Much of the diamicton is matrix supported. These other deposits (older outwash and diamicton) are not clearly apparent as separate deposits in most well records. The diamicton at sites P2 and P3 (Map Sheet; Figs. 5 and 6), and where else well records note diamicton amid outwash gravel, could be either till as suggested on the map, or outwash from cataclysmic floods like the Tanwax–Ohop Valley flood as suggested elsewhere near Tenino (Pringle and Goldstein, 2002; Parker and others, 2008). Similar deposits suggested by some well records deeper in the subsurface are one reason Cross Section A–A′ lumps pre-Vashon drift into an undivided drift unit. The ~100 ft of Vashon outwash shown above undivided pre-Vashon drift in Cross Section A–A′ may also include diamictons (till and (or) debris flow deposits)—most well records do not offer clear evidence for or against it, and at least the diamicton in the above-mentioned gravel pit does not form a contiguous hydrologic barrier. Unit Qgog covers Rock, Violet, Grand Mound, and Fords prairies. Patches of this unit can also be found in Frost Prairie and in the Skookumchuck River valley, where the unit occupies some terraces along the margins of the valley. The tendency of areas mapped as unit Qgog to form prairies rather than forests results from high permeability and transmissivity, which efficiently drains the surface and leads to summer drought, but which also permits the unit to form rich aquifers. The same permeability and transmissivity also render these aquifers particularly vulnerable to contamination from the surface. Unit Qgog shares its high permeability and transmissivity with units Qpog, and Qpd. Unit Qgog appears to

Figure 3. *(next page)* Lidar-derived hillshade images of Grand Mound, Violet, and Rock Prairies and adjacent hills. Regional view is shown in **A** with close-up shown in **B**. Images show a transition in the character of landforms from the glaciated Puget Lowland to unglaciated hills farther south. Letters highlight features that illustrate each landform. (A) Widespread striations are flutes and drumlins. (A2) More subdued striations where Vashon ice did not extend but pre-Vashon ice did. (B) Mostly stagnant ice deposits mapped as unit Qgic. (C) Distinctly sinuous eskers, formed by subglacial and englacial meltwater. (D) Wetlands and peat deposits that commonly develop in depressions amid the glaciated surfaces. (E) Outwash surfaces that lack upslope drainage basins, implying that the outwash was deposited by meltwater that emerged from adjacent ice. (F) Early recessional ice front. (G) Mima mounds, clusters of small, regularly sized bumps (Fig. 4). (H) Sand and gravel mines. (I) Broad outwash surfaces with relict fluvial terraces and anastomosing meltwater channels. (J) More elevated outwash surfaces formed by periglacial drainage when ice across Grand Mound and Mima prairies blocked westbound drainage. (K) Formerly deeper valleys with floors filled with sediment impounded by outwash deposition downstream. (L) Rough surfaces marking maximum ice extent. (M) Smoother unglaciated landforms farther south. (N) Landslides. (L) Rough glaciated surfaces.

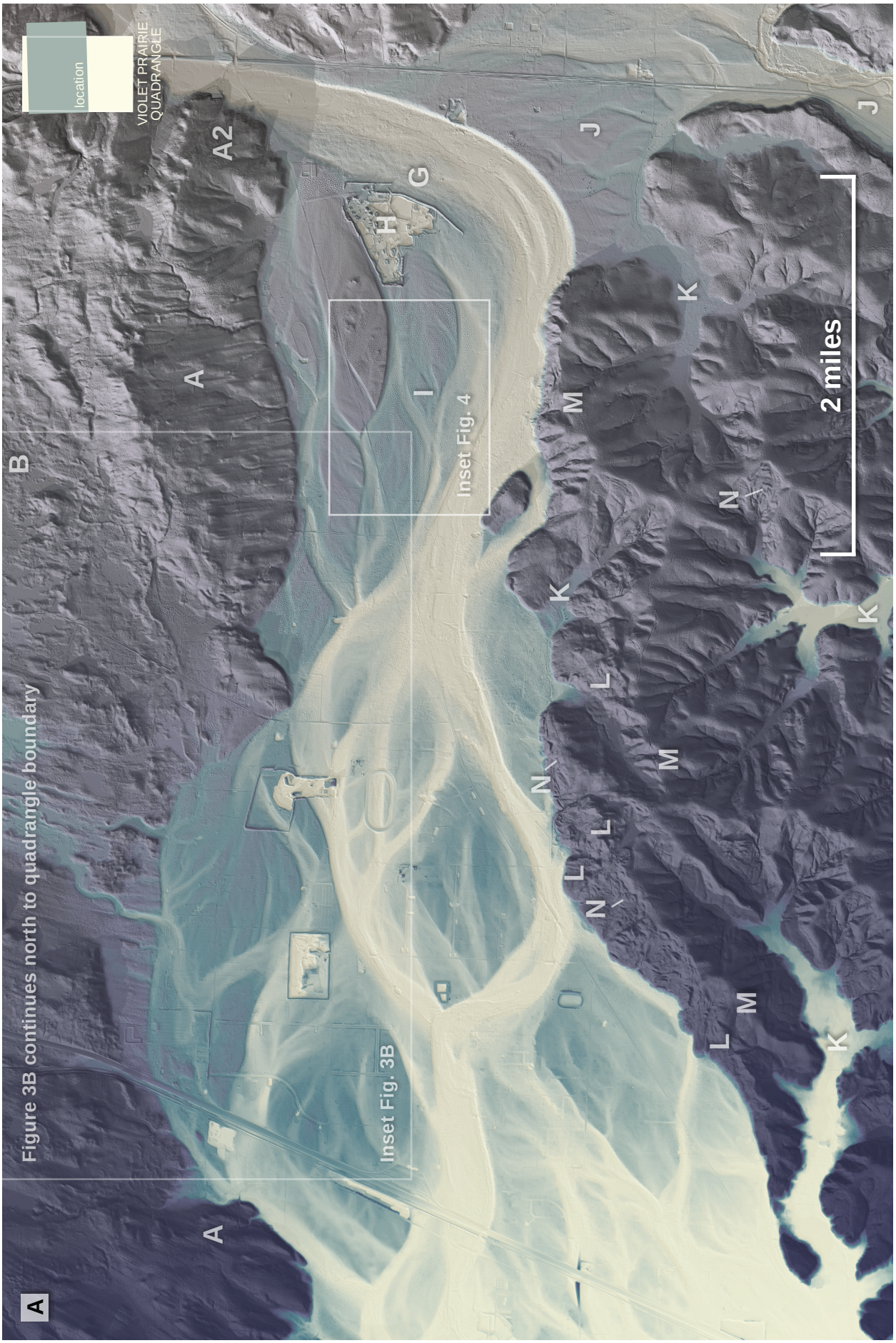
A
Figure 3B continues north to quadrangle boundary
Inset Fig. 3B
A
B
A2
VIOLET PRAIRIE
QUADRANGLE
location
Inset Fig. 4
I
H
G
J
K
M
N
L
2 miles

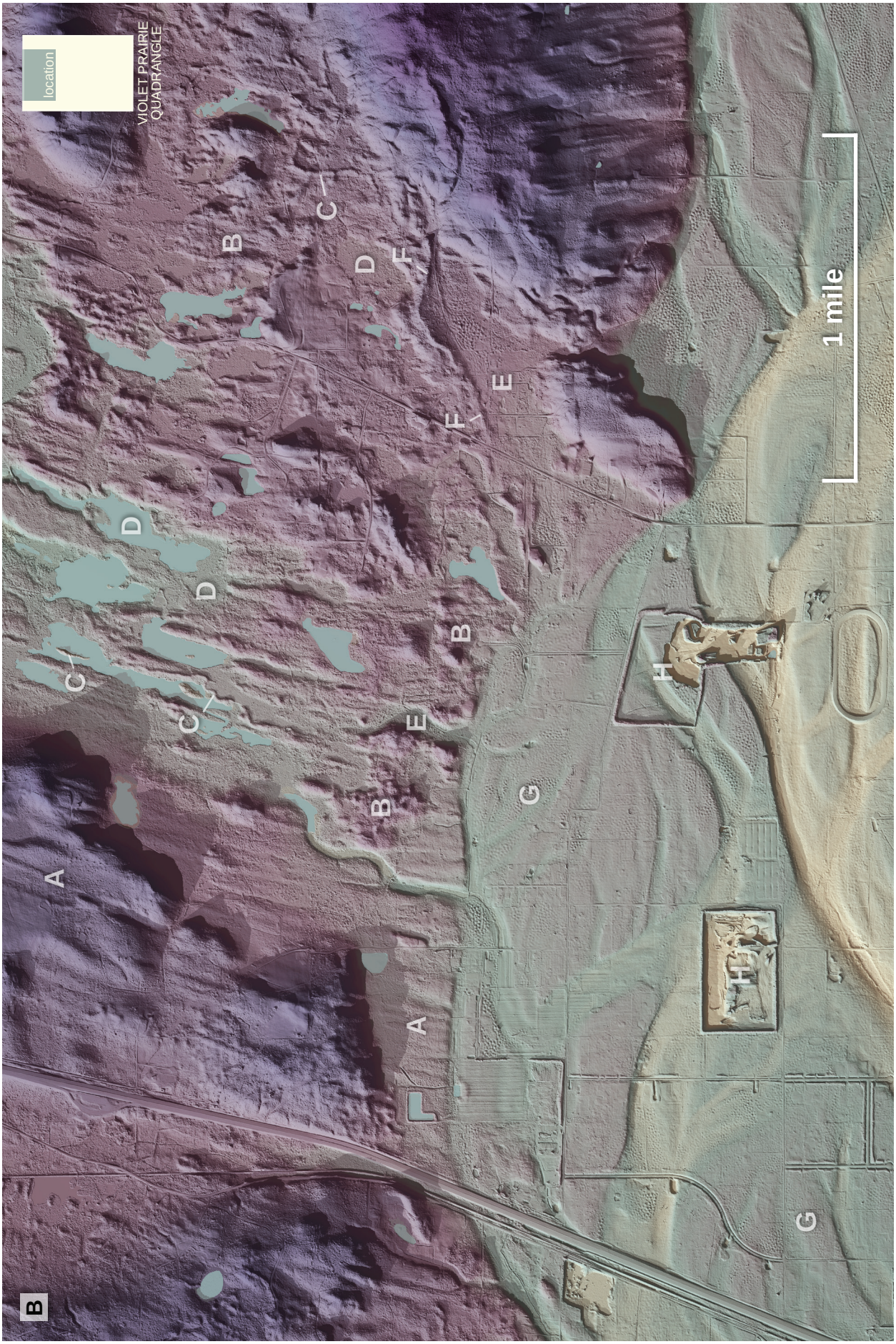
B
location
VIOLET PRAIRIE QUADRANGLE
A
C
D
B
E
F
G
H
1 mile
0

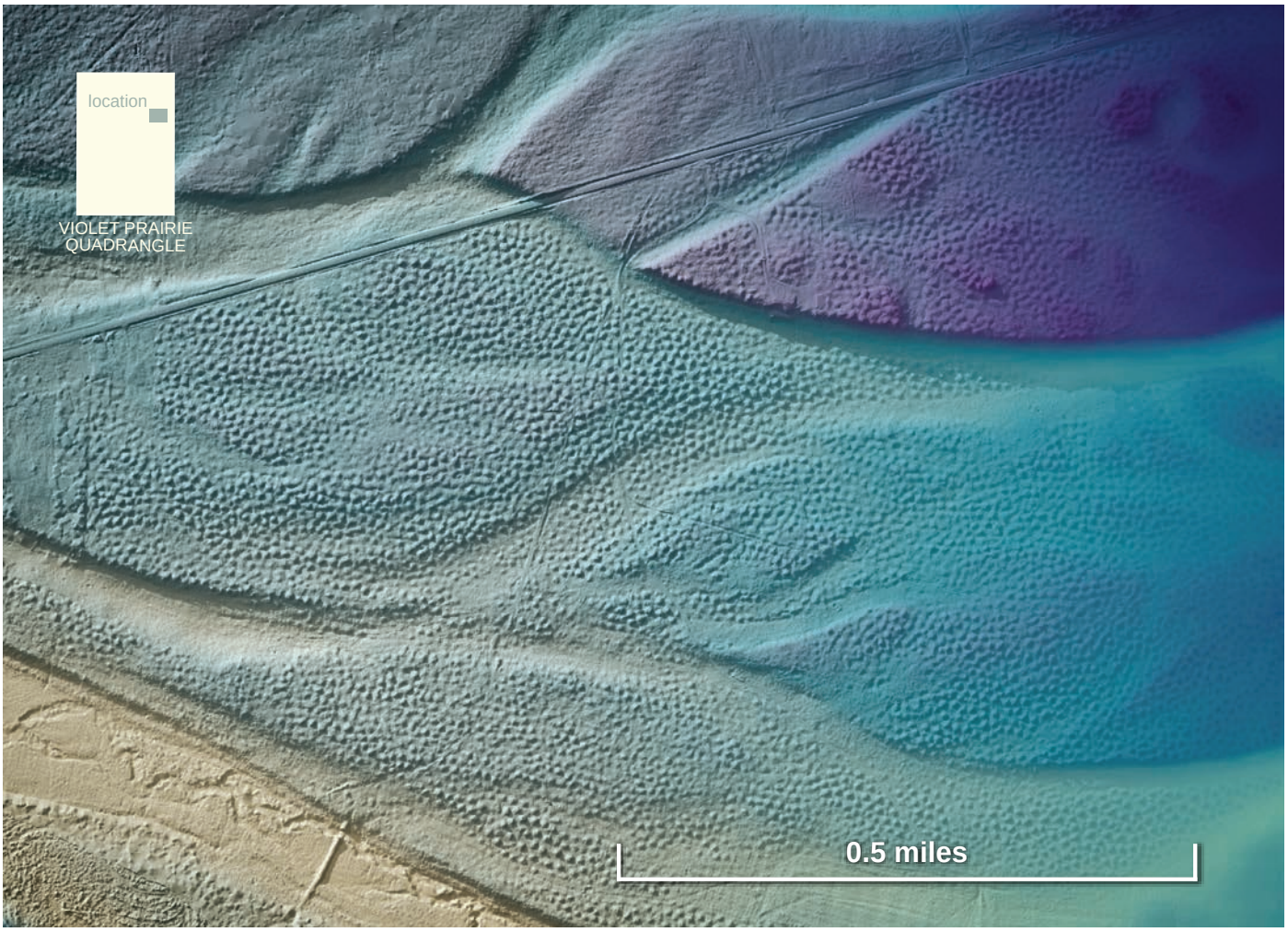

Figure 4. Lidar-based image of mima mounds and relict outwash channels in Rock Prairie. Mima mounds in this area consist of sandy, dark, organic-rich soil with pebbles or cobbles. The mounds rest on a substrate of glacial outwash rich with Cascade Mountains-derived andesite clasts (clast counts C5–C12, Table DS3; Pringle and Goldstein, 2002). Despite an abundance of theories and decades of debate, the development of the mounds remains enigmatic.

be largely equivalent to the high-permeability hydrogeologic unit A (and C) of Gendaszek (2011). Compared to Cross Section A–A′ of this report, Gendaszek showed a thinner unit A beneath thicker pre-Vashon drift (his unit D and unit Qpd of this report). However, we agree with Gendaszek (2011) that the boundary between these units is difficult to recognize in well records and suggest that in the prairies beneath Scatter Creek and the Chehalis River valley, the aquifers are not effectively separated, despite scattered, locally confining lenses or layers in both aquifers. Correlation to sub-units of Qgo presented by Walsh and Logan (2005) and Logan and others (2009) is discussed below (see *Outwash Pathways and Lithologic Associations*).

Qgic **Vashon ice-contact deposits**—Mostly till, locally ranges to pebbles, cobbles, sand, silt, and clay, in varied amounts; pale gray to reddish brown; loose to compact, with lodgment till mostly less compacted and more porous than in unit Qgt, but locally ranging to equally compact; ablation till and ice proximal outwash mostly loose; particle sizes, rounding, sorting and presence of bedding highly varied and resembling unit Qgt in till facies (ice-deposited diamicton, loose or compact) and units Qgo, Qgog, and Qa in waterlain facies (better sorted, commonly bedded, and mostly loose). Unit Qgic in the Violet Prairie quadrangle was deposited by the Olympia lobe and exposures lithologically tend to resemble the mix of mostly northern provenances associated with that lobe (Fig. 1). Unit Qgic is associated with irregular landforms such as eskers, kettles, and an overall bumpy surface morphology, commonly superimposed over drumlins and flutes (Fig. 3B). The kettles and eskers indicate a late-glacial presence of stagnant ice that permits preservation of subglacial landforms (Haugerud, 2009; Polenz and others, 2009, 2010) that would be obliterated by moving ice. Melting ice can also deposit locally thick ablation till and patchy outwash, whereas buried ice blocks can locally persist for centuries or millennia before their collapse leads to formation of kettles, as documented by Porter

Figure 5. Diamicton in gravel mine at photo site P2. Unbedded, unsorted, stony deposits within the same pit range from locally well-developed, compact diamicton to loose and pervious diamicton. Lack of bedding, less sorting, and locally lack of clast support, distinguish the diamicton from adjacent outwash. Interpreted as either Vashon Till or debris flow deposits (see units Qgog and Qpd). Surface is disturbed, depth below original surface not established but likely less than 15 ft.

and Carson (1971). Unit Qgic is widespread north of Violet and Grand Mound prairies. In the Violet Prairie quadrangle the unit could reasonably be considered a terminal moraine of the Olympia ice lobe but was not labeled as such because, as a deposit of mappable volume and extent, it was observed only at least two miles north of the ice margin, and ice likely persisted there when recessional periglacial meltwater had already begun to flow across what are now Rock, Violet, and Grand Mound prairies, obliterating or burying moraine deposits there. However, at least parts of the deposit do mark a temporary recessional ice front where outwash surfaces are truncated on their upstream end by ice contact deposits of unit Qgic, (Fig. 3B). Divided into:

Qge **Vashon esker**—Pebbles and sand; medium gray; lightly to moderately weathered, with most weathering rinds less than 2 mm thick; mostly loose; clasts well rounded; well sorted; distinctly channel-bedded in most exposures, with beds commonly oversteepened because source water, confined beneath ice, locally flowed uphill. Unit Qge was deposited by subglacial, supraglacial, or englacial meltwater and is found amid or adjacent to units Qgic and Qgim. Unit Qge was identified by its distinctive sinuous hill landforms. Its sedimentary characteristics were inferred by analogy to deposits observed elsewhere in the southern Puget Lowland.

Qgt **Vashon lodgment till**—Compact diamicton, matrix-supported with clasts ranging from pebbles to boulders; matrix of sand, silt, and clay in varied amounts; pale gray where fresh, ranging to light brown with surficial rust staining; lightly to moderately weathered; mostly compact to very compact (locally concrete-like) and, due to low permeability, usually less weathered than other Vashon-age deposits; clasts angular to well rounded; poorly sorted with particle sizes from boulders to clay; unbedded, but locally banded. Unit Qgt in the Violet Prairie quadrangle was deposited by the Olympia lobe and exposures lithologically tend to resemble the mix of mostly northern provenances associated with that lobe, shown in Figure 1. Unit Qgt is more compact than unit Qgic and tends to form a better geotechnical foundation and hydrologic barrier. Unit Qgt is associated with drumlins and fluted surfaces, although ice scour can also form both of these on underlying deposits. Unit Qgt is found on Lemon Hill and farther west along a two-mile-wide corridor across the northern end of the map area.

Pre-Vashon Glacial Deposits

Qpog? **Pre-Vashon recessional outwash gravel**—Pebbles and cobbles with sparse to moderately voluminous, sandy to clayey matrix; pale gray; weathers pale brown to tan and light orange; lightly to moderately weathered; moderately compact; moderately to well sorted; rounded to subangular clasts; readily apparent granitic and other northern-sourced clasts confirm association with northern-sourced Puget Lowland glaciation. Clast lithologies are roughly 50% basalt, 20% each of intermediate igneous and quartz/chert, and less than 10% granitic clasts. Exposures are limited to elevated terraces along the margins of the Skookumchuck River valley and can be interpreted either as evidence of channel-side levees from meltwater discharge volumes large enough to turn the entire valley width into a single channel, or as a record of a valley floor that was about 20 to 30 ft more elevated during the outwash deposition than it is now. Unit Qpog? is queried because the inference of

Figure 6. Diamicton (unit Qgic?) and outwash (unit Qgog) in a gravel mine at photo site P3. Diamicton on right side of image is unbedded, unsorted, and mostly loose, and does not provide a significant hydrologic barrier. Lack of bedding in the diamicton distinguishes it from (south–dipping) pebble and cobble gravel outwash on the left side of the image.

pre-Vashon age is questionable; it rests entirely on clast weathering (clast counts C22 and C23, Table DS3). Note that Lea (1984) also identified the deposit at C23 as pre-Vashon outwash. The weathering at C22 and C23 is distinctly more advanced than weathering of clasts from outwash in the center of the valley, where there is little doubt that Vashon meltwater would have deposited fresh material, and where clast weathering is fully consistent with that of other Vashon-aged deposits (clast counts C24 and C25, Table DS3). Clast weathering at sites C22 and C23 also exceeds that of other Vashon outwash clast counts. However, the deposits at sites C22 and C23 are less weathered than unambiguously pre-Vashon-aged deposits farther north in the map area. They rest on elevated, valley-marginal terraces, where microclimate could conceivably have accelerated weathering of Vashon-age deposits. For instance, their perch may have subjected these deposits to more frequent cycles of wetting and drying than most Vashon deposits have experienced. Well records near site C23 suggest between 41 and 110 ft of unit thickness. The lithologic assemblages in clast count sites C22 and C23 suggest derivation from a Yelm ice lobe (Fig. 1). If the deposits are Vashon-aged this would suggest correlation to sub-units of Qgo that Walsh and Logan (2005) and Logan and others (2009) associated with the Yelm ice lobe. Like unit Qgog, unit Qpog? is highly permeable and offers a rich aquifer that is, however, vulnerable to contamination from the surface.

Qpos? **Pre-Vashon? outwash sand**—Sand, slightly silty, with 1 to 3% matrix of silt and clay; contains about 40% quartz, 20% feldspar, and 25% lithic fragments that include readily apparent andesite and smaller amounts of widely varied minerals and rock fragments, including at least some from high-grade metamorphic rocks; pale yellowish brown to pale gray; slightly to moderately weathered, with most grains and rock fragments showing at least a thin weathering rind; compact; fine- to medium-grained; subangular; well sorted. Lithologic and mineralogic mix suggests outwash sand with contributions from northern distal sources as well as eastern Cascade Mountains sources. The observed weathering noticeably exceeds what is typical of Vashon outwash sand and thereby suggests, but does not establish, pre-Vashon age. Observed in a single exposure near the northern map edge, directly adjacent to a spring, which raises the possibility that the weathering at this exposure may have more to do with wetting and drying cycles than age. Unit directly underlies Vashon Till.

Qpt **Pre-Vashon lodgment till**—Matrix-supported diamicton consisting of pebbles, cobbles, and boulders, in varied amounts, in a matrix of clay, silt and sand, in varied amounts; pale brown to reddish brown; typically lightly to moderately weathered; compact where well developed (commonly referred to as "hardpan" and locally resembling concrete); subangular to subrounded; unsorted; unstratified. Clast composition is up to ~50% basalt, ~20 to 50% intermediate igneous, up to ~40% quartz/chert, and less than 10% granitic and metamorphic. Unit Qpt is found in the northwest and northeast corners of the map area.

Qpim **Pre-Vashon terminal moraine**—Diamicton of silt, clay, sand, pebbles and cobbles, in varied amounts; matrix-supported in most exposures; brownish gray to pale reddish brown, moderately to strongly weathered, with at least some secondary clay. Some volcanic clasts reveal a fresh core but their pitted surface appears to be at least 2 to 3 mm of severely weathered rind. Unit Qpim is mostly loose and disintegrates when excavated, although some deposits may have loosened with weathering. Clast rounding is subangular to well-rounded, and the unit is poorly sorted to unsorted, and unbedded. Composition of clasts is roughly 35% basalt, ~20 to 45% intermediate igneous, ~5 to 30% quartz/chert, and less than 10% granitic and metamorphic, and locally includes lithic fragments of tuff. Found in the hills south of Scatter Creek valley, associated with more irregular topography and greater surface roughness than unglaciated areas farther south (Fig. 3A), and marks the southern limit of pre-Vashon glaciation.

Qpd **Pre-Vashon drift (cross section only)**—Mostly pebble gravel and cobble gravel, with varied amounts of boulders, sand, silt, and till; gray to light brown. Outwash portion is clast-supported pebble and cobble-gravel similar to units Qpog? and Qgog, with well-rounded clasts, good sorting, and bedding. Till is matrix-supported but cobble- and pebble-rich diamicton. Some diamictons within the unit may be debris flow deposits as those suggested east of the map area by Pringle and Goldstein (2002 and written commun., 2018) and Parker and others (2008). Clast rounding in the diamictons is subangular to rounded, sorting poor, similar to units Qpt, Qpim, Qgt, Qgic, and Qgim. Clast count at site C17 from a well cutting 113 ft below the surface revealed ~38% basalt, ~36% intermediate igneous clasts, ~14% quartz/chert, and <5% each of granitic and metamorphic clasts (Table DS3). Although this suggests association with a pre-Vashon Yelm ice lobe and Cascade Mountains-sourced meltwater, the unit, like its Vashon-aged equivalents, likely contains facies of Olympia ice-lobe affinity as well (Fig. 1). The unit captures all glacial deposits stratigraphically below Vashon Till, although some of the outwash is likely to be of Vashon age. Most observed well cuttings are lightly weathered similar to Vashon Drift, as illustrated by light to moderate weathering in clast count C17. We speculate that lightly weathered deposits include both Vashon advance outwash and older deposits in which waterlogging inhibited weathering. Unit Qpd is inferred beneath Grand Mound, Rock, and Violet prairies, based on well records, which suggest a thickness in the order of 50 ft, although we suspect that upsection deposits mapped as unit Qgog include some unrecognized older deposits. Unit Qpd is mostly outwash gravel

and shares the high permeability and transmissivity of units Qgog, and Qpog?. The high permeability and transmissivity permit all three units to host rich aquifers that are, however, vulnerable to contamination from the surface. Unit Qpd appears to be largely equivalent to the high-permeability hydrogeologic unit D of Gendaszek (2011).

Tertiary Volcanic and Sedimentary Bedrock

Mcw? **Wilkes Formation (Miocene)**—Inferred from adjacent Centralia quadrangle based entirely on geomorphic continuity and field relations, and therefore shown only queried in the Violet Prairie quadrangle, and described as similar to Wilkes Formation in the Centralia quadrangle (Sadowski and others, 2018): Pebbly sandstone to sandy conglomerate; light gray to medium brown with occasional olive tint; sands weakly to moderately cemented; very coarse- to fine-grained sand matrix with pebbles and cobbles; sub-angular to sub-rounded; moderately to well sorted; pebbly conglomerate is sub-angular to rounded, moderately to strongly weathered; bedding is massive to cross laminated, to undulatory with lenses of coarser material; heterolithic clasts include basalt to andesite (10–80%), quartzite (10–17%, as low as 3%), trace sandstone, siltstone, and chert. Minerals include quartz (5–20%), potassium feldspar (sanidine?) (2–8%), plagioclase (oligoclase–andesine?)(<1–3%), mica (muscovite and biotite)(<1–2%), and trace chalcedony and pyroxene. Unit thickness may exceed 200 ft but is thought to quickly pinch out in the Violet Prairie quadrangle. Wilkes Formation is inferred in a single polygon along the southern map boundary, about 1,000 ft east of Interstate 5; deposits are terrestrial to nearshore (nonmarine)(Snavely and others, 1958); contact relationships in the Centralia quadrangle suggest northwest-southeast-oriented former channels wherein Wilkes Formation rests unconformably on less heterolithic Lincoln Creek Formation. Dip directions typically differ by as much as 90° from underlying attitudes in the Lincoln Creek Formation. Sadowski and others (2018) interpreted the youngest single grains from two U-Pb analyses on detrital zircons from the Centralia quadrangle as indicative of deposition ≤8.57 ±0.92 Ma and ≤7.54 ±1.04 Ma ago. This and strong mid-Miocene zircon age peaks in both samples (Fig. 7) suggest a late(?) Miocene unit age consistent with the Wilkes Formation (Roberts, 1958), and we interpret the Wilkes Formation in the map area as equivalent to the Miocene non-marine sedimentary rock unit of Snavely and others (1958).

ΦEmlc **Lincoln Creek Formation (Oligocene–Eocene)**—Very fine sandstone to siltstone with rare medium sandstone; variedly tuffaceous; ivory to pale gray where fresh, weathers tan to orange brown; fractured surfaces commonly are weathered dark brownish red; weakly to moderately indurated; sub-angular to sub-rounded; moderately to well sorted; bedding mostly not apparent, but some exposures reveal faint, planar or cross-bedding; bedding commonly obscured by widespread hackly structure or spheroidal weathering. Petrographic thin section analysis revealed 33 to 80% quartz, 15 to 60% feldspar, and <1 to 17% lithic fragments. Volcaniclastic fragments include basalt, ash, <2% muscovite, and opaque grains (<1% each of magnetite and volcanic glass). Based on the geographic extent of the formation in the map area and sparse observations of southwest-down bedding dips between about 20° and 30°, we estimate a unit thickness between 720 and 1,650 ft. Lincoln Creek Formation was identified exclusively near the southwest corner of the Violet Prairie quadrangle. Contact relations with the underlying Skookumchuck Formation were not observed. Macrofossil casts of clam shells and other unspecified macrofossils from site GD30, 0.8 mi east of the southwest corner of the Violet Prairie quadrangle, were not preserved well enough to permit identification to species level but indicate a marine shallow shelf depositional environment. Snavely and others (1958) asserted that the contact is conformable, locally gradational, but mostly marked by a distinct lithologic break or possible paleosol. Although some exposures of the formation within the map area appear to contain microfossils, for instance, in sandstone at site GD31, no sample yielded identifiable specimens. All exposed fossils are easily smeared with a fingernail and probably replaced by clay. At site GD26, 1 cm clam shells and a possible fossil imprint resembling reed grass eluded sampling and identification. The age of the unit is discussed below (see *Ages of Deposits and Paleoenvironmental Interpretations*).

Ensk **Skookumchuck Formation (late to middle Eocene)**—Sandstone and siltstone, micaceous, feldspathic, tuffaceous, locally carbonaceous; rare, calcite-cemented concretions; pale gray to bluish gray, weathers light brown to reddish brown; strongly weathered in surface exposures, such that nearly all samples can be readily broken with bare hands; no unweathered or lightly weathered surface exposure observed in map area—the only resistant field-observed rock is a concretion cemented by secondary calcite mineralization (see below). Although Fillmore Drilling Company (1949) also described subsurface samples from the Bannse No. 1 oil exploration well (hereinafter referred to as 'the Bannse well')(HC2; Fig. 8) as friable, siltstone from sample site GD10 (Table DS2) still indicates that the less weathered rocks in the deeper subsurface are moderately lithified and not as easily crushed. Bedding is in most exposures only subtly defined by micaceous partings, silt interbeds, carbonaceous layers, or bedding-parallel iron staining. Cross-cutting Liesegang banding is also common. Sandstone in the unit is very fine to medium grained, angular to rounded, moderately to well-sorted, poorly to well-bedded, with channel crossbeds apparent in some larger exposures, but bedding in most exposures is only faintly suggested by orientation of mica flakes

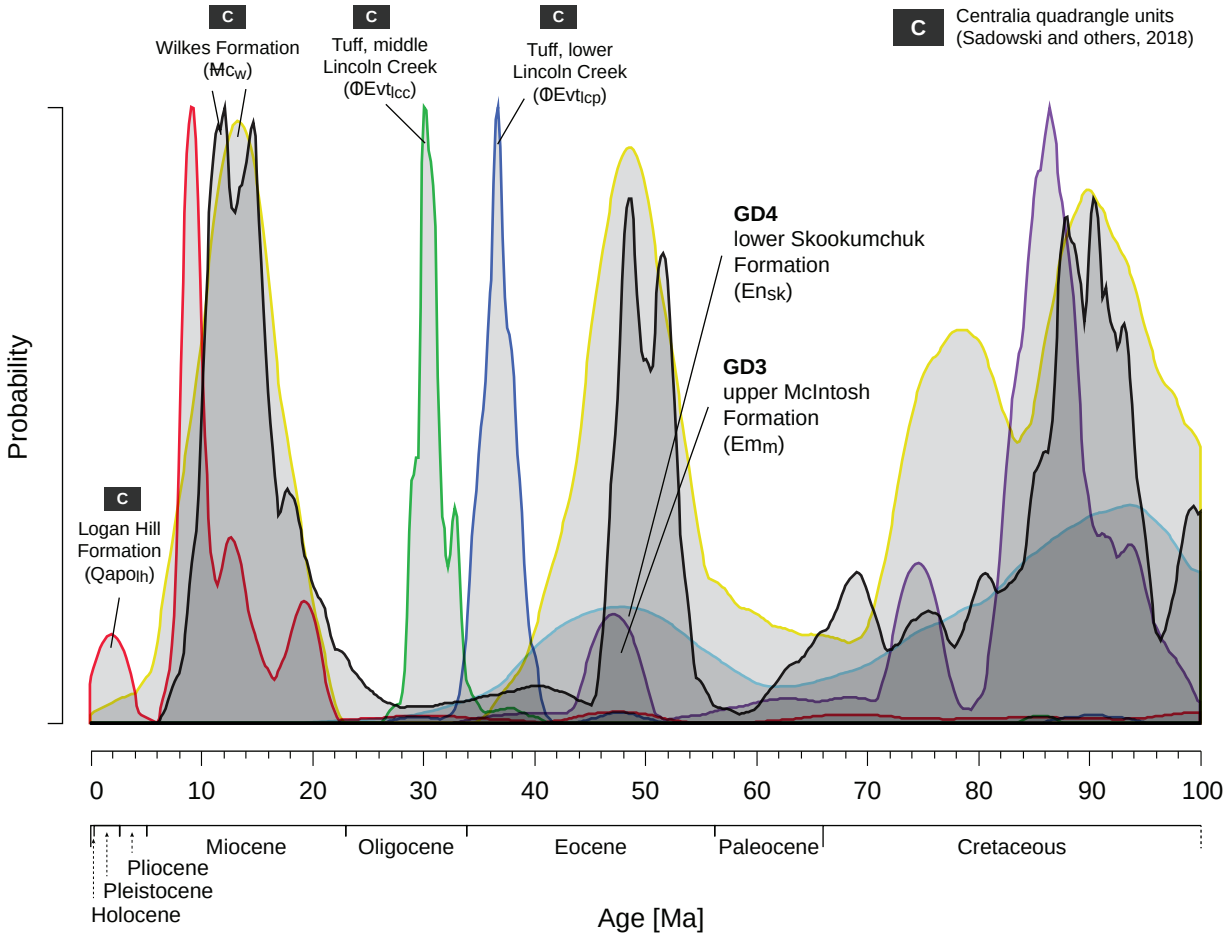

Figure 7. Combined zircon age peaks from U-Pb analysis of five detrital samples (red, black, yellow, pale blue, and lilac curves) and two tuff samples (green and blue lines) from the Violet Prairie and Centralia quadrangles. The tuff samples each have only one peak and provide depositional ages from the lower (blue) and middle (green) Lincoln Creek Formation. The detrital samples each have multiple peaks. For each sample, size of each peak corresponds to the relative abundance of zircons with the age of that peak. Peaks of similar ages in different samples may point to shared sediment sources.

or subtly preferential partings. Many exposures are marked by hackly jointing and (or) onionskin weathering, although these traits may be more widespread in Lincoln Creek Formation. The rock mass consists of 65 to 90% clastic material, including quartz, feldspar, biotite, muscovite, and lithic fragments (aphanitic basalt, quartzite, schist, feldspathic sandstone). Moderately weathered, subangular to rounded, monocrystalline and polycrystalline quartz grains comprise 40 to 70% of the rock. Plagioclase (andesine) grains, some of which are zoned, make up 30 to 60% of the overall rock composition. Some samples contain <5% potassium feldspar (sanidine and microcline). Moderate to highly weathered, subrounded to rounded lithic fragments constitute <10% of the rock. A matrix of clay minerals, carbonaceous material, chloritic material, and volcanic glass makes up 10 to 35% of the rock mass. Biotite and muscovite grains make up at least 5% of the rock, with more biotite than muscovite. Minor minerals in the sandstone are hornblende, augite, chlorite, glass, magnetite, pyrite, zircon, chalcedony, garnet, and apatite. Fossil fragments of plants and shells are common where exposure is good and weathering has not destroyed them. Hard, calcite-cemented feldspathic sandstone (paleomagnetic sample M2), observed in a 6x6 ft patch amid otherwise heavily weathered rock in the valley-side slope of an unnamed northwestern tributary of Zenkner Valley (Fig. 9), appears to be a rare concretion, which Snavely and others (1959) indicated can be found anywhere in the formation. The implied secondary cementation of this exposure is consistent with paleomagnetic analysis that suggests pervasive remagnetization of several samples of Skookumchuck Formation from the Violet Prairie quadrangle and the Centralia quadrangle adjacent to the south (Bernard Housen, Western Washington Univ., written commun., 2018).

Snavely and others' (1958) interpretation of the Crescent oil well (HC1 along Cross Section A–A′) implies a minimum Skookumchuck Formation unit thickness of 1,300 ft in the map area. The greater thickness at the east end of Cross Section A–A′ is conjecture. Farther south in the map area we estimate 1,100 ft thickness (see *Bannse Well* below).

Although Skookumchuck Formation appears to cover nearly all hills in the southern half of the map area, the vast majority of exposures are strongly weathered

and offer little insight. The depositional environment of the Skookumchuck Formation has been interpreted as a deltaic system ranging from freshwater fluvial, floodplain and wetland to littoral marine settings, which yielded interfingering offshore, near-shore, and coastal facies (Snavely, 1958; Armentrout, 1987; Buckovic 1979; Flores and Johnson, 1995).

Snavely and others (1958) identified 13 named coal beds concentrated in two zones within the unit, although surficial exposures are rare in the map area and historic mines (such as at significant sites S6–S11; Snavely and others, 1958; Washington Geological Survey, 2017) likely obliterated some exposures. Neither the base nor the top of the Skookumchuck Formation was observed during this study, nor was the basaltic sandstone member that was included in the unit by Snavely and others (1951, 1958)(see *Ages of Deposits and Paleoenvironmental Interpretations*). Snavely and others (1958) cited surface mapping west of the Violet Prairie quadrangle as indicative of a gradational contact between the Skookumchuck Formation and underlying marine sediments of the McIntosh Formation but also noted that both formations interfinger with Northcraft Formation. They added that in the eastern part of the Centralia coal district, Skookumchuck Formation at least locally onlaps unconformably onto Northcraft Formation. Based on this study, the partly terrestrial Skookumchuck Formation is generally less lithified and more carbonaceous than the McIntosh Formation in the Violet Prairie quadrangle.

ⓟEvcn **Northcraft Formation (Oligocene–Eocene)**—Volcanic flows of andesite and basaltic andesite with tan to lilac-gray, aphanitic matrix and volcaniclastic sedimentary rocks derived from the former; observed exposures in the map area were few and small (on the order of 1 ft^2 or less) and, except for the moderately weathered G8, heavily weathered and therefore poorly characterized; abundant pebbles, cobbles and boulders of well-rounded dark gray basaltic andesite (and absence of till) upslope to a minimum distance of 0.3 mi north to northeast of site G8 suggest the unit in the shallow subsurface there. Petrographic analysis reveals a mix of 75% clasts and 25% matrix with porphyritic and volcaniclastic textures; monocrystalline and polycrystalline quartz grains average 55 to 60% of the rock mass; lithic fragments include porphyritic and aphanitic basalt, quartzite, and volcanic glass fragments (a few lithic fragments show trachytic and vesicular textures); phenocrysts and granules of augite 5 to 15% (in basalt and calcic andesite?); pyroxene and zoned and fractured plagioclase phenocrysts (andesine to labradorite) for which Snavely and others (1958) suggest post-crystallization movement; groundmass includes cryptocrystalline plagioclase laths, augite and magnetite granules, and glass fragments, where the latter two comprise at least 5%; some groundmass samples are micaceous and palagonitic; secondary minerals observed are chlorite, biotite, chalcedony, quartz, zeolites, hematite, and ilmenite (5–20%). Volcaniclastic rock sampled from geochemistry site G19 from 1,026 ft below the surface in the Bannse well (Fig. 8) is well-lithified and too fine-grained to see particles or texture except under microscope (sample was insufficient for thin section preparation.) Reddish brown claystone from 1,283 to 1,298 ft below the surface in the same well was characterized as "vitreous tuff" in the core log (Fillmore Drilling Company, 1949) but proved calcareous enough to vigorously effervesce on exposure to hydrochloric acid, suggesting that calcareous claystone may be a better characterization than tuff. No other Northcraft Formation sample available for this report reacted to hydrochloric acid. Igneous rock from geochemistry site G20 from 4,191 ft below the surface in the same well is sufficiently coarse-grained to suggest intrusive origin, as previously noted in core descriptive log (Fillmore Drilling Company, 1949). Rocks at site G20 contain 1 to 2 mm plagioclase grains that are fairly fresh but moderately chloritized. Other notable minerals in the rocks from site G20 include clinopyroxene (0.65 mm), orthopyroxene (0.7 mm), mildly iddingsitized olivine (0.5–1.2 mm), hypersthene and about 6% opaque minerals. Petrographic examination of more weathered samples revealed abundant plagioclase laths and vesicles filled with chalcedony or yellow clay. Geochemical analysis, especially of samples from sites G8 and G20 establishes a good geochemical fit with Northcraft Formation samples elsewhere (see *Geochemistry* below). Based on exposures outside the map area, Northcraft Formation flows range from andesitic to basaltic in composition.

Lavas and flow breccias are found mostly in the upper part of the formation, pyroclastic rocks throughout the formation, and basaltic conglomerate and sandstone in the lower part of the unit (Snavely and others, 1958; Armentrout, 1987). Snavely and others (1958) interpreted (all?) sedimentary rocks within the formation as non-marine. Inferences of Northcraft Formation in the map area interfingering with McIntosh and Skookumchuck formations (Cross Section A–A′) are based mainly on prior reports not specific to the Violet Prairie quadrangle (Pease and Hoover, 1957; Armentrout, 1987; Hagen, 1987) and conceptual models (Buckovic, 1979; Rau, 1981; Flores and Johnson, 1995), but intersection of volcanic rocks in shallow water wells W7, 8, 10, and 11 along Cross Section A–A′, and surficial exposures near wells W10 and W11 also suggest interfingering with Skookumchuck Formation. Unit thickness in the Crescent oil exploration well (HC1) has been interpreted as 830 ft (Snavely and others, 1958).

A Northcraft Formation volcanic source east of the map area (Snavely and others, 1958; Hagen, 1987) suggests that the Northcraft lavas thin westward across the map area. Such westward thinning and the assumption of interfingering contacts with the McIntosh and Skookumchuck formations are schematically inferred in Cross Section A–A′. Northcraft Formation has been documented in the map area only north of

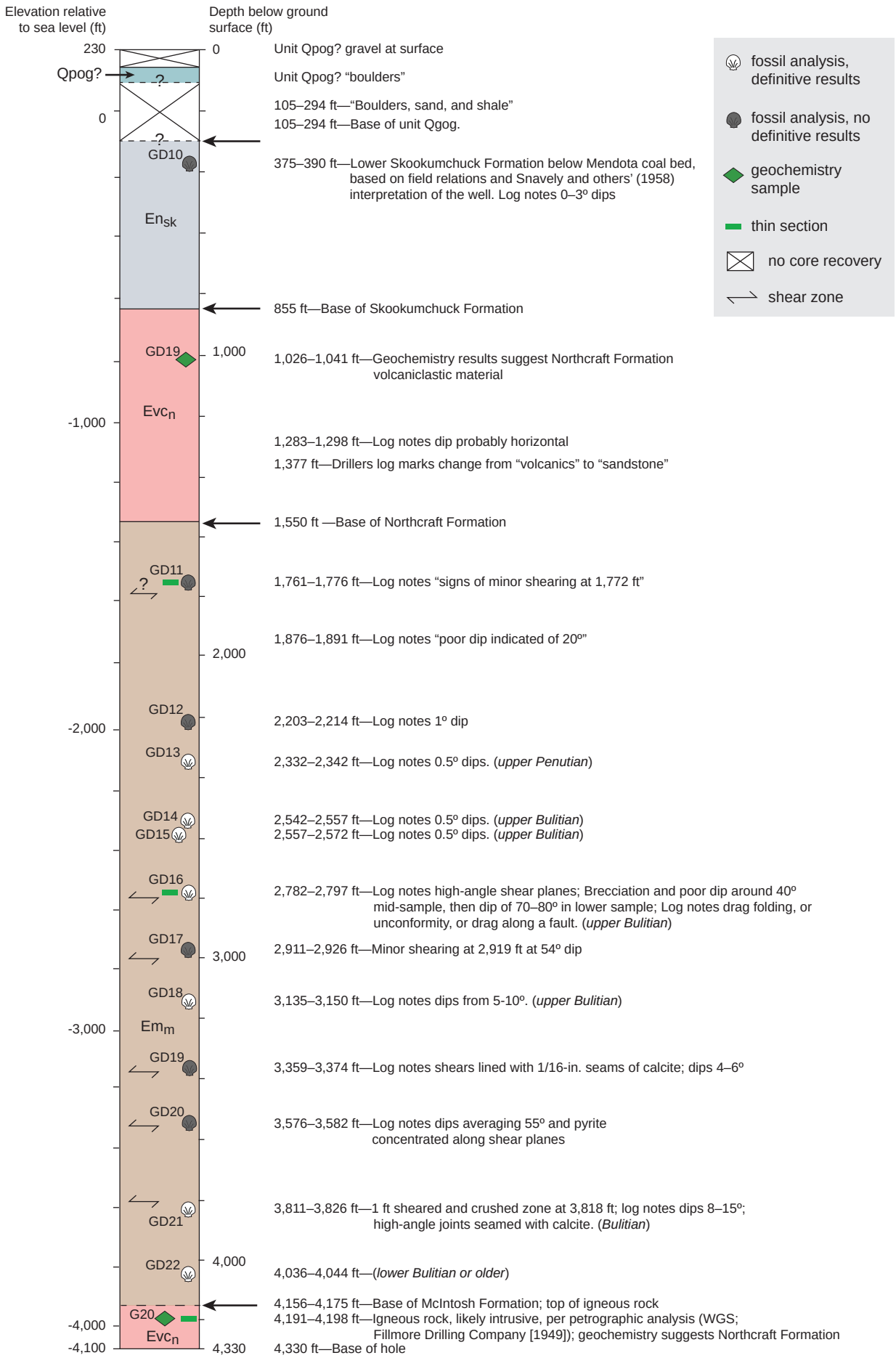
Elevation relative to sea level (ft)
Depth below ground surface (ft)
230
0
Qpog?
?
0
?
GD10
Ensk
GD19
1,000
Evcn
-1,000
GD11
?
2,000
GD12
-2,000
GD13
GD14
GD15
GD16
GD17
3,000
GD18
-3,000
Emm
GD19
GD20
GD21
GD22
4,000
G20
-4,000
Evcn
-4,100
4,330
Unit Qpog? gravel at surface
Unit Qpog? "boulders"
105–294 ft—"Boulders, sand, and shale"
105–294 ft—Base of unit Qgog.
375–390 ft—Lower Skookumchuck Formation below Mendota coal bed, based on field relations and Snavely and others' (1958) interpretation of the well. Log notes 0–3º dips
855 ft—Base of Skookumchuck Formation
1,026–1,041 ft—Geochemistry results suggest Northcraft Formation volcaniclastic material
1,283–1,298 ft—Log notes dip probably horizontal
1,377 ft—Drillers log marks change from "volcanics" to "sandstone"
1,550 ft —Base of Northcraft Formation
1,761–1,776 ft—Log notes "signs of minor shearing at 1,772 ft"
1,876–1,891 ft—Log notes "poor dip indicated of 20º"
2,203–2,214 ft—Log notes 1º dip
2,332–2,342 ft—Log notes 0.5º dips. (upper Penutian)
2,542–2,557 ft—Log notes 0.5º dips. (upper Bulitian)
2,557–2,572 ft—Log notes 0.5º dips. (upper Bulitian)
2,782–2,797 ft—Log notes high-angle shear planes; Brecciation and poor dip around 40º mid-sample, then dip of 70–80º in lower sample; Log notes drag folding, or unconformity, or drag along a fault. (upper Bulitian)
2,911–2,926 ft—Minor shearing at 2,919 ft at 54º dip
3,135–3,150 ft—Log notes dips from 5-10º. (upper Bulitian)
3,359–3,374 ft—Log notes shears lined with 1/16-in. seams of calcite; dips 4–6º
3,576–3,582 ft—Log notes dips averaging 55º and pyrite concentrated along shear planes
3,811–3,826 ft—1 ft sheared and crushed zone at 3,818 ft; log notes dips 8–15º; high-angle joints seamed with calcite. (Bulitian)
4,036–4,044 ft—(lower Bulitian or older)
4,156–4,175 ft—Base of McIntosh Formation; top of igneous rock
4,191–4,198 ft—Igneous rock, likely intrusive, per petrographic analysis (WGS; Fillmore Drilling Company [1949]); geochemistry suggests Northcraft Formation
4,330 ft—Base of hole
fossil analysis, definitive results
fossil analysis, no definitive results
geochemistry sample
thin section
no core recovery
shear zone

Scatter Creek, close to the stratigraphic transition from McIntosh Formation to Skookumchuck Formation, and in deep wells (HC1 and HC2). Unit age is discussed below (see *Ages of Deposits and Paleoenvironmental Interpretations*).

Emm **McIntosh Formation (middle Eocene)**—Volcanic lithic, marine sandstone, siltstone, and claystone; gray to slightly pale brownish gray; lightly to heavily weathered; moderately lithified; fine to medium grained; angular to rounded; moderately to well sorted; with very faint meso-scale to large-scale cross bedding. This bedding is suggested for the map area by exposure of a 100 ft-thick section of upper McIntosh Formation with such bedding in the Hercules No. 1 sandstone quarry in Tenino, 0.5 mi east of the map area (Fig. M1, geochemistry sample site G33). Petrographic study of McIntosh Formation samples from the map area revealed 70–85% clastic grains and 15–30% matrix consisting of clay minerals, chlorite, glass, and chalcedony. Some samples contain a micaceous matrix of mostly biotite and chlorite with traces of muscovite. Major minerals are: monocrystalline and polycrystalline quartz (30–60%) with inclusions and overgrowths of muscovite and biotite; feldspar (30–50%), where zoned and perthitic textured plagioclase (andesine) comprises 25–70% of all feldspar, and potassium feldspar (microcline and sanidine) 5% of all feldspar; biotite and muscovite (15% or less). Rounded lithic fragments (<10–25%) include metamorphic rock (quartzite), aphanitic and porphyritic basalt (trachytic texture), and feldspathic sedimentary rock. Glass fragments are common and some are altered to chalcedony. Other minerals identified are magnetite, ilmenite, augite, hornblende, glauconite, and zircon. Although not observed among the few, small, and mostly weathered exposures in the map area, the formation contains tuff interbeds within a few miles of the map area (Snavely and others, 1958; Polenz and others, 2017). Walsh and Logan (2005) reported interbeds of volcanic breccia, and Snavely and others (1958) reported "volcanic rocks interbedded with" McIntosh Formation. The McIntosh Formation observed in the map area corresponds to Snavely and others' (1958, 1959) siltstone, shale, and feldspathic sandstone; their (basal and upper) basaltic-lithic sandstone was not observed.

The McIntosh Formation is at least 2,500 ft thick beneath the map area at the Bannse well (Fig. 8). McIntosh Formation exposures were observed in the map area in only a few outcrops north of Scatter Creek, and most of these are heavily weathered. Similarly spotty exposures have been reported in adjacent quadrangles northwest, north, and northeast of the map area (Snavely and others, 1958, 1959; Walsh and Logan, 2005; Logan and others, 2009; Polenz and others, 2017).

Microfossil content analysis of three samples from upper McIntosh Formation exposed in and near Tenino 0.2 to 0.5 mi east of the map area yielded no biostratigraphic constraint (age sites GD35, GD36, and GD37, Fig. M1; Table DS2). A fossil leaf fragment from age site GD34, 5.3 mi east of the northeastern map corner (collocated with site GD12 of Polenz and others, 2017) remains unidentified but suggests a shallow marine or terrestrial depositional setting there.

AGES OF DEPOSITS AND PALEOENVIRONMENTAL INTERPRETATIONS

Cenozoic Volcanic and Sedimentary Bedrock

Regional models have suggested that a thick package of dense, strongly magnetic rock underlies the map area, perhaps some combination of Crescent Formation and (or) underlying, slightly denser mantle rocks (Finn, 1990; Trehu and others, 1994; Gao and others, 2011; Schmandt and Humphreys, 2011). To help define structures and constrain the depth of this dense rock beneath the map area, we collected ground-based transects of magnetic and gravity field strength data along Cross Section A–A′ (Figs. M2 and M3). Our modeling of these and regional aeromagnetic and gravity data is consistent with the presence of such a thick package of strongly magnetic rock beneath the cross section. However, we were unable to constrain the depth of this package, at least in part because gravity and magnetic measurements were also affected by shallower igneous rocks of the Northcraft Formation. Surficial bedrock units upsection of the strongly magnetic igneous basement rocks include, from oldest to youngest: (1) the Eocene McIntosh Formation marine sedimentary rocks; (2) the Eocene volcanic and volcaniclastic Northcraft Formation which interfingers with McIntosh Formation (Buckovic, 1979; Rau, 1981; Armentrout, 1987; Flores and Johnson, 1995) and may also bracket it in the map area; (3) the Eocene Skookumchuck Formation, which also interfingers with Northcraft Formation (Buckovic, 1979; Rau, 1981; Armentrout, 1987; Flores and Johnson, 1995) and consists of tuffaceous, coal-bearing, deltaic terrestrial to shallow marine sedimentary rocks; (4) the Oligocene–Eocene Lincoln Creek Formation, which consists of tuff-rich marine sedimentary rocks; and (5) the Miocene, terrestrial Wilkes Formation.

Figure 8. *(facing page)* Well section for the Bannse No. 1 oil exploration well (Union Oil Co. of California (1948–1949); Fillmore Drilling Company [1949]). Depth intervals on right identify core samples analyzed in preparation of this report, for geochemistry (sites G19–20), fossil assemblages (sites GD10–GD22), and thin section petrography. Elizabeth Nesbitt and Ruth Martin (Burke Museum) identified fossil species and suggested that all foraminiferal stages (italicized) correspond to the middle(?) Eocene. Paleogene sections with chronometric age control have been developed in California (Mallory, 1959; McDougall, 2008). Ages and stages for comparable fossil assemblages in Washington and Oregon hinge on correlation to the California sections. This correlation remains questionable; assignments of ages and stages for these fossil assemblages in Washington and Oregon await substantiated correlation or local chronometric age control. See Table DS2 for details on new fossil species identification. Shears document subsurface offset that is not explained by mapped faults.

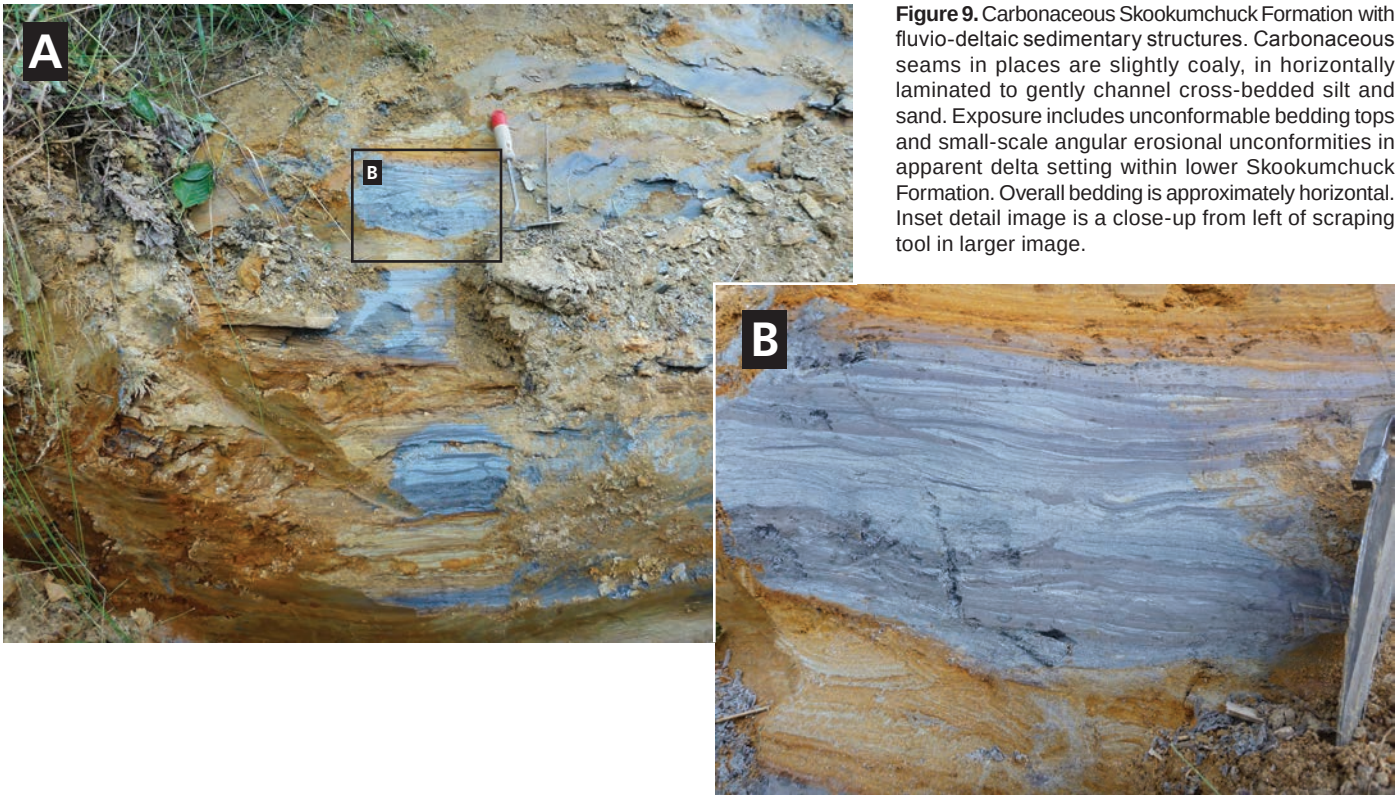

Figure 9. Carbonaceous Skookumchuck Formation with fluvio-deltaic sedimentary structures. Carbonaceous seams in places are slightly coaly, in horizontally laminated to gently channel cross-bedded silt and sand. Exposure includes unconformable bedding tops and small-scale angular erosional unconformities in apparent delta setting within lower Skookumchuck Formation. Overall bedding is approximately horizontal. Inset detail image is a close-up from left of scraping tool in larger image.

DETRITAL ZIRCON GEOCHRONOLOGY

Seven samples from the sedimentary bedrock units in the map area and the adjacent Centralia quadrangle were processed for U-Pb analysis of zircon grains. U-Pb dating of detrital zircons can provide information about sediment provenance and depositional age (Fedo and others, 2003). Five new detrital zircon samples from this study and the adjacent Centralia quadrangle exhibit a range of ages among the sediments from the units in the combined map areas (Fig. 7). The youngest peak from each analysis provides a maximum age for the deposit; the older ages provide information about the mix of sedimentary provenances. The ages can be grouped into late Mesozoic to early Cenozoic and Proterozoic, with minor Paleozoic and Archean. Two additional zircon age analyses targeted tuffs within the lower and middle Lincoln Creek Formation; these each yielded a single age peak representing a depositional age.

A new analysis of 100 detrital zircons from rocks that we interpreted as Tenino sandstone within the upper McIntosh Formation near Tenino yielded one zircon with a 41 ±2 Ma age (age site GD3). A more robust constraining age is provided by the youngest peak around 47 Ma and a ≤47.23 ±0.8 Ma concordia age for several of the youngest grains (Fig. B1A), but the 41 ±2 Ma age probably more accurately constrains the age of the deposit because the ~47 Ma age is as old as Polenz and others' (2017) ~47 Ma "basal" McIntosh Formation depositional age. Detrital zircons from the lower Skookumchuck Formation at age site GD4 yielded a young peak and corresponding Concordia age of ≤41.4 ±1.4 Ma; the youngest single zircon at 38 ±2 Ma again suggests that this sample is a few million years younger than 41.4 Ma.

The samples from the upper McIntosh and overlying lower Skookumchuck formations have similar Cenozoic to late Cretaceous age spectrums. Major age peaks from Cretaceous to Jurassic seem to be shifted by 5 to 10 million years in the Skookumchuck Formation. The Proterozoic age distribution is vastly different, with a single Proterozoic grain from the McIntosh Formation (1.36 Ga, ~1% of total), whereas the overlying Skookumchuck Formation contains 32 Proterozoic grains (1.08–2.68 Ga, 33% of total). This contrast suggests that a different sediment source was tapped during deposition of the Skookumchuck Formation. Prominent age peaks within the older population of grains in the Skookumchuck Formation are 1.36 Ga and ~1.76 Ga, with scattered ages in between. Minor peaks include 1.08, 1.18, 2.0 Ga, and three Archean grains. These age peaks are consistent with derivation from the Belt/Purcell supergroup and (or) the overlying Windermere supergroup (Evans and others 2000; Anderson and Davis, 1995; Lewis and others, 2010; Ross and others 1992), located east and northeast of the map area. Alternatively, these populations could be derived from reworked accreted terranes and their associated basins (Lamaskin, 2012). Sources for the younger zircons are likely from Jurassic, Cretaceous, and Eocene volcanic and (or) intrusive activity, including Idaho Batholith and Challis-aged volcanic events (Gaschnig and others, 2010; LaMaskin, 2012).

Three other detrital samples from the Centralia quadrangle (age sites GD6–GD8 of Sadowski and others, 2018) are from units mapped as the Wilkes Formation and overlying Logan Hill Formation (Fig. 7). A prominent Quaternary age peak at 2 Ma in the Logan Hill Formation (which we only identified outside the Violet Prairie quadrangle) and other Neogene peaks at 10 and 14 Ma in the Wilkes Formation constrain the maximum ages of deposition for these younger units. Age spectra from early

Cenozoic to Mesozoic and Proterozoic/Archean groupings are mostly similar to each other and the Skookumchuck Formation sample, though older peaks are faint in the Logan Hill Formation sample. This pattern suggests that the Logan Hill sediments are mostly derived from a combination of Miocene sources similar to those in the Wilkes Formation, and slightly younger sources. Minor differences among the older spectra in the two Wilkes Formation samples may be attributed to the greater number of zircons analyzed in the sample represented by the black line in Figure 7 (n=300), which is more likely to pick up less prominent populations. The mostly similar Eocene and older age spectra suggest that inferred provenances for the samples from the Logan Hill and Wilkes formations are also similar to those from the Skookumchuck Formation.

UNION OIL COMPANY BANNSE NO. 1 OIL EXPLORATION WELL

Union Oil Company of California drilled the Bannse well in 1948 to 1949 in the southern center of the map area (HC2; Fig. 8). The well reached a depth of 4,330 ft. According to Snavely and others (1958), the well penetrated the Skookumchuck, Northcraft and McIntosh formations.

Based on a new geochemical analysis (site G20 at 4,191 to 4,198 ft depth; see *Geochemistry*), 155 to 174 ft of basaltic andesite at the base of the well is shown in Fig. 8 as Northcraft Formation. Petrographic examination of the sample from site G20 suggests that this lower interval of Northcraft Formation is probably intrusive (this study; Fillmore Drilling Company, 1949).

Driller's and core logs (Fillmore Drilling Company, 1949) and Snavely and others' (1958) interpretations suggest 2,606 to 2,625 ft of McIntosh Formation sedimentary rock upsection of the basal Northcraft Formation. Bedding generally dips gently, and we infer that the 2,600 ft likely provides a good proxy for minimum stratigraphic unit thickness in this part of the map, despite multiple shears (Fig. 8). The section provides a minimum thickness estimate because additional McIntosh Formation could be present below the intrusive(?) Northcraft Formation rocks at the bottom of the well.

New biostratigraphic assessments of several McIntosh Formation samples from the Bannse well (sites GD12–GD22) suggest a middle Eocene age, but identifications of lower Bulitian (or older) to upper Penutian foraminiferal stages can at present be only questionably correlated to chronometrically dated sections in California (Table DS2). New detrital U-Pb analyses from upper McIntosh and lower Skookumchuck formations (age sites GD3 and GD4) suggest that all McIntosh Formation samples from the Bannse Well are at least ~41 Ma old.

Figure 8 shows 695 ft of section above the McIntosh Formation as Northcraft Formation, based mainly on Snavely and others' (1958) interpretation. The driller's and core logs (Fillmore Drilling Company, 1949) suggest a mix of tuff, breccia, and sedimentary rocks. Geochemical analysis of a sample from site G19 at 1,026 to 1,041 ft depth provides some support for association with Northcraft Formation (see *Geochemistry*), although the remaining core did not offer enough sample to petrographically verify the core log's characterization of the sample as "tuff" or "ash" (as opposed to volcaniclastic). More than 15% loss on ignition (LOI, Table DS4) in the sample from site G19 suggests relatively strong alteration.

Snavely and others' (1958) interpretation shows about 675 ft of Skookumchuck Formation in the Bannse well, from about 180 to 855 ft below the surface. We infer 1,100 ft unit thickness in the vicinity of the well based on the -625 ft elevation of the base of the Skookumchuck Formation in the well and a 470 ft hilltop surface elevation 0.4 mi northwest of the well. That inference assumes essentially flat-lying beds, which are suggested by bedding measurements within and near the well (see *Structures in the Map Area*; Fig. 8). A Skookumchuck Formation sample from site GD10 in the well failed to yield biostratigraphic constraints.

PALEOENVIRONMENT

The stratigraphy of the Paleogene and Neogene units exposed in the map area reflects a changing near-shore sedimentary paleoenvironment flanked on the east by a volcanic center. Marine deposition of McIntosh Formation was followed by deltaic terrestrial to shallow marine deposition of Skookumchuck Formation. This Eocene transition may be partly a (late stage) response to regional shortening associated with accretion around 51 to 48 Ma (Wells and others, 2014; Eddy and others, 2016; 2017) of the Siletzia terrane to western North America. Pease and Hoover (1957) asserted that, somewhere west of the Violet Prairie quadrangle, Crescent Formation interfingers with lower McIntosh Formation. If accretion and shortening shrank the marine basin in which the McIntosh Formation had been deposited between the North American continent and the Siletzia oceanic plateau, this may help explain the transition from the McIntosh Formation's marine basin into the Skookumchuck Formation's deltaic terrestrial to shallow marine setting. A change in the sediment supply may also have contributed to the development of an Eocene delta (Buckovic, 1979; Flores and Johnson, 1995) in which the Skookumchuck Formation was deposited. Emergence of the Northcraft volcanics (Snavely and others, 1951, 1958; Gard, 1968; Buckovic, 1974, 1979; Hagen, 1987) during deposition of the McIntosh Formation, and later addition of different Proterozoic sedimentary constituents during deposition of the Skookumchuck Formation (see *Detrital Zircon Geochronology*), may both point to increased sedimentation rates. This increase can be attributed to emergence of nearby mountains suggested by Northcraft volcanism and to drainage capture suggested by later addition of distal sediment sources not apparent in older sediment. In any case, marine conditions re-emerged throughout deposition of the Oligocene–Eocene Lincoln Creek Formation.

MCINTOSH FORMATION

Estimates of the thickness of the McIntosh Formation come primarily from well logs. Snavely and others (1959) defined the McIntosh Formation as more than 4,000 ft of middle Eocene, dark gray, tuffaceous marine siltstone and claystone with interbedded feldspathic and basaltic sandstone, based on the Mottman Campbell No. 1 oil exploration well just northeast of the Violet Prairie quadrangle (HC5; Fig. M1).

The base of the McIntosh Formation is poorly defined. At the southern margin of the Black Hills, four miles west of the Violet Prairie quadrangle, Snavely and others (1958) mapped basaltic rocks in contact with McIntosh sedimentary rocks as

part of the McIntosh Formation. Others instead mapped basalt in the Black Hills as Crescent Formation (Pease and Hoover, 1957; Globerman 1981; Walsh and others, 1987; Logan, 1987; Polenz and others, 2017), and Polenz and others (2017) produced an approximately 47 Ma U-Pb depositional age on tuff from McIntosh Formation sedimentary rocks that locally overlie basalt in the southern Black Hills. Polenz and others interpreted this age as the base of the McIntosh Formation as formally defined by Snavely and others (1959)—which excludes informal additions of a lower unit member.

Biostratigraphy provides tentative constraints on the age of the McIntosh Formation in the map area. Foraminiferal stage assessments for newly identified fossils from McIntosh Formation in the Bannse well range from Penutian to lower Bulitian stages, with a consistent trend of stages getting older with depth (Fig. 8; Table DS2). Regional correlation tables (Rau, 1958; Armentrout and others, 1983; Wells and others, 2014) could be interpreted to suggest a middle (to early?) Eocene age for these new fossil identifications, but stage assignments in the Pacific Northwest remain difficult to interpret, and fossils identified by Snavely and others (1958) in earlier samples from the same well should be reassessed. New and recent U-Pb age analyses from the McIntosh Formation therefore presently provide better guidance, although they are not collocated with biostratigraphically insightful fossil samples (Polenz and others, 2017).

Two new U-Pb ages on detrital zircons constrain the time of transition from deposition of marine McIntosh Formation to mostly terrestrial Skookumchuck Formation. Tenino sandstone at the upper end of the McIntosh Formation 1,150 ft east of the Violet Prairie quadrangle (age site GD3) suggests an age of <41 ±2 Ma. U-Pb data at age site GD4 (Fig. M1) suggest an age of <38 ±2 Ma for rocks that, based on nearby boring records (B1, B2, B6), are interpreted as lower Skookumchuck Formation.

Together, these ages suggest that deposition of the McIntosh Formation in the map area ended close to ~41 Ma or later. The age of the lower end of the formation either is close to Polenz and others' (2017) ~47 Ma age, or older and at least partly coeval to some fraction of the Crescent Formation, if addition of a lower McIntosh Formation is accepted.

NORTHCRAFT FORMATION

Snavely and others (1951, 1958) proposed the Northcraft Formation as a sequence of calcic andesitic and basaltic lava flows and flow breccias in the upper section and volcaniclastic conglomerate, sandstone and pyroclastic rocks in the lower part. Hagen (1987) identified breccia pipes as evidence for a Northcraft volcanic center southeast of the Violet Prairie quadrangle.

Buckovic (1979) described three terrestrial andesitic lithofacies of the Northcraft Formation, each of which grades laterally away from vent areas into adjacent facies that fine, thin, and eventually intertongue with deltaic feldspathic sediments (represented in the map area by the McIntosh and Skookumchuck formations). The observed exposures of Northcraft Formation in the Violet Prairie quadrangle are too few, small, and weathered to categorize the formation within this quadrangle, but the model of an Eocene deltaic depositional system near the then-active Northcraft volcanic system (Buckovic, 1979; Flores and Johnson, 1995) provides a fitting framework for the character and three-dimensional distribution of all the Eocene bedrock units in the map area.

The age of the Northcraft Formation appears to range approximately from <47 to 33 Ma. Snavely and others (1958) used paleontologic studies of the overlying Skookumchuck Formation and underlying McIntosh Formation to assign the Northcraft Formation a late Eocene age. U-Pb analyses on zircon grains from these correlative sedimentary rock units near the map area range from approximately 47 to <41 Ma for McIntosh Formation, as discussed above (see *McIntosh Formation*) to approximately <41 to 37 Ma for the Skookumchuck Formation, as discussed below (see *Skookumchuck Formation*). Philips and others (1986) presented K-Ar ages that Hagen (1987) used to infer an age range of 32.7 ±1.5 to 38.8 ±1.9 Ma for five samples Hagen identified as Northcraft Formation east of the Violet Prairie quadrangle.

The approximately 33–39 Ma Northcraft Formation age range suggested by the K-Ar ages of Phillips and others (1986) overlaps the about <41 to >37 Ma age range of Skookumchuck Formation and thereby adds support to the conceptual expectation that the Northcraft and Skookumchuck formations interfinger as suggested in Cross Section A–A′, Buckovic (1979), and Flores and Johnson (1995). The spatial distribution of observed outcrops and identifications of both formations in wells within and near the Violet Prairie quadrangle are consistent with but do not require such interfingering. The affected contacts in Cross Section A–A′ are therefore queried.

SKOOKUMCHUCK FORMATION

The Skookumchuck Formation in the map area consists of nearshore to terrestrial feldspathic sandstone, siltstone and coal beds, with subtle bedding. The stratigraphic position of coal beds in and near the Violet Prairie quadrangle and generally gentle bedding dips indicate that the Skookumchuck Formation in the map area is generally the lower member from downsection of the Mendota coal bed. Two exceptions are southwest of the Kopiah fault and in the center of a southeast-plunging syncline that crosses the southern half of the eastern map edge (Fig. 10). Despite this, the basal, basaltic-lithic sandstone and conglomerate member of Snavely and others (1958) was not observed in the map area.

Macrofossils from four localities of Skookumchuck Formation in the Violet Prairie quadrangle (GD7, 24, 29, and 38, Table DS2) are consistent with deposition in marine shelf to tidal conditions and Snavely and others' (1951, 1958) prior assertions of correlation to the Cowlitz Formation of Weaver (1937). Although microfossils were present in multiple samples, preservation was mostly too poor to permit species identification. Abundant, sand-sized glauconite pellets in rocks at age site GD33 appear to be coprolites similar to invertebrate fecal pellets presented by Carter (2017) but yielded no biostratigraphic constraint.

New U-Pb analyses constrain the age of the Skookumchuck Formation. The transition from McIntosh Formation to Skookumchuck Formation in the map area likely occurred approximately <41 Ma (see *McIntosh Formation* above). The upper end of the Skookumchuck Formation may be as young as ~37 Ma, based on Sadowski and others' (2018) 36.7 ±0.32 Ma depositional age on tuff from the apparent base of the overlying Lincoln Creek Formation just south of the Violet Prairie quadrangle. Therefore U-Pb ages suggest an age range of approximately

<41 to >37 Ma for the Skookumchuck Formation in the map area. Notably, most of the Skookumchuck Formation in the Violet Prairie quadrangle is from below the Mendota coal bed (Fig. 10; Snavely and others, 1958), suggesting that it was deposited closer to the <~41 Ma age of the base of the formation than the ~37 Ma basal Lincoln Creek Formation age. Exposures in the southeast and southwest of the map area extend farther upsection (Fig. 10; Snavely and others, 1958). However, Triplehorn and others (1980) asserted that six K-Ar ages from the Big Dirty and Smith coal beds indicate a ~40 Ma age for these coal beds. This suggests that only the southwestern corner of the Violet Prairie quadrangle contains Skookumchuck Formation younger than ~40 Ma.

LINCOLN CREEK FORMATION

The Lincoln Creek Formation (Beikman and others, 1967) is a massive tuffaceous, fossiliferous and concretionary marine siltstone ranging up to 9,000 ft in thickness (Snavely and others, 1958; Beikman and others, 1967; Armentrout, 1987; Prothero and Armentrout, 1985; Sadowski and others, 2018). Sandstone and conglomerate of the Lincoln Creek Formation east of the map area have been interpreted as strandline and continental deposits (Snavely and others, 1958) correlative to the Toutle Formation (Roberts, 1958). Snavely and others (1958) described Lincoln Creek Formation farther west in the eastern Centralia–Chehalis area as deltaic, near-shore, and continental deposits of basaltic sandstone, which was not observed in the Violet Prairie quadrangle. West of the Chehalis River, the formation thickens into a shallow water offshore marine environment and conformably overlies marine rocks of Cowlitz Formation (Armentrout, 1987). Closer to the map area (but still west of it), the formation thins and unconformably onlaps older Eocene rocks that now form the Doty Hills, Black Hills (Fig. M1) and Minot Peak (Pease and Hoover, 1957).

Lincoln Creek Formation in the Violet Prairie quadrangle corresponds to the undivided Lincoln Creek Formation member in the adjacent Centralia quadrangle farther south (Sadowski and others, 2018). Sadowski and others (2018) obtained a U-Pb age (Fig. 7) from a basal lapilli tuff 1.1 mi southeast of where the contact between the Lincoln Creek and Skookumchuck formations crosses the southern boundary of the Violet Prairie quadrangle. Stratigraphic continuity into the Violet Prairie quadrangle suggests a similar section and unit age for the Lincoln Creek Formation in the Violet Prairie quadrangle.

Outcrops of Lincoln Creek Formation near the southern map edge include some conglomerate in addition to sandstone and siltstone. This rock content suggests that the Lincoln Creek Formation in the map area may be part of an eastern sandstone and conglomerate facies (Snavely and others, 1958) in the lower to middle Lincoln Creek Formation. A 36.7 ±0.32 Ma depositional age on tuff at the base of the formation just south of the map area (Sadowski and others, 2018) approximates the age of the base of the formation shown by Wells and others (2014) and may also approximate the base of the formation in the Violet Prairie quadrangle. However, the tuff was not observed within the quadrangle, and *Nuculana washingtonensis* fossils from age site GD39 along the southern map edge were collected within 300 ft (map distance) of the inferred contact with the underlying Skookumchuck Formation. We interpret *Nuculana washingtonensis* as a shallow water indicator that suggests a stratigraphic position at or slightly above the Eocene-Oligocene boundary (33.9 Ma, U.S. Geological Survey Geologic Names Committee, 2010). This may suggest that the base of the Lincoln Creek Formation in the map area is somewhat higher in section than the base of the Lincoln Creek formation farther south in the adjacent Centralia quadrangle, and global magnetostratigraphic correlation of a Lincoln Creek section a few miles northwest of the map area suggested to Prothero and Armentrout (1985) that the base of the formation may also be older outside the map area. Molluscan and foraminiferal collections from outside the map area indicate late Eocene to early Miocene age (Beikman and Gower, 1958). Recent work also suggests the unit age may range to early Miocene (Nesbitt, 2018).

WILKES FORMATION

Roberts (1958) described the late Miocene Wilkes Formation as a sequence of terrestrial fluvial, lacustrine, and brackish-water deposits. The lithology of the formation suggests that these rocks were deposited in a shallow-water environment. Roberts proposed a unit thickness of more than 760 ft. Some lacustrine deposits contain well-preserved leaves, and delicate lamination in some beds suggests deposition in quiet water. Similar rocks at the same stratigraphic position are shown as “Miocene and Pliocene(?), Nonmarine sedimentary rocks” on Snavely and others’ (1958) map. Reassignment to the Wilkes Formation in the Centralia quadrangle south of the map area resulted primarily from two new U-Pb ages there (Fig. 7; Sadowski and others, 2018). The Wilkes Formation was tentatively extended into the Violet Prairie quadrangle based on geomorphic field relations.

Quaternary Units

PLEISTOCENE GLACIAL DEPOSITS

Pre-Vashon Glacial Deposits

Glacial and periglacial deposits cover most of the surface across roughly the northern half of the Violet Prairie quadrangle, and repeated northern-sourced ice incursions (Noble and Wallace, 1966; Lea, 1984) have left a strong geomorphic signature there (Figs. 3A and B). Clast counts from these deposits (Fig. 1) reveal less basalt, more quartz and chert, and somewhat more intermediate igneous rocks than Polenz and others (2017) documented, on average, in drift deposits in the Littlerock quadrangle just northwest of the Violet Prairie quadrangle. In the Littlerock quadrangle, most drift is clearly associated with the Olympia lobe of ice in the western Puget Lowland, and basalt from the Black Hills likely increased the basalt content of many samples. Clast counts from the Violet Prairie quadrangle more uniformly suggest a sizable contribution of Cascade Mountains-sourced sediment, presumably transported into the map area mainly by discharge from the Cascade Mountains, which would have periglacially drained along the ice front. Meltwater from the “Yelm lobe” of the eastern Puget Lowland (Noble and Wallace, 1966; Walsh and Logan, 2005; Logan and others, 2009) would also have carried ample sediment derived, directly or indirectly, from the Cascade Mountains.

Clasts and matrix in many exposures of till slightly south, east, and southwest of the Vashon ice limit are so distinctly and

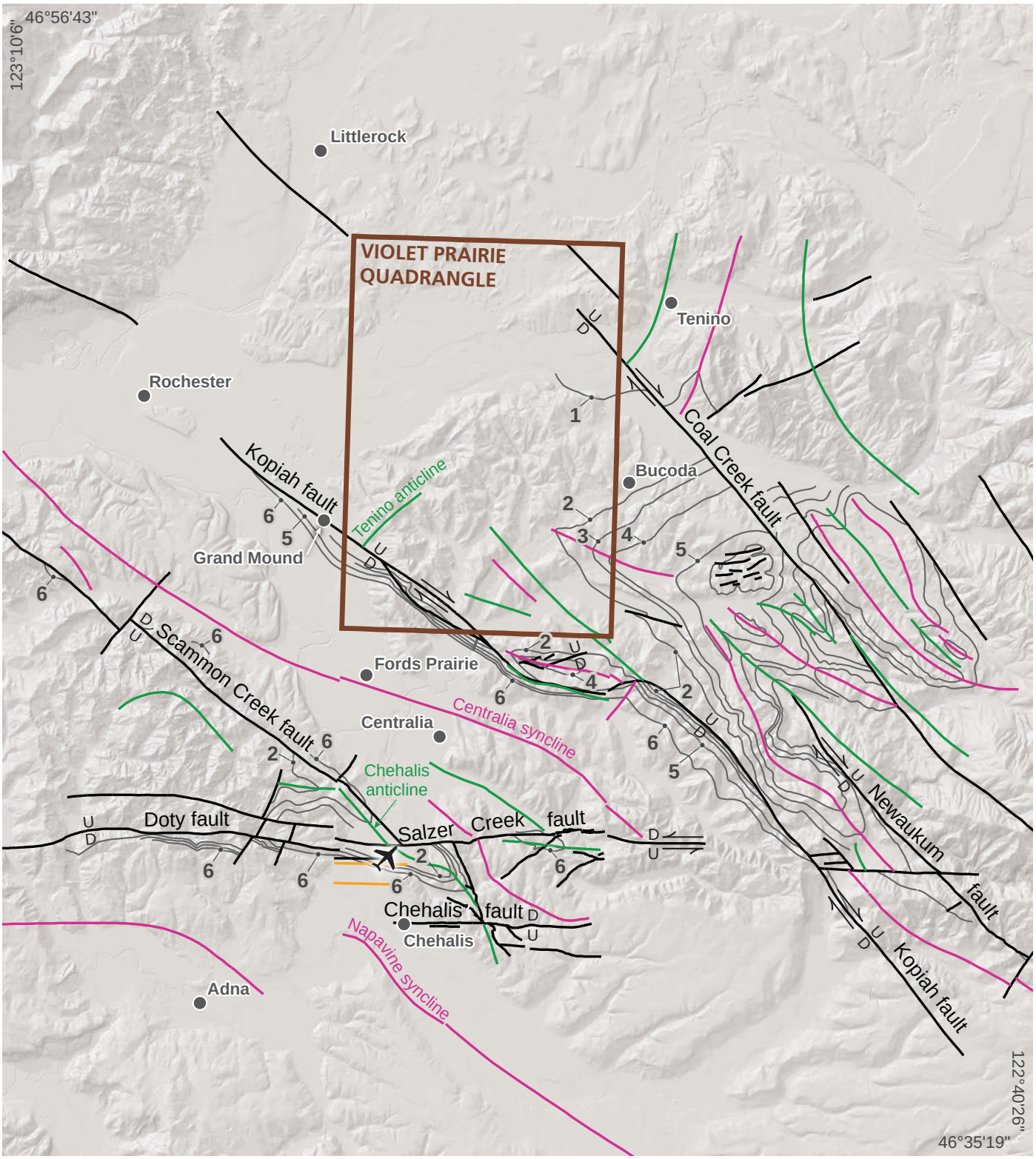

fault
U
D
horizontal motion
vertical motion

syncline

anticline

monocline

uppermost
coal bed
lowermost

6–Tono No.1
5–Upper Thompson
4–Big Dirty
3–Smith
2–Mendota
1–Black Bear

0 miles 5

Chehalis-Centralia Airport

pervasively more weathered than Vashon drift that there is no doubt they are of pre-Vashon age. We used clast counts to help separate moderately weathered Vashon and pre-Vashon deposits. Not surprisingly, the counts show that deposits interpreted as pre-Vashon in age are on average more weathered than deposits mapped as Vashon age (Fig. 2). But weathering in some counts varies widely between individual clasts, the dataset makes no distinction between till and outwash, and in highly weathered exposures it is unclear if the deposits were initially compact or loose. Moreover, weathering in whisker plots of 13 Vashon and 11 pre-Vashon deposits reveals more overlap than distinction, and notably, two clast counts of post-glacial alluvium (unit Qa) were on average more weathered than the Vashon age deposits (Fig. 2).

The overlap in the strength of weathering of post-glacial, Vashon-aged, and older deposits is attributed to microclimate and other factors in addition to age, and the strength of weathering at individual outcrops, even on a relative scale, is only a crude suggestion of relative age. For this reason, map unit age assignments at some sites were influenced by field relations as much as weathering, and drift age at some sites is interpreted as inconclusive. For instance, all instances of unit Qpog? are queried, and southwest of Rock Prairie, clast count site C13 from the upper 3 ft of the soil revealed moderately weathered clasts and was mapped as queried unit Qpt.

There is no evidence that the Possession ice advance (MIS4) reached the map area (Troost, 2016). Polenz and others (2017) found Possession outwash in the Littlerock quadrangle, adjacent to and northwest of the Violet Prairie quadrangle. Assuming their supporting luminescence age control is accurate, this implies that Possession meltwater and outwash deposition along the ancestral Black River valley at least came close to Grand Mound Prairie in the northwestern part of the map area. Whether this led to enough outwash aggradation in the valleys of the Black and Chehalis rivers (Fig. M1) to dam upstream areas and send Possession-aged slack water deposits into the map area remains at best speculative. No such sediment is therefore suggested in Cross Section A–A′.

Snavely and others (1958) widely mapped Cascade Mountains-sourced pre-Vashon outwash of the Logan Hill Formation on hilltops in and near the map area. We only observed this unit outside the map area.

Vashon Drift of the Fraser Glaciation

The most recent incursion of the Cordilleran ice sheet into the map area occurred during the Vashon Stade of the late Wisconsinan Fraser Glaciation (MIS2). Based on radiocarbon data from farther north in the Puget Lowland, Polenz and others (2015) estimated that this took place between about 16 and 15.3 ka, revising Porter and Swanson's (1998) estimate of an earlier glacial maximum. The ice incursion triggered deposition of voluminous outwash (units Qgog and Qgo), terminal moraines (unit Qgim), compact lodgment till (unit Qgt) and undivided ice contact deposits (unit Qgic).

Based on the presence of some mildly weathered drift in the north-facing slope south of Grand Mound Prairie, such as at clast count site C19 (in a gravel pit mapped as unit ml) this map agrees with Bretz's (1913) interpretation that Vashon ice advanced to just south of Violet and Grand Mound prairies—as indicated by Vashon and pre-Vashon ice limit lines on the map plate, nearly to the position of the most extensive pre-Vashon ice advance. The supporting deposits of mildly weathered drift are too spotty and thin to show on the map, such that the Vashon ice limit line provides the only evidence of this interpretation.

Outwash Pathways and Lithologic Associations

The ice mass across Violet Prairie routed meltwater from mainly the eastern Puget Lowland south to Centralia, via Frost Prairie, Bucoda and the Skookumchuck River valley. Relict channel forms and a south-down slope across Frost Prairie just east of the map area provide evidence of this southbound meltwater flow from Tenino to Bucoda (assuming isostatic rebound tilt can be neglected), although Walsh and Logan (2005) and Logan and others (2009) also pointed out that meltwater flow and glacial outwash deposition into the Skookumchuck River valley occurred via the Stony Point channel of Bretz (1913), which enters the Skookumchuck River valley upstream of Bucoda (Fig. M1). South of the map area, Sadowski and others (2018) used geomorphic analysis of lidar data to infer Vashon outwash as far as Salzer Creek, 8.5 mi south of the Vashon ice limit shown on this map. Since the ice dam across the corridor of Scatter Creek marks the maximum ice extent west of Tenino, the time of southbound drainage to the Skookumchuck River also marks the glacial maximum. Constraints on the timing of Vashon ice advance and retreat farther north in the Puget Lowland (fig. 3 in Polenz and others, 2015) suggest that the meltwater drainage to the Skookumchuck River valley did not last long.

Clast counts provide some insight into pro-glacial meltwater pathways and outwash sediment provenance. Clast counts of Vashon and pre-Vashon outwash in the Skookumchuck River valley suggest that this outwash is derived mainly from the Olympia ice lobe, meaning most exposures contain somewhat more quartz, chert and basalt, and fewer intermediate igneous rocks than clast assemblages associated with the Yelm lobe of the eastern Puget Lowland (Fig. 1; clast counts C20–C25). The association with the Olympia lobe suggests correlation to Olympia lobe outwash subunits of Walsh and Logan (2005) and Logan and others (2009), and (or) their pre-Vashon equivalents. Cross-cutting relations south of Tenino indicate that Vashon outwash in Frost Prairie and the Skookumchuck River valley are older than the early recessional outwash in Rock, Violet, and Grand Mound prairies west of Tenino. Lithologic trends of clast counts west of Tenino (C5–C12, C17) reveal a mix of deposits,

Figure 10. *(facing page)* Map of faults, folds, and major named coal beds in the Skookumchuck Formation, as mapped by Snavely and others (1958) in and near the Violet Prairie and Centralia quadrangles. Northeast of the Kopiah fault, bedding orientations in the Violet Prairie quadrangle dip gently and vary in strike and coal beds are spaced correspondingly far apart. Strikingly, this area of gentle bedding approximates a region of subdued aeromagnetic anomalies (Fig. M2). With few biostratigraphic markers and exposures of bedding in the quadrangle, coal beds provide the best guide to stratigraphic position within the Skookumchuck Formation. Coal beds in the Violet Prairie quadrangle generally indicate exposures of lower Skookumchuck Formation (below the Mendota coal bed), except southwest of the Kopiah fault, where moderate to steep bedding dips systematically southwest-down and a tightly spaced succession of coal beds extends up to the Tono No. 1, which marks the middle of the upper coal group in the upper Skookumchuck Formation.

including some that, like the outwash in the Skookumchuck River valley, suggest association with the Olympia ice lobe and associated outwash subunits of Walsh and Logan (2005) and Logan and others (2009)(C7, C8, C9, C11), whereas others suggest association with provenance from the Cascade Mountains and the Yelm ice lobe and associated subunits of Walsh and Logan (2005) and Logan and others (2009)(C10, C12, C17). A third group may be best characterized as mixed (C5, C6). The varied lithologic assemblages west of Tenino suggest that association with outburst flood(s) from glacial lake Carbon (Goldstein and others, 2002, 2010; Pringle and Goldstein, 2002; Parker and others, 2008) is correct for some of these deposits, but probably not all. However, the at least partial association with outburst floods suggests that episodes of high discharge volumes may provide a mechanism for valley widening in Rock, Violet, and Grand Mound prairies.

HOLOCENE TO PLEISTOCENE NONGLACIAL DEPOSITS

Postglacial deposits include both Pleistocene and Holocene sediments because the onset of the Holocene at 11.7 ka (USGS Geologic Names Committee, 2010) does not coincide with the end of the Vashon glaciation. We estimate that Vashon ice was present in the map area sometime between 16 and 15.3 ka on the basis of age-control data farther north in the Puget Lowland (fig. 3 in Polenz and others, 2015). North of the Vashon ice limit, no pre-Vashon sediments were specifically identified as nonglacial, and all sediments mapped as nonglacial are post-glacial. Areas south of the ice limit were only indirectly affected by either glaciation or the Pleistocene-Holocene transition, and ages of some nonglacial deposits likely straddle glacial-nonglacial transitions.

We agree with Lea (1984) that outwash gravel of likely pre-Vashon age dammed an unnamed northern tributary of the Skookumchuck River and triggered valley floor aggradation. However, we are unconvinced that clast weathering in the outwash at the bottom end of this valley (C23) necessitates a pre-Vashon age for either the outwash at C23 or the upvalley sediment, and a Vashon age for the gravel bar also appears consistent with the record of valley floor aggradation in a peat bog core presented by Rigg (1958) at significant site S16 north of clast count site C23. Surficial peat, and clay described from 5 to 11.5 ft below the surface in the bog core, may have been deposited during the late Pleistocene and Holocene in response to valley damming by Vashon-aged outwash. Deeper peat and underlying clay and sand likely are a record of similar valley damming by a pre-Vashon ice advance.

If the above interpretation of Rigg's (1958) peat section is correct, re-sampling of the section could yield insights of regional significance. Outwash deposition in the valley of the Skookumchuck River necessarily marks the maximum extent of the Vashon glaciation. Throughout the Puget Lowland, calculations of fault activity (recurrence intervals on shallow-crustal faults) rest on an assumption that the length of the post-glacial period is known. Estimates of when this occurred have so far rested on data from farther north in the Puget Lowland (Porter and Swanson, 1998; Polenz and others, 2015). It is in most instances not clear how closely these estimates constrain the time of glacial retreat. An accurate assessment of the timing of the glacial maximum at or near Rigg's (1958) core site could improve these estimates and consequently improve fault hazard assessments elsewhere in the Puget Lowland. Radiocarbon analysis of twigs from gray clay that Rigg (1958) noted from 7 to 10 ft below the surface should yield an age estimate for after Vashon outwash had begun to dam the valley; fibrous peat and twigs from 11.5 ft below the surface (just below the clay) should mark the end of pre-Vashon conditions. Luminescence analysis of the sediment at the base of Rigg's section (17.5 to 19 ft below the surface) could additionally test Lea's (1984) hypothesis that the penultimate glaciation of the map area was the Double Bluff ice advance (MIS6).

Landslides

Sedimentary bedrock units of the map area are prone to landslides because of their poor induration, abundance of weak layers such as ash or coal, heavy alteration and deep weathering. Landslides and landforms that suggest unstable slopes abound south of Scatter Creek (at or south of the glacial maximum). Landforms associated with slope failures (such as disrupted drainages, uneven or benched slopes, mid-slope scarps, concave upper or convex lower slopes and other slope irregularities), range from obvious to very subtle both in lidar-based images and on the ground. Field visits of most landslide landforms in and near the map area reveal few or no signs of historic activity even in some relatively distinct and crisp landforms, as previously noted by Fiksdal (1978).

We observe three categories of landslides. The first category does not appear clearly on lidar-based images, but careful examination of these images and (or) field visits can document historic landslide activity. An example is the slope at significant site S5 west of Coffee Creek near Centralia, WA, where a small, concave scallop (head scarp) on the northern side of a road bed documents historic landslide movement, yet lidar-based images show an otherwise mostly smooth slope.

More common are landslides that can be recognized by geologists on the ground but are not clearly expressed in the lidar data and, unlike the first category above, lack clear evidence of recent movement. Two examples are at significant site S14 (3 mi southwest of Tenino) and S15 (in an unnamed, southern tributary of Prairie Creek). The areas marked by the mass wasting overlay pattern likely contain many landslides in these two categories. Their demonstrable presence in some locations indicates that many land-use decisions in areas covered by the overlay would benefit from a site-specific assessment.

A third, widespread category of landslides is marked by distinct landforms that are clearly apparent in lidar and on the ground (where not obscured by vegetation). Their features range from crisp to smoothed, commonly within a single landslide or landslide complex. An example is at significant site S2 (in the eastern headwaters of Prairie Creek), where a landslide with smoothed but distinct landforms includes a head scarp as high as 80 ft, and an upright, 7 ft-diameter old growth stump on a bench below a lateral scarp suggests that the most recent movement in this part of the landslide predates historic forest management. It is possible that this landslide has not moved since the end of the Pleistocene, as Fiksdal (1978) suggested is typical of "old" landslides in the area. However, the landowner at a different,

large landslide complex of this third category reported that he had, throughout the past few decades, observed open cracks in the hilltop ridge at the upper end of the landslide complex. Movement in a morphologically crisp part of that landslide had in recent years caused road damage, but the landowner's comments suggested that he observed open cracks in a part of the landslide complex that was morphologically more subdued and smoothed. This relationship casts doubt on the notion that morphologic crispness in lidar-based images is a fully reliable proxy for recency of landslide movement in this map area.

Most mapped landslides best fit the third category above, with geomorphically distinct landforms that can be readily discerned in lidar-based images—with or without field-based corroborating data, and with or without evidence of historic movement. Strikingly, these include some large landslides on relatively gentle slopes and a morphology suggestive of lateral spreading or earth flows (Fig. 11). Seismic implications are further discussed in *Structures in the Map Area*. It seems likely that many of these features are "old", especially where morphologically smoothed, but actual ages of landslide activity are largely undocumented. Multiple attempts to recover datable material from sag ponds in the course of this mapping were unsuccessful.

Geochemistry

IGNEOUS ROCK GEOCHEMISTRY

Five samples of igneous (or volcaniclastic) rock from the Violet Prairie quadrangle were selected for whole-rock chemical analysis; three collected from outcrop and two from the Bannse well. With the exception of the deepest well sample (G20), all of the samples are moderately to severely weathered and (or) altered and this is reflected in their chemical compositions (for instance, LOI as much as 15.5 wt. %, Al_2O_3 as much as 25 wt. %) (Table DS4). However, the two least affected samples (sites G8 and G20), both with LOI <4 wt. %, appear to largely retain their igneous chemistries. These two samples are medium-K andesites (56.8–57.1 wt. % SiO_2, 0.9–1.1 wt. % K_2O) and classify as calc-alkaline (Figs. 12A, B). They are moderately light rare earth element (LREE) enriched (La/Yb = 5.2–7.6)(Fig. 12C) and on a MORB-normalized spider diagram (Fig. 12D) display enrichments in large ion lithophile elements (K, Rb, Ba) and depletions in high field strength elements (Ta, Nb) that are characteristic of subduction zone magmas. Similar LREE enrichments and spider diagram patterns are observed in the more weathered samples as well (Figs. 12C, D), suggesting all five samples share the same igneous parentage. Sample G20 has adakite traits (Defant and Drummond, 1990) including Sr/Y >20, Sr >400 ppm, Yb <1.8 ppm, and Al_2O_3 >15 wt. % that are indicative of derivation from an eclogitic source. Taken together, the geochemical data suggest these rocks formed in a subduction setting and likely represent an early phase of Cascade arc magmatism.

Geochemical correlation of these rocks with volcanic units in nearby quadrangles is hindered by a paucity of data, particularly trace element data, for the Northcraft Formation and the Goble Volcanics. However, numerous chemical similarities point to correlation with the Northcraft Formation including: (1) both the Violet Prairie quadrangle volcanic samples and samples mapped as Northcraft Formation elsewhere are dominantly andesitic and calc-alkaline (Figs. 12A, B); (2) both show similar patterns on rare earth element and spider diagrams (Figs. 12C, D); (3) both contain rocks with adakite affinities; and (4) the less altered

Figure 11. Lidar-based image of a large landslide in the Skookumchuck Formation north of Hanaford Valley. The landslide (dark brown) is marked by a low average slope (about 8%, with 212 ft relief from head scarp to valley floor, and a 0.5 mi run-out distance), widely spread sag ponds and mid-slide ridges, and a large size (186 acres, excluding deposits that may be concealed beneath the valley floor). The prominent ridge in the eastern center of the landslide is 150 ft high. These attributes suggest possible seismic triggering of this and other large landslides in the map area.

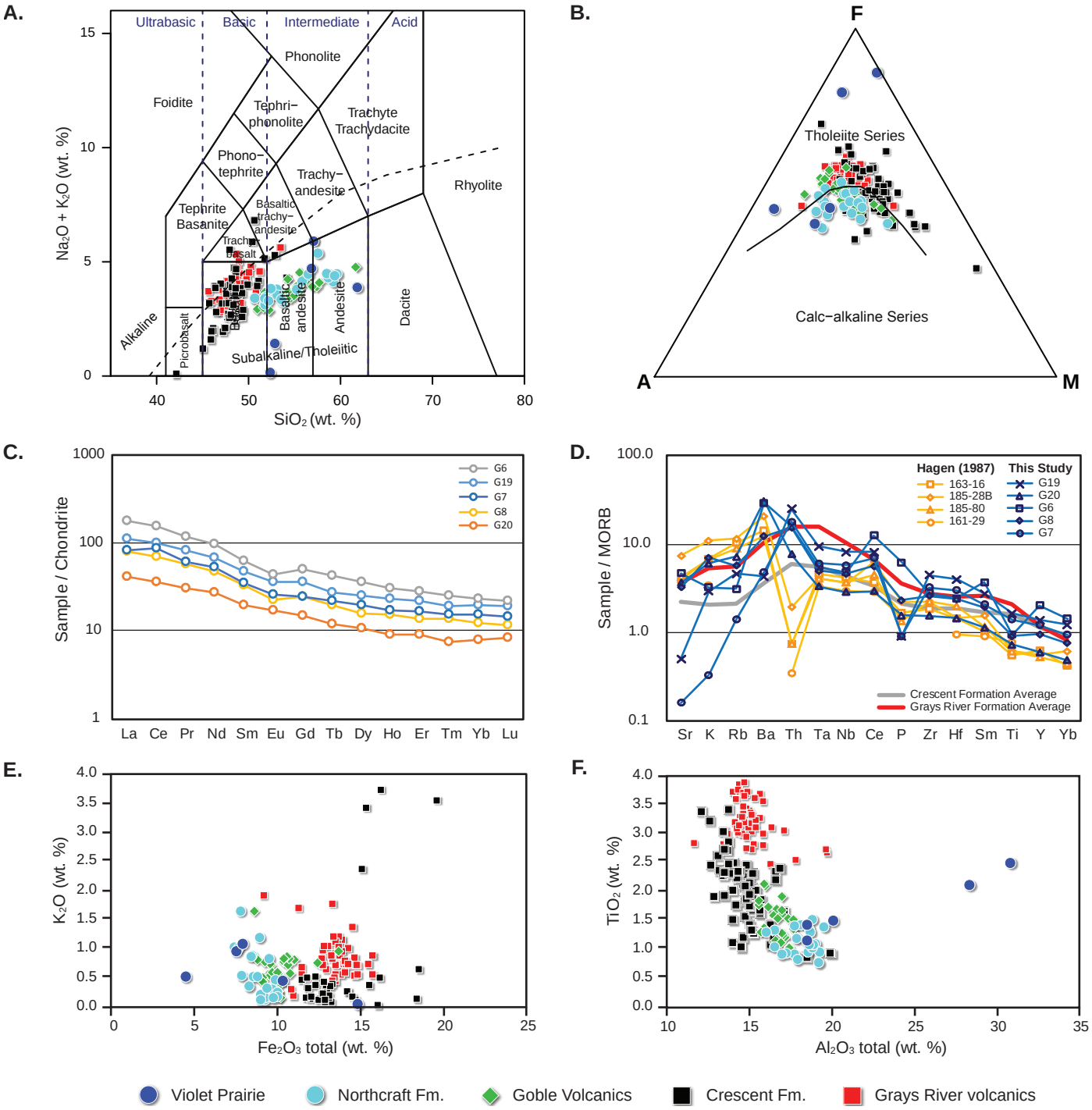

Figure 12. Geochemical data. **A.** Total alkalies vs. silica plot (Le Bas and others, 1986) for selected volcanic units from southwest Washington. Violet Prairie data are from this study. Northcraft data are from Hagen (1987). Goble Volcanics data are from Phillips and others (1989). Grays River volcanics data are from Chan and others (2012). Crescent Formation data are from Moothart (1993), Schasse and Logan (1998), Schasse and Wegmann (2000), Schasse and Polenz (2002), Schasse and Slaughter (2005), Schasse and others (2003, 2004), Walsh and others (2003), Logan and others (2009), Contreras and others (2012), and Polenz and others (2004, 2012a, b, 2014, 2015, 2016, 2017). **B.** AFM diagram (Irvine and Baragar, 1971) for select volcanic units from southwest Washington. Note that the two least altered Violet Prairie samples plot in the calc-alkaline field along with other Northcraft Formation samples. **C.** Rare earth element data for Northcraft Formation samples from the Violet Prairie quadrangle, normalized to chondrite values of Boynton (1984). The close similarity of patterns suggests all five Violet Prairie samples share a common origin. **D.** MORB-normalized spider diagram (Sun and McDonough, 1989) comparing Northcraft Formation samples from the Violet Prairie quadrangle and from Hagen (1987) with data from other volcanic units in southwest Washington. All Violet Prairie samples display relative depletions in Ta and Nb and enrichments in Rb and Ba, diagnostic features of subduction-related magmas that are also seen in other Northcraft Formation samples. Conversely, no Ta-Nb depletions are seen in the Crescent or Grays River data, indicating those units are not correlative with the Violet Prairie rocks. Low Sr and K in some Violet Prairie samples likely reflects loss of these mobile elements during alteration and weathering. **E.** Variation diagram showing overlap between Violet Prairie and other Northcraft Formation data. Other volcanic units in the region (Grays River volcanics, Crescent Formation, Goble Volcanics) have generally higher total Fe_2O_3. **F.** Variation diagram showing overlap between Violet Prairie and other Northcraft Formation data. Other volcanic units in the region (Grays River volcanics, Crescent Formation, Goble Volcanics) have generally lower Al_2O_3 and (or) higher TiO_2. Violet Prairie samples with Al_2O_3 > 25 wt. % lost >15 wt. % on ignition (LOI) and appear to be weathered.

Violet Prairie samples overlap in major oxide compositions, specifically Al_2O_3 and total Fe_2O_3, with data for Northcraft lavas (Figs. 12E, F).

SEDIMENTARY ROCK GEOCHEMISTRY

Geochemical analysis of sedimentary rock units suggests that systematic differences may exist between the mostly terrestrial Skookumchuck Formation compared to the marine McIntosh and Lincoln Creek formations. Plots of (1) Rb/Al_2O_3 vs Zr/Al_2O_3 and (2) Ti/Al_2O_3 vs Zr/Al_2O_3 appear to systematically separate Skookumchuck Formation from the two marine units. However, more work will be needed to confirm if this relationship resulted from something other than depositional environment.

GEOCHEMISTRY BY X-RAY DIFFRACTION

Clay mineral analysis by X-ray diffraction was performed on 47 samples of rocks or rock weathering products from the Violet Prairie and adjacent Centralia quadrangles. The analyses revealed no clear differences between the sedimentary rock and drift units in the Violet Prairie quadrangle and are consistent with preliminary findings of Polenz and others (2017). The results are presented by Sadowski and others (2018).

STRUCTURES IN THE MAP AREA

Faults

With the exception of a single, queried southwest-trending segment of what Snavely and others (1958) had inferred as the Tenino Anticline, all known faults and folds in the map area strike or trend northwest. More regional aeromagnetic data reinforce this structural fabric by revealing a broader pattern of northwest-oriented aeromagnetic anomalies. This fabric is locally weakened or discontinuous and mostly faint in the Violet Prairie quadrangle. However, the fabric surrounds the quadrangle and strengthens east and southeast of the quadrangle (Fig. M2). The fabric provides support for the northwest-striking faults mapped by Snavely and others (1958)(Fig. 10), and Polenz and others (2017) invoked it, among other reasons, to suggest northwest-striking faults in the lowlands and Black Hills northwest of the Violet Prairie quadrangle.

The new mapping in the Violet Prairie quadrangle revealed no definitive surface exposures of faults. All but one of the faults shown are therefore compiled with only minor adjustments from Snavely and others (1958). However, unlike on Snavely and others' (1958) map, all faults are shown as right-lateral, with strike-slip as the main component of motion. This interpretation rests partly on the conclusions TransAlta geologists drew from thousands of exploration boreholes and mining-related excavations in and near the map area (Will Greenough, TransAlta, oral commun., 2017). TransAlta geologists concluded that their data generally support Snavely and others' mapping of structures in and near the Violet Prairie quadrangle, including the northeast-up offset on the Coal Creek and Kopiah faults, but they also noted that the main offset on the northwest-striking cluster of faults mapped by Snavely and others is right-lateral (Will Greenough, oral commun., 2017). This is consistent with Stanley and others' (1994) more regional geophysical evaluation of deep seismic, magnetic, and gravity data—note specifically the northwest striking "strike slip fault" in their figure 13, which approximates the location of the northwest-striking faults in and southeast of the Violet Prairie quadrangle.

Aside from the fact that proprietary data convinced TransAlta geologists to interpret the faults in the map area as mainly right-lateral, Sadowski and others (2018) provided evidence for right-lateral offset on the Kopiah fault south of the Violet Prairie quadrangle. Folding northeast of the Kopiah fault (see *Folds* below) adds evidence of northeast-southwest compression in the map area, consistent with the compressional setting interpreted by Sadowski and others (2018) farther south. Evidence for north-up offset is discussed below in the context of individual fault strands.

Existing and new geophysical data contributed to our interpretation of folds and faults. Combined modeling of regional and newly acquired local gravity measurements (unpublished data, WGS) offers no evidence for notable gravity anomalies within the map area (Fig. M3). The significance of a gradual gravity decrease from the Violet Prairie quadrangle east, south, and west into adjacent areas remains unclear, but the lack of sharp transitions even along the closely spaced measurements along Cross Section A–A′ may suggest that the generally flat-lying Skookumchuck Formation sedimentary rocks at the surface rest on similarly flat-lying strata of other units at greater depth, consistent with mostly gentle bedding orientations recorded below the Skookumchuck Formation in the Bannse well (Fig. 8).

Aeromagnetic data supplemented by several ground magnetic survey lines in and near the map area (Fig. M2) show somewhat more evidence of anomalies in support of the mapped faults. The data suggest additional possible faults, such as an unmapped northwest-striking fault to connect the Newaukum fault southeast of the map area to an unnamed, concealed, and questionable fault suggested northwest of the map area by Polenz and others (2017). Near the northwestern map corner, such a northeast-up fault could help explain the distribution of McIntosh Formation exposures northeast of the fault in contrast to Skookumchuck Formation exposures southwest of the fault. But fault offset does not appear to be required for the mapped distribution of units in this area, and inference of such a fault is therefore not sufficiently supported by this mapping.

Whether any shallow crustal faults in and near the map area are active remains to be determined. However, the nearly north-south compressional setting implied by the geometry of folding and faulting south of and in the map area is consistent with on-going north-south compression that is accommodated farther north in the Puget Lowland by a system of (1) northwest-striking, right-lateral faults such as the Southern Whidbey Island fault zone and (2) west-striking faults such as the Seattle and Tacoma faults.

Some faults in the area may be non-tectonic. Clayified tephra layers in the Skookumchuck Formation commonly act as slip planes and there is considerable localized, and locally intense, apparently non-tectonic folding and faulting within the Skookumchuck Formation (Will Greenough, oral commun., 2017). This deformation likely amounts to landslide movement. These inferences appear to be consistent with distinctions Nelson (1981) made between tectonic and non-tectonic faults in the context of coal mining.

KOPIAH FAULT AND ASSOCIATED FAULTS

The Kopiah fault is compiled from Snavely and others (1958) but is shown as an oblique reverse right-lateral fault with two strands and mostly strike-slip motion. Compilation from Snavely and others' 1:48,000-scale map implies that the fault location is approximate, but Snavely and others (1958, p. 87) noted that the fault location is "fairly accurately delineated because it dislocates the coal bearing rocks" and added that each fault strand has about 200 to 250 ft of throw on it. Snavely and others (1958) justify the bifurcation of the Kopiah fault in the map area by asserting that the block of Skookumchuck Formation between the strands is rotated relative to adjacent areas. The southern strand appears to be anchored in part by thrust faults with displacements of as much as 3 ft in the Perth coal mine (roughly located by significant site S11), although this offset could be interpreted as non-tectonic.

The Kopiah fault follows the northeastern edge of a gravity low crudely defined by regional gravity data. Regional gravity data (Bowman, 2013) supplemented by new gravity measurements (this study) suggest more complexity but also seem consistent with the Kopiah fault's presence and alignment, as do multiple aeromagnetic anomalies aligned with or parallel to the fault in and near the Violet Prairie quadrangle (Figs. M2 and 3).

The Kopiah fault in and near the Violet Prairie quadrangle marks a systematic change in bedding orientations. Gently dipping beds with varied strike orientations in Skookumchuck Formation northeast of the fault contrast with bedding that systematically dips southwest in the Skookumchuck and Lincoln Creek formations southwest of the fault. Snavely and others (1958) and Sadowski and others (2018) noted that beds are locally overturned near the fault (not observed in the Violet Prairie quadrangle). Coal mine records indicate that bedding dips flatten farther southwest, away from the Kopiah fault. Exposures along a railroad cut 0.2 to 1 mi south of the map area, described in detail by Snavely and others (1958, p. 27) suggest that the consistent southwest-dips in the upper Skookumchuck Formation extend upsection into the base of the Lincoln Creek Formation, wherein deposition of tuff is newly dated by a 36.7 ±0.32 Ma zircon U-Pb analysis (Fig. 7; Sadowski and others, 2018). This suggests a conformable transition from Skookumchuck to Lincoln Creek Formation, and folding of both after 36.7 ±0.32 Ma. An angular unconformity between the Lincoln Creek and Wilkes formations implies that significant folding had occurred before the Wilkes Formation was deposited during the Late(?) Miocene (Sadowski and others, 2018). This map follows prior mapping (Snavely and others, 1958; Schasse, 1987; Walsh and others, 1987) and agrees with Sadowski and others (2018) south of the map area in showing northeast-up offset on the Kopiah fault. Such offset is also supported by stratigraphic relations west of the map area, based on Snavely and others' (1958) bedding orientations and unit interpretations at surface exposures and in borings B1, B2, B6, and HC4 (Fig. M1).

Multiple scarps parallel to the mapped alignment of the Kopiah fault may be fault expressions. If so, they imply additional unmapped fault strands. North of the mapped fault a large landslide complex covers about a mile of the hillside east of Zenkner Valley (Fig. 13). About 2,000 ft northeast of the mapped fault, a southeast-trending, southwest-down scarp at paleomagnetic site M1 crosses this landslide from top to bottom, a length of 2,000 ft. The scarp is largely straight and trends about 140°, roughly parallel to the Kopiah fault. The scarp has a maximum height of about 80 ft. A second scarp with similar orientation and southwest-down offset of up to about 60 ft also crosses the landslide top to bottom about 800 ft farther northeast. Neither scarp extends outside the landslide area, but among hundreds of landslides in the map area, this set of scarps stands out for: (1) being straight; (2) paralleling each other and nearly paralleling a known nearby fault; (3) having consistent southwest-down offset just like that fault; and (4) crossing the entire landslide area, at an orientation oblique to the slope and not aligned with bedding or any apparent joints. In addition, a small, straight drainage on the opposite side of Zenkner valley is aligned with the larger of the scarps but also located in a landslide. Finally, about 950 ft southwest of the southwestern strand of the Kopiah fault near the southern map edge, and 660 ft southwest of significant site S9, lidar-based images reveal a slight but distinct, 1,100 ft-long, straight scarp that parallels the Kopiah fault on the slope southwest of a ridge that also trends approximately along the same orientation.

COAL CREEK FAULT

Snavely and others (1958) first inferred the northwest end of the Coal Creek fault in the Violet Prairie quadrangle as a concealed high-angle reverse(?) fault with displacement of about 400 ft. This map adopts their fault with queries but without modifying its position and orientation. Snavely and others cited offset coal beds southeast of the Violet Prairie quadrangle as evidence for the fault. The fault is queried because it is entirely concealed within the quadrangle and we encountered no field evidence to support its position or extent. The mapped trend of the fault does coincide with an aeromagnetic anomaly across Rock Prairie (Fig. M2), and the presence of a fault in this area beneath Rock Prairie is consistent with our combined modeling of aeromagnetic and new field-based magnetic ground surface transects and existing and new gravity transects along Cross Section A–A′. The aeromagnetic anomaly is part of a fabric of northwest-oriented aeromagnetic anomalies that surround the quadrangle. The fabric is discontinuous and mostly faint in the Violet prairie quadrangle but strengthens east and southeast of the quadrangle. It provides support for the cluster of northwest-striking faults mapped by Snavely and others (1958), and Polenz and others (2017) invoked it to suggest that the northwest-striking faults in the lowlands and Black Hills northwest of the Violet Prairie quadrangle may be related to the faults identified by Snavely and others.

Estimate of vertical offset

We used boring log interpretations presented by Snavely and others (1958) to help estimate vertical offset across the Coal Creek fault. Snavely and others (1958) identified specific coal beds in borings on opposite sides of the Coal Creek fault. For two pairs of wells, we estimated the surface elevation from a DEM and the depth to the top of a specific coal bed in each boring. Then we computed the vertical difference between the coal bed elevations in the borings. Snavely and others' mapped bedding attitudes and distribution of coal bed exposures suggest gentle coal bed orientations, and we inferred that the difference in coal bed elevations across borings limits vertical offset

across the Coal Creek fault. This calculation was applied to (1) the Big Dirty coal bed using B7 and B8 (boreholes GS-M and WU-1, Snavely and others, 1958, located 3.8 and 2.7 mi east of the Violet Prairie quadrangle, respectively) and (2) the Black Bear coal bed using B4 and B9 (boreholes GW-1 and GS-A of Snavely and others, 1958, respectively located inside and 1.6 mi east of the Violet Prairie quadrangle). Based on limited coal bed elevation differences across the borings (80 ft west-down between B4 and B9, and 519 ft west-down between B7 and B8) we inferred ~100 ft of northeast up displacement on the Coal Creek fault. This displacement is reflected on our cross section and is smaller than that implied by the cross section of Snavely and others (1958). The northeast-up offset across the Coal Creek fault is consistent with a general, gentle trend of northeast-rising units between the eastern edge of the Violet Prairie quadrangle and the Kopiah fault near the southwest corner of the quadrangle. This trend is clearly expressed in Cross Section A–A′ but does not require Coal Creek fault offset.

Interpretation of coal bed deformation along Coal Creek fault

Coal beds in the map area may provide evidence of Coal Creek fault offset. Snavely and others (1958, p. 107) reported "minor folds and faults" in the Great Western coal mine (S6) that followed the Black Bear coal bed 1.3 mi southwest of the Coal Creek fault in the Violet Prairie quadrangle. Along with the reported elevation of the Black Bear coal bed in nearby boring B4, and sparse but varied bedding orientation measurements near the Coal Creek fault in the Violet Prairie quadrangle, these minor folds and faults may be either evidence for non-tectonic, small folding and faulting, or the folds and faults may be tectonic offsets that would likely be related to the nearby Coal Creek fault but are too complex to be adequately defined and interpreted based on the limited available data.

UNNAMED FAULT NORTHEAST OF COAL CREEK FAULT

A newly inferred, questionable concealed fault is shown across Lemon Hill west of Tenino. The fault is shown parallel to and 0.8 mi northeast of the Coal Creek fault and was inferred based on (1) several perennial springs anomalously located on a hilltop at the northern edge of the Violet Prairie quadrangle and (2) a northwest-oriented aeromagnetic anomaly parallel to the nearby Coal Creek fault. Gravity data points are not spaced densely enough to permit clear inferences in this area, but a magnetic ground-level survey line and more densely spaced gravity measurements, as well as modeling of combined gravity and magnetic data support the presence of a disturbance approximately where the southeastern projection of the inferred fault intersects the northwestern projection of Cross Section A–A′ east of the Violet Prairie quadrangle. Notably, Snavely and others (1958) show a similarly oriented northeast-up fault that parallels the Coal Creek fault between five and eight miles southeast of where the newly inferred fault strand meets the eastern edge of the Violet Prairie quadrangle. Snavely and others' (1958) fault farther southeast is about the same distance northwest of the Coal Creek fault as the newly inferred fault strand we show in the Violet Prairie quadrangle. As with the Coal Creek fault, we view the newly inferred fault in the context of the fabric of northwest-oriented aeromagnetic anomalies in and near the Violet Prairie quadrangle.

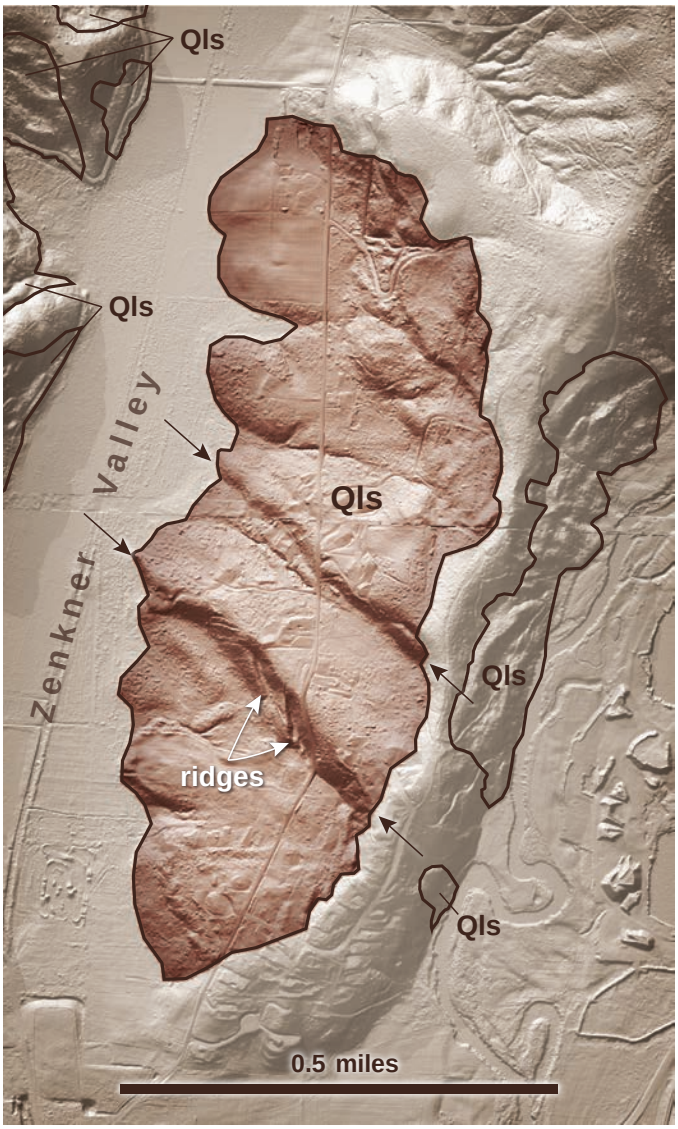

Figure 13. Lidar-based image of large landslide with anomalous scarps (brown arrows). A large landslide on the east side of Zenkner Valley is situated between 0 and 0.9 mi northeast of the northwest-striking Kopiah fault (Map Sheet). The landslide landform is distinct but the surface morphology is mostly smoothed and subdued. No evidence of recent or ongoing landslide movement was observed during a field visit in 2017. Two prominent scarps cross the entire landslide oblique to slope, from top to valley floor. They are essentially straight, as tall as 80 ft, northeast-up, and parallel to the Kopiah fault. Along the southwestern of the two scarps, two smaller ridges (white arrows) splay acutely away from the scarp, rotated 15 and 28 degrees respectively, clockwise relative to the scarp. Their orientation approaches the strike of bedding measured at 182/06 nearby along the scarp. This suggests that the failures are bedding-parallel.

Folds

Despite abundant landslides and a paucity of exposures that extend beyond the soil into underlying bedrock, two exposures near the southern map edge revealed enough bedding to suggest local folding. An outcrop at site GD29, 0.5 mi northeast of where the Kopiah fault crosses the southern map boundary, exposes 3 ft

of medium gray to tan, fine-grained, micaceous and fossiliferous sandstone and siltstone that weathers reddish-brown and is part of the lower Skookumchuck Formation. Although exposure is poor, two bedding measurements imply a synclinal axis with a trend of 123° and a plunge of 14°, shown on the map as a small syncline (Fig. 14A). A third bedding exposure 180 ft farther west-southwest implies a similarly oriented anticline southwest of the syncline. Together, these small folds imply shortening normal to the Kopiah fault, consistent with the oblique, reverse right-lateral fault interpretation shown on the map.

An outcrop of lower Skookumchuck Formation 0.5 mi east of the above-mentioned fold exposure at age site GD29 exposes pale yellow sandstone with reddish brown, iron-cemented surfaces. The exposure is about 4 ft high by 10 ft wide. Bedding is difficult to see in most of the exposure, but prominent, apparent laminations near the east end of the exposure suggest an anticline. A stereonet plot of six strike and dip measurements along the apparent anticline yielded an axial trend of 274° and plunge of 0° (Fig. 14B). This anticline is represented on the map by a small, local fold symbol that approximates the orientations of the local fold at site GD29 and a west-northwest-trending, unnamed anticline compiled from Snavely and others (1958) about 1,000 ft north of this outcrop. Snavely and others' mapping of the larger fold farther north suggests that the small folds observed at this site and site GD29 belong to the same set of two sub-parallel anticlines and two synclines shown by Snavely and others (1958) northeast of the Kopiah fault near the southern edge of the Violet Prairie quadrangle. This suggestion contributed to the decision to compile Snavely and others' (1958) set of four folds across the southern part of the map area, although three are queried as we observed no supporting evidence for them and are unsure what argument(s) underpinned Snavely and others' (1958) mapping of the folds.

We omit most of Snavely and others' (1958) Tenino anticline because we do not believe available bedding orientation data justified this structure along most of its length.

Structural Implications of Landslides in the Map Area

The Violet Prairie quadrangle map shows more than 300 landslide polygons, many of which capture large landslide complexes with multiple inset landslides that have varied levels of morphologic crispness. The ten largest landslide polygons range from 70 to 252 acres. Some complexes combine sub-areas that clearly move in different directions and may be causally unrelated. Nevertheless the sheer size of the larger landslide complexes suggests that the larger landslides are seismically triggered (Stephen Slaughter, WGS, oral commun., 2018). Keefer (1984) established that seismic triggering of earthflows and lateral spreads tends to require earthquakes of local magnitude 5.

Following the May 12, 2008, Wenchuan earthquake in Sichuan Province, China, an earthquake which the U.S. Geological Survey reported as an event of magnitude 7.9[3], Gorum and others (2011) analyzed 60,000 landslides identified in the aftermath of the earthquake. Gorum and others (2011) found that most of the landslides occurred within 10 km (6 mi) of the fault, and

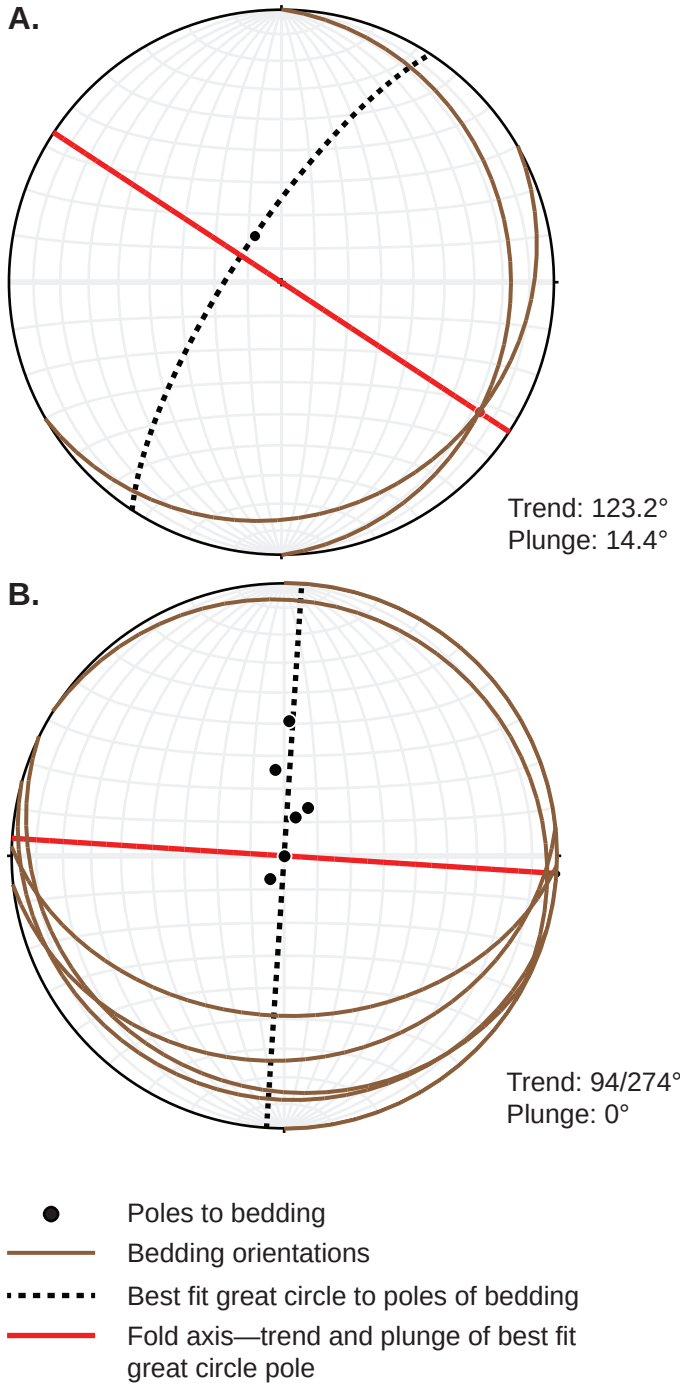

Figure 14. Stereonet diagrams for bedding planes at and near site GD29. **A.** Equal area plot of one gently east-dipping and one gently south-dipping bedding plane and poles to bedding, located at site GD29. A northwest-west-trending, horizontal syncline axis inferred from the bedding planes is shown in red. A third bedding exposure 180 ft farther west (not shown) implies an approximately parallel, local anticline. **B.** Equal area plot of four south-dipping, one gently north-dipping, and one horizontal bedding plane and poles to bedding, located half a mile east of site GD29. An approximately west-trending, horizontal fold axis inferred from the six bedding planes is shown in red.

[3] https://earthquake.usgs.gov/earthquakes/eventpage/usp000g650

landslides were heavily concentrated in the hanging wall of fault segments with mostly thrust displacement on a fault plane with a dip angle of about 45°. This suggests not only that many of the landslides in the map area may be seismically triggered, but also that thrust movement on local faults is a very effective trigger.

We cannot rule out that seismic triggering (if any) of landslides in and near the map area is entirely attributable to megathrust events on the active Cascadia subduction zone, or earthquakes on more distant but demonstrably active shallow-crustal faults, such as the Tacoma and Seattle faults. Yet in the map area and the adjacent Centralia quadrangle to the south, local faults, including at least one fault segment with thrusting as the apparent main mechanism, spatially coincide with large landslides with characteristics typical of seismically triggered slope failures. Earthquakes on local faults, especially thrust offset, would provide an ideal trigger. In the Violet Prairie quadrangle, no fault is presently identified as a thrust fault. Our mapping of the Kopiah fault as oblique reverse right lateral implies a compressional setting in which unrecognized thrust faults could also be present.

None of the above proves that landslides in the map area are seismically induced by activity on local faults. Nevertheless, the simultaneous presence of local faults and a large number of potentially seismically-triggered landslides presents local faults as a likely trigger. The likelihood of seismic landslide induction suggests that future earthquakes should be expected to induce additional landslides in presently unaffected slopes because Keefer (1984) noted that earthquake-induced landslides tend to develop preferentially in areas that have not previously failed.

Neither the observations from this geologic mapping project, nor the regional context discussed above demonstrate that the shallow crustal faults in the map area are active, but ongoing structural activity in the map area seems likely given the regional tectonic framework, despite the paucity of recorded seismicity.

ACKNOWLEDGMENTS

This geologic map was funded in part by the U.S. Geological Survey (USGS) National Cooperative Geologic Mapping program under award no. G17AC00262. We thank: Elizabeth Nesbitt and Ruth Martin (both at the Burke Museum) for analysis of biostratigraphic samples for fossils and their ages; Will Greenough (TransAlta) and Grant Newport (Weyerhaeuser) for helpful discussions and insights from proprietary exploration records; Richard Blakely (USGS) for aeromagnetic anomaly maps; Kat Szatkowski, Lauren Burch, Spenser Scott, and WGS staff, Rachel Noonan, Ian Hubert, Kara Jacobacci, and Guy McWethy for help with field work; the WGS landslide hazard group (Kara Jacobacci, Kate Mickelson, Trevor Contreras, and Stephen Slaughter) for lidar-based reconnaissance assessment of potentially unstable slopes; the WGS lidar group (Abigail Gleason and Guy McWethy) for compiling and processing the best-available lidar for our area of interest; Mitchell Allen (DNR Forest Practices Division) for assistance with GIS project set-up and field work; Bernard Housen and William Callebert (Western Washington University) for paleomagnetic analyses; and Timothy Walsh and Alex Steely (both WGS) for helpful discussions. We thank private and public landowners for sharing local knowledge and permitting us to map on their land. Among co-authors, Jeff Tepper and Todd Lau focused on geochemical analysis and interpretation; Recep Cakir and Todd Lau on geophysical data collection and analysis; Angela Blanks-Bennett on petrographic and geochemical sample analysis and geophysical data collection; Gabriel Legorreta Paulín on satellite data; and Andy DuFrane on U-Pb sample processing, analysis, and implications for affected rock unit ages and provenances

REFERENCES

Allmendinger, R. W.; Cardozo, N. C.; Fisher, D., 2013, Structural geology algorithms: Vectors & Tensors: Cambridge, England, Cambridge University Press, 289 p.

Anderson, T., 2002, Correction of common lead in U–Pb analyses that do not report ^{204}Pb: Chemical Geology, v. 192, p. 59-79.

Anderson, H. E.; Davis, D. W., 1995, U - Pb geochronology of the Moyie sills, Purcell Supergroup, southeastern British Columbia: implications for the Mesoproterozoic geological history of the Purcell (Belt) basin: Canadian Journal of Earth Science, v. 32, p. 1180-1193.

Armentrout, J. M., 1987, Cenozoic stratigraphy, unconformity-bounded sequences, and tectonic history of southwestern Washington. *In* Schuster, J. E., editor, Selected papers on the geology of Washington: Washington Division of Geology and Earth Resources Bulletin 77, p. 291-320. [https://www.dnr.wa.gov/Publications/ger_b77_papers_on_wa_geology_pt3of3.pdf]

Armentrout, J. M.; Hull, D. A.; Beaulieu, J. D.; Rau, W. W., 1983, Correlation of Cenozoic stratigraphic units of western Oregon and Washington: Oregon Department of Geology and Mineral Industries Oil and Gas Investigation 7, 90 p., 1 plate. [http://www.oregongeology.org/pubs/ogi/OGI-07.pdf]

Babcock, R. S.; Burmester, R. F.; Engebretson, D. C.; Warnock, A. C.; Clark, K. P., 1992, A rifted margin origin for the Crescent basalts and related rocks in the northern Coast Range volcanic province, Washington and British Columbia: Journal of Geophysical Research, v. 97, no. B5, p. 6799-6821. [http://cedar.wwu.edu/geology_facpubs/31/]

Babcock, R. S.; Suczek, C. A.; Engebretson, D. C., 1994, The Crescent "terrane", Olympic Peninsula and southern Vancouver Island, *In* Lasmanis, Raymond; Cheney, E. S., convenors, Regional geology of Washington State: Washington Division of Geology and Earth Resources Bulletin 80, p. 141-157. [http://www.dnr.wa.gov/publications/ger_b80_regional_geol_wa_2.pdf]

Beikman, H. M.; Gower, H. D., 1958, Coal resources of southwestern Washington: U.S. Geological Survey Open-File Report 59-6, 54 p. (Published as Washington Division of Mines and Geology Bulletin 47) [http://www.dnr.wa.gov/publications/ger_b47_coal_reserves_wa.pdf]

Beikman, H. M.; Rau, W. W.; Wagner, H. C., 1967, The Lincoln Creek Formation, Grays Harbor basin, southwestern Washington: U.S. Geological Survey Bulletin 1244-I, 14 p. [http://pubs.er.usgs.gov/publication/b1244I]

Berg, A. W., 1990, Comment and reply on "Formation of Mima mounds—A seismic hypothesis"; Reply: Geology, v. 18, no. 12, p. 1260-1261.

Blakely, R. J.; Sherrod, B. L.; Wells, R. E.; Weaver, C. S.; McCormack, D. H.; Troost, K. G.; Haugerud, R. A., 2004, The Cottage Lake aeromagnetic lineament—A possible onshore extension of the southern Whidbey Island fault, Washington: U.S. Geological Survey Open-File Report 2004-1204, 60 p. [http://pubs.er.usgs.gov/publication/ofr20041204]

Booth, D. B.; Troost, K. G.; Clague, J. J.; Waitt, R. B., 2004, The Cordilleran ice sheet. *In* Gillespie, A. R.; Porter, S. C.; Atwater, B. F., editors, The Quaternary period in the United States: Elsevier, p. 17-43.

Bowman, J. D., 2013, Washington State aeromagnetic and gravity anomaly data—GIS data: Washington Division of Geology and Earth Resources Digital Data Series 2, 4.42 MB. [http://www.dnr.wa.gov/publications/ger_portal_geophysical_data.zip]

Bowman, J. D.; Czajkowski, J. L., 2016, Washington State seismogenic features database—GIS data: Washington Division of Geology and Earth Resources Digital Data Series 1, version 4.1, originally issued December 2013. [http://www.dnr.wa.gov/publications/ger_portal_seismogenic_features.zip]

Boynton, W. V., 1984, Cosmochemistry of the rare earth elements: meteorite studies. *In* Henderson, P., editor, Rare Earth Element Geochemistry: Elsevier, p. 63-114.

Bretz, J Harlen, 1911, The terminal moraine of the Puget Sound glacier: Journal of Geology, v. 19, no. 2, p. 161-174.

Bretz, J Harlen, 1913, Glaciation of the Puget Sound region: Washington Geological Survey Bulletin 8, 244 p., 3 plates. [http://www.dnr.wa.gov/publications/ger_b8_glaciation_pugetsound.pdf]

Buckovic, W. A., 1974, The Cenozoic stratigraphy and structure of a portion of the west Mount Rainier area, Pierce County, Washington: University of Washington Master of Science thesis, 123 p., 1 plate.

Buckovic, W. A., 1979, The Eocene deltaic system of west-central Washington. *In* Armentrout, J. M.; Cole, M. R.; Ter Best, Harry, Jr., editors, Cenozoic paleogeography of the western United States: Society of Economic Paleontologists and Mineralogists Pacific Section, Pacific Coast Paleogeography Symposium 3, p. 147-163.

Cardozo, N., and Allmendinger, R. W., 2013, Spherical projections with OSXStereonet: Computers & Geosciences, v. 51, p. 193–205.

Carter, Lori, 2017, The scoop on fossilized poop: Rock & Gem, v. 47, no. 1, p. 28-33.

Chan, C. F.; Tepper, J. H.; Nelson, B. K., 2012, Petrology of the Grays River volcanics, southwest Washington: Plume-influenced slab window magmatism in the Cascadia forearc: Geological Society of America Bulletin, v. 124, p. 1324-1338.

Clague, J. J., 1997, Evidence for large earthquakes at the Cascadia subduction zone: Reviews of Geophysics, v. 35, no. 4, p. 439-460.

Clowes, R. M.; Brandon, M. T.; Green, A. G.; Yorath, C. J.; Sutherland Brown, A.; Kanasebretwich, E. R.; Spencer, C. J., 1987, LITHOPROBE—Southern Vancouver Island—Cenozoic subduction complex imaged by deep seismic reflections: Canadian Journal of Earth Sciences, v. 24, no. 1, p. 31-51.

Colman, S. M.; Pierce, K. L., 1981, Weathering rinds on andesitic and basaltic stones as a Quaternary age indicator, western United States: U.S. Geological Survey Professional Paper 1210, 56 p. [https://pubs.er.usgs.gov/publication/pp1210]

Contreras, T. A.; Spangler, Eleanor; Fusso, L. A.; Reioux, D. A.; Legorreta Paulin, Gabriel; Pringle, P. T.; Carson, R. J.; Lindstrum, E. F.; Clark, K. P.; Tepper, J. H.; Pileggi, Domenico; Mahan, S. A., 2012, Geologic map of the Eldon 7.5-minute quadrangle, Jefferson, Kitsap, and Mason Counties, Washington: Washington Division of Geology and Earth Resources Map Series 2012-03, 1 sheet, scale 1:24,000, with 60 p. text. [http://www.dnr.wa.gov/Publications/ger_ms2012-03_geol_map_eldon_24k.zip]

Culver, H. E., 1919, The coal fields of southwestern Washington: Washington Geological Survey Bulletin 19, 155 p. http://www.dnr.wa.gov/publications/ger_b19_coal_fields_sw_wa.pdf]

Dalquest, W. W.; Scheffer, V. B., 1942, The origin of the Mima mounds of western Washington: Journal of Geology, v. 50, no. 1, p. 68-84.

Defant, M.J.;Drummond, M.S., 1990, Derivation of some modern arc magmas by melting of young subducted lithosphere, Nature, v. 347, p. 662-665.

Eddy, M. P.; Bowring, S. A.; Umhoefer, P. J.; Miller, R. B.; McLean, N. M.; Donaghy, E. E., 2016, High-resolution temporal and stratigraphic record of Siletzia's accretion and triple junction migration from nonmarine sedimentary basins in central and western Washington: Geological Society of America Bulletin, v. 128, no. 3/4, p. 425-441.

Eddy, M. P.; Clark, K. P.; Polenz, Michael, 2017, Age and volcanic stratigraphy of the Eocene Siletzia oceanic plateau in Washington and on Vancouver Island: Lithosphere, v. 9, no.4, p. 652-664,

Evans, K. V.; Aleinikoff, J. N.; Obradovich, J. D.; Fanning, C. M., 2000, SHRIMP U–Pb geochronology of volcanic rocks, Belt Supergroup, western Montana: evidence for rapid deposition of sedimentary strata: Canadian Journal of Earth Sciences, v. 37, p. 1287-1300.

Fedo, C. M.; Sircombe, K. N.; Rainbird, R. H., 2003, Detrital zircon analysis of the sedimentary record: Reviews in Mineralogy and Geochemistry, v. 53, p. 277-303.

Fiksdal, A. J., 1978, Slope stability of the Centralia–Chehalis area, Lewis County, Washington: Washington Division of Geology and Earth Resources Open File Report 78-2, 4 p., 1 plate, scale 1:62,500. [http://www.dnr.wa.gov/publications/ger_ofr78-2_slope_stability_centralia_chehalis_62k.pdf]

[Fillmore Drilling Company], [1949], Driller's log and core log descriptions for Union Oil Company of California well: Bannse No. 1 (API: 046-067-00011; WA File No.: T-11): Washington Geological Survey Oil and Gas File T-11.

Finn, C. A., 1990, Geophysical constraints on Washington convergent margin structure: Journal of Geophysical Research, v. 95, no. B12, p. 19,533-19,546.

Flores, R. M.; Johnson, S. Y., 1995, Sedimentology and lithofacies of the Eocene Skookumchuck Formation in the Centralia coal mine, southwest Washington. *In* Fritsche, A. E., editors, Cenozoic paleogeography of the western United States—II: Society for Sedimentary Geology (SEPM) Pacific Section Book 75, p. 274-290.

Gabet, E. J.; Perron, J. T.; Johnson, D. L., 2014, Biotic origin for Mima mounds supported by numerical modeling: Geomorphology, v. 206, p. 58-66.

Gao, Haiying; Humphreys, E. D.; Yao, Huajian; van der Hilst, R. D., 2011, Crust and lithosphere structure of the northwestern U. S. with ambient noise tomography: Terrane accretion and Cascade arc development: Earth and Planetary Science Letters, v. 304, p. 202-211.

Gard, L. M., Jr., 1968, Bedrock geology of the Lake Tapps quadrangle, Pierce County, Washington: U.S. Geological Survey Professional Paper 388-B, 33 p., 2 plates. [http://pubs.er.usgs.gov/usgspubs/pp/pp388B]

Gaschnig, R. M.; Vervoort, J. D.; Lewis, R. S.; McClelland, W. C., 2010, Migrating magmatism in the northern US Cordillera: in situ U–Pb geochronology of the Idaho batholith: Contributions to Mineralogy and Petrology, v. 159, p. 863-883.

Gendaszek, A. S., 2011, Hydrogeologic framework and groundwater/surface-water interactions of the Chehalis River basin, southwestern Washington: U.S. Geological Survey Scientific Investigations Report 2011-5160, 42 p., 1 sheet, scale 1:250,000. [http://pubs.usgs.gov/sir/2011/5160]

Glassley, W. E., 1974, Geochemistry and tectonics of the Crescent volcanic rocks, Olympic Peninsula, Washington: Geological Society of America Bulletin, v. 85, no. 5, p. 785-794.

Globerman, B. R., 1981, Geology, petrology, and paleomagnetism of Eocene basalts from the Black Hills, Washington coast range: Western Washington University Master of Science thesis, 373 p., 1 plate.

Goldfinger Chris; Galer, Steve; Beeson, Jeffrey; Hamilton, Tark; Black, Bran; Romsos, Chris; Patton, Jason; Nelson, C. H.; Hausmann, Rachel; Morey, Ann, 2016, The importance of site selection, sediment supply, and hydrodynamics—A case study of submarine paleoseismology on the northern Cascadia margin, Washington USA: Marine Geology, v. 384, p. 4-16,17,25-46.

Goldstein, B. S.; Pringle, P. T.; Anderson, N. A., 2002, A late-glacial outburst flood from glacial Lake Carbon, Washington State, USA [abstract]: Geological Society of America Abstracts with Programs, v. 34, no. 5, p. A-24.

Goldstein, B.S.; Pringle, Patrick; Parker, B.; Futornick, Z. O., 2010, Tracking the late-glacial outburst flood from glacial Lake Carbon, Washington State, USA [abstract]. *In* Northwest Scientific Association, From Mount St. Helens to Oak-Prairie Lowlands—Disturbances, biological legacies, and conservation: Northwest Scientific Association, p. 57. [http://www.centralia.edu/academics/earthscience/nwsa/NWSA_CPOP_2010_Program.pdf]

Gorum, Tolga; Fan, Xuanmei; van Westen, C. J.; Huang, R. Q.; Xu, Qiang; Tang, Chuan; Wang, Gonghui, 2011, Distribution pattern of earthquake-induced landslides triggered by the 12 May 2008 Wenchuan earthquake, Geomorphology, v. 133, n. 3-4, p. 152-167.

Hagen, R. A., 1987, The geology and petrology of the Northcraft Formation, Lewis County, Washington: University of Oregon Master of Science thesis, 252 p., 1 plate.

Haugerud, R. A., 2009, Preliminary geomorphic map of the Kitsap Peninsula, Washington; version 1.0: U.S. Geological Survey Open-File Report 2009-1033, 2 sheets, scale 1:36,000. [http://pubs.usgs.gov/of/2009/1033/]

Henriksen, Donald Anton, 1956, Eocene stratigraphy of the lower Cowlitz River-eastern Willapa Hills area, southwestern Washington: Washington Division of Mines and Geology Bulletin 43, 122 p. [http://www.dnr.wa.gov/publications/ger_b43_eocene_stratigraphy.pdf]

Horwath Burnham, J. L.; Johnson, D. L., editors, 2012, Mima Mounds—The case for polygenesis and bioturbation: Geological Society of America Special Paper 490, 205 p.

Irvine T. N.; Baragar, W. R. A., 1971, A guide to the chemical classification of common volcanic rocks: Canadian Journal of Earth Sciences, v. 8, p. 523-548.

Irving, E., 1979. Paleopoles and paleolatitudes of North America and speculations about displaced terrains: Canadian Journal of Earth Sciences, v. 16, no. 3, p. 669-694.

Jackson, S. E., Pearson, N. J., Griffin, W. L., Belousova, E. A., 2004, The application of laser ablation-inductively coupled plasma-mass spectrometry to in situ U–Pb zircon geochronology, Chemical Geology, v. 211, p. 47-69.

Jeschke, D. A.; Eungard, D. W.; Troost, K. G.; Wisher, A. P, 2016, Subsurface database of Washington State—GIS data: Washington Division of Geology and Earth Resources Digital Data Series 11, version 1.2, previously released October 2015 [http://www.dnr.wa.gov/publications/ger_portal_subsurface_database.zip]

Johnson, S. Y.; Blakely, R. J.; Stephenson, W. J.; Dadisman, S. V.; Fisher, M. A., 2004, Active shortening of the Cascadia forearc and implications for seismic hazards of the Puget Lowland: Tectonics, v. 23, n. TC1011, 27 p.

Johnson, S. Y.; Potter, C. J.; Armentrout, J. M.; Miller, J. J.; Finn, C. A.; Weaver, C. S., 1996, The southern Whidbey Island fault—An active structure in the Puget Lowland, Washington: Geological Society of America Bulletin, v. 108, no. 3, p. 334-354, 1 plate.

Keefer, D. K., 1984, Landslides caused by earthquakes: Geological Society of America Bulletin, v. 95, no. 4, p. 406-421.

LaMaskin, T. A., 2012, Detrital zircon facies of Cordilleran terranes in western North America: GSA Today, v. 22, no. 3, p. 4-11. [http://www.geosociety.org/gsatoday/archive/22/3/article/i1052-5173-22-3-4.htm]

Lea, P. D., 1984, Pleistocene glaciation at the southern margin of the Puget lobe, western Washington: University of Washington Master of Science thesis, 96 p., 3 plates.

Le Bas M. J.; LeMaitre, R. W.; Streckeisen, A.; Zanettin, B., 1986, A chemical classification of volcanic rocks based on the total alkali silica diagram: Journal of Petrology, v. 27, p. 745-750.

Lewis, J. C.; Unruh, J. R.; Twiss, R. J., 2003, Seismogenic strain and motion of the Oregon coast block: Geology, v. 31, no. 2, p. 183-186.

Lewis, R. S.; Vervoort, J. D.; Burmester, R. F.; Oswald, P. J., 2010, Detrital zircon analysis of Mesoproterozoic and Neoproterozoic metasedimentary rocks of north central Idaho—Implications for development of the Belt-Purcell basin: Canadian Journal of Earth Sciences, v. 47, p. 1383-1404.

Logan, R. L., compiler, 1987, Geologic map of the Chehalis River and Westport quadrangles, Washington: Washington Division of Geology and Earth Resources Open File Report 87-8, 16 p., 1 plate, scale 1:100,000. [http://www.dnr.wa.gov/Publications/ger_ofr87-8_geol_map_chehalisriver_westport_100k.zip]

Logan, R. L.; Walsh, T. J., 2009, Mima Mounds formation and their implications for climate change [abstract]. In Northwest Scientific Association, The Pacific Northwest in a changing environment—Northwest Scientific Association 81st annual meeting; Program with abstracts: Northwest Scientific Association, p. 38-39. [http://www.northwestscience.org/Resources/Final%20Annual%20Meeting%20Abstracts%20and%20Programs/2009%20NWSA%20Program%20and%20Abstracts.pdf]

Logan, R. L.; Walsh, T. J.; Stanton, B. W.; Sarikhan, I. Y., 2009, Geologic map of the Maytown 7.5-minute quadrangle, Thurston County, Washington: Washington Division of Geology and Earth Resources Geologic Map GM-72. [http://www.dnr.wa.gov/publications/ger_gm72_geol_map_maytown_24k.pdf]

Ludwig, K. R., 2003. User's manual for Isoplot 3.00. A geochronological toolkit for Microsoft Excel. Berkeley Geochronology Center, Special Publication No. 4a,Berkeley, California.

Mallory, V. S., 1959, Lower Tertiary biostratigraphy of the California Coast Ranges: American Association of Petroleum Geologists, 416 p., 7 plates.

McCaffrey, Robert; King, R. W.; Payne, S. J.; Lancaster, Matthew, 2013, Active tectonics of northwestern U. S. inferred from GPS-derived surface velocities: Journal of Geophysical Research Solid Earth, v. 118, 15 p. [http://onlinelibrary.wiley.com/doi/10.1029/2012JB009473/epdf]

McCaffrey, Robert; Qamar, A. I.; King, R. W.; Wells, Ray; Khazaradze, Giorgi; Williams, C. A.; Stevens, C. W.; Vollick, J. J.; Zwick, P. C., 2007, Fault locking, block rotation and crustal deformation in the Pacific Northwest: Geophysical Journal International, v. 169, no. 3, p. 1315-1340.

McDougall, Kristin, 2008, California Cenozoic biostratigraphy—Paleogene, *In* Scheirer, A. H., editor, 2007, Petroleum systems and geologic assessment of oil and gas in the San Joaquin Basin Province, California: U.S. Geological Survey Professional Paper 1713, 56 p. [Accessed May 6, 2013 at http://pubs.usgs.gov/pp/pp1713/]

Moothart, S. R., 1993, Geology of the middle and upper Eocene McIntosh Formation and adjacent volcanic and sedimentary rock units, Willapa Hills, Pacific County, southwest Washington: Oregon State University Master of Science thesis, 265 p., 3 plates. [http://ir.library.oregonstate.edu/xmlui/handle/1957/12293]

Morrison, R. B., 1991, Introduction. *In* Morrison, R. B., editor, Quaternary nonglacial geology—Conterminous U.S.: Geological Society of America DNAG Geology of North America, v. K-2, p. 1-12.

Nilsen, T. H., 1976, Washington gravity base station network: Washington Division of Geology and Earth Resources Information Circular 59, 83 p. [http://www.dnr.wa.gov/Publications/ger_ic59_wa_gravity_base_network.pdf]

Nelson, J. W., 1981, Faults and their effect on coal mining in Illinois: Illinois Institute of Natural Resources, State Geological Survey Division Circular 523, 38 p. [https://www.ideals.illinois.edu/bitstream/handle/2142/44642/faultstheireffec523nels.pdf?sequence=2]

Nesbitt, E. A., 2018, Cenozoic Marine Formations of Washington and Oregon—an annotated catalogue: PaleoBios, v. 35, 20 p. [https://escholarship.org/uc/item/04q5f9cr]

Newcomb, R. C., 1952, Origin of the Mima Mounds, Thurston County region, Washington: Journal of Geology, v. 60, no. 5, p. 461-472.

Noble, J. B.; Wallace, E. F., 1966, Geology and ground-water resources of Thurston County, Washington: Washington Division of Water Resources Water-Supply Bulletin 10, v. 2, 141 p., 5 plates. [https://fortress.wa.gov/ecy/publications/summarypages/wsb10b.html]

Parker, B. L.; Goldstein, B. S.; Futornick, Z. O.; Pringle, P. T., 2008, Sedimentological evidence for an enriched glacial outburst flood in Thurston County, Washington [abstract]: Geological Society of America Abstracts with Programs, v. 40, no. 1, p. 70.

Pease, M. H., Jr.; Hoover, L., Jr., 1957, Geology of the Doty-Minot Peak area, Washington: U.S. Geological Survey Oil and Gas Investigations Map OM-188, 1 sheet, scale 1:62,500. [http://pubs.er.usgs.gov/publication/ om188]

Petrus, J. A.; Kamber, B. S., 2012, VizualAge: A novel approach to laser ablation ICP-MS U-Pb geochronology data reduction: Geostandards and Geoanalytical Research, v. 36, n. 3, p. 247-270.

Phillips, B. A.; Kerr, A. C.; Mullen, E. K.; Weis, Dominique, 2017, Oceanic mafic magmatism in the Siletz terrane, NW North America—Fragments of an Eocene oceanic plateau: LITHOS, [http://www.sciencedirect.com/science/article/pii/S0024493717300105]

Phillips, W. M.; Korosec, M. A.; Schasse, H. W.; Anderson, J. L.; Hagen, R. A., 1986, K-Ar ages of volcanic rocks in southwest Washington: Isochron/West, no. 47, p. 18-24.

Phillips, W. M.; Walsh, T. J.; Hagen, R. A., 1989, Eocene transition from oceanic to arc volcanism, southwest Washington. *In* Muffler, L. J. P.; Weaver, C. S.; Blackwell, D.D., editors, Proceedings of workshop XLIV—Geological, geophysical, and tectonic setting of the Cascade Range: U.S. Geological Survey Open-File Report 89-178, p. 199-256. [http://pubs.er.usgs.gov/publication/ofr89178]

Polenz, Michael; Alldritt, Katelin; Hehemann, N. J.; Sarikhan, I. Y.; Logan, R. L., 2009, Geologic map of the Belfair 7.5-minute quadrangle, Mason, Kitsap, and Pierce Counties, Washington: Washington Division of Geology and Earth Resources Open File Report 2009-7, 1 sheet, scale 1:24,000. [http://www.dnr.wa.gov/Publications/ger_ofr2009-7_geol_map_belfair_24k.pdf]

Polenz, Michael; Allen, M. D.; Legorreta Paulín, Gabriel; Eungard, D. W.; Cakir, Recep; Scott, S. P.; Mahan, S. A., 2016, Geologic map of the Shelton Valley 7.5-minute quadrangle, Mason County, Washington: Washington Division of Geology and Earth Resources Map Series 2016-02R, originally published 2016, 1 sheet, scale 1:24,000, 45 p. text. [http://www.dnr.wa.gov/publications/ger_ms2016-02_geol_map_shelton_valley_24k.zip]

Polenz, Michael; Contreras, T. A.; Czajkowski, J. L.; Legorreta Paulin, Gabriel; Miller, B. A.; Martin, M. E.; Walsh, T. J.; Logan, R. L.; Carson, R. J.; Johnson, C. N.; Skov, R. H.; Mahan, S. A.; Cohan, C. R., 2010, Supplement to geologic maps of the Lilliwaup, Skokomish Valley, and Union 7.5-minute quadrangles, Mason County, Washington—Geologic setting and development around the Great Bend of Hood Canal: Washington Division of Geology and Earth Resources Open File Report 2010-5, 27 p. [http://www.dnr.wa.gov/Publications/ger_ofr2010-5_lilliwaup_skokomish_valley_union_suppl_24k.pdf]

Polenz, Michael; Favia, J. G.; Hubert, I. J.; Legorreta Paulín, Gabriel; Cakir, Recep, 2015, Geologic map of the Port Ludlow and southern half of the Hansville 7.5-minute quadrangles, Kitsap and Jefferson Counties, Washington: Washington Division of Geology and Earth Resources Map Series 2015-02, 1 sheet, scale 1:24,000, 40 p. text. [http://www.dnr.wa.gov/publications/ger_ms2015-02_geol_map_port_ludlow_hansville_24k.zip]

Polenz, Michael; Gordon, H. O.; Hubert, I. J.; Contreras, T. A.; Patton, A. I.; Legorreta Paulin, Gabriel; Cakir, Recep, 2014, Geologic map of the Center 7.5-minute quadrangle, Jefferson County, Washington: Washington Division of Geology and Earth Resources Map Series 2014-02, 1 sheet, scale 1:24,000, with 35 p. text. [http://www.dnr.wa.gov/Publications/ger_ms2014-02_geol_map_center_24k.zip]

Polenz, Michael; Miller, B. A.; Davies, Nigel; Perry, Benjamin B.; Hughes, J. F.; Clark, K. P.; Walsh, T. J.; Tepper, J. H.; Carson, R. J., 2012a,Analytical data from the Hoodsport 7.5-minute quadrangle, Mason County, Washington--Supplement to Open File Report 2011-3: Washington Division of Geology and Earth Resources Open File Report 2011-4, 42 p. [http://www.dnr.wa.gov/Publications/ger_ofr2011-4_hoodsport_supplement.pdf]

Polenz, Michael; Petro, G. T.; Contreras, T. A.; Stone, K. A.; Legorreta Paulin, Gabriel; Cakir, Recep, 2013, Geologic map of the Seabeck and Poulsbo 7.5-minute quadrangles, Kitsap and Jefferson Counties, Washington: Washington Division of Geology and Earth Resources Map Series 2013-02, 1 sheet, scale 1:24,000, with 39 p. text. [http://www.dnr.wa.gov/Publications/ger_ms2013-02_geol_map_seabeck-poulsbo_24k.zip]

Polenz, Michael; Spangler, Eleanor; Fusso, L. A.; Reioux, D. A.; Cole, Ryan A.; Walsh, T. J.; Cakir, Recep; Clark, K. P.; Tepper, J. H.; Carson, R. J.; Pileggi, Domenico; Mahan, S. A., 2012b, Geologic map of the Brinnon 7.5-minute quadrangle, Jefferson and Kitsap Counties, Washington: Washington Division of Geology and Earth Resources Map Series 2012-02, 1 sheet, scale 1:24,000, with 47 p. text. [http://www.dnr.wa.gov/Publications/ger_ms2012-02_geol_map_brinnon_24k.zip]

Polenz, Michael; Vermeer, J. L.; Legorreta Paulín, Gabriel; Tepper, J. H.; Mahan, S. A.; Cakir, Recep, 2017, Geologic map of the Littlerock 7.5-minute quadrangle, Thurston County, Washington: Washington Geological Survey Map Series 2017-01, 1 sheet, scale 1:24,000, 36 p. text. [http://www.dnr.wa.gov/publications/ger_ms2017-01_geol_map_littlerock_24k.zip]

Polenz, Michael; Wegmann, K. W.; Schasse, H. W., 2004, Geologic map of the Elwha and Angeles Point 7.5-minute quadrangles, Clallam County, Washington: Washington Division of Geology and Earth Resources Open File Report 2004-14, 1 sheet, scale 1:24,000. [http://www.dnr.wa.gov/Publications/ger_ofr2004-14_geol_map_elwha_angelespoint_24k.pdf]

Porter, S. C., 1975, Weathering rinds as a relative-age criterion—Application to subdivision of glacial deposits in the Cascade Range: Geology, v. 3, no. 3, p. 101-104.

Porter, S. C.; Carson, R. J., 1971, Problems of interpreting radiocarbon dates from dead-ice terrain, with an example from the Puget Lowland of Washington: Quaternary Research, v. 1, no. 3, p. 410-414.

Porter, S. C.; Swanson, T. W., 1998, Radiocarbon age constraints on rates of advance and retreat of the Puget lobe of the Cordilleran ice sheet during the last glaciation: Quaternary Research, v. 50, no. 3, p. 205-213.

Pratt, T. L.; Johnson, S. Y.; Potter, C. J.; Stephenson, W. J.; Finn, C. A., 1997, Seismic reflection images beneath Puget Sound, western Washington State—The Puget Lowland thrust sheet hypothesis: Journal of Geophysical Research, v. 102, no. B12, p. 27,469-27,489.

Pringle, P. T.; Goldstein, B. S., 2002, Deposits, erosional features, and flow characteristics of the late-glacial Tanwax Creek–Ohop Creek Valley flood—A likely source for sediments composing the Mima Mounds, Puget Lowland, Washington [abstract]: Geological Society of America Abstracts with Programs, v. 34, no. 5, p. A-89.

Prothero, Donald R.; Armentrout, John M., 1985, Magnetostratigraphic correlation of the Lincoln Creek Formation, Washington—Implications for the age of the Eocene/Oligocene boundary: Geology, v. 13, no. 3, p. 208-211.

Rau, W. W., 1958, Stratigraphy and foraminiferal zonation in some of the Tertiary rocks of southwestern Washington: U.S. Geological Survey Oil and Gas Investigations Chart OC-57, 2 sheets. [https://pubs.er.usgs.gov/publication/oc57]

Rau, W. W., 1981, Pacific Northwest Tertiary benthic foraminiferal biostratigraphic framework—An overview. *In* Armentrout, J. M., editor, Pacific Northwest Cenozoic biostratigraphy: Geological Society of America Special Paper 184, p. 67-84.

Rau, W. W., 2004, Pacific Northwest Tertiary foraminiferal collections of the U.S. Geological Survey and the State of Washington: Washington Division of Geology and Earth Resources Digital Report 4, 1 CD-ROM. [http://www.dnr.wa.gov/Publications/ger_dr4_pacific_nw_foram_collections.zip]

Rigg, G. B., 1958, Peat resources of Washington: Washington Division of Mines and Geology Bulletin 44, 272 p. [http://www.dnr.wa.gov/publications/ger_b44_peat_reasources_wa_3.pdf]

Ritchie, A. M., 1953, The erosional origin of the Mima mounds of southwest Washington: Journal of Geology, v. 61, no. 1, p. 41-50.

Roberts, Albert Eugene, 1958, Geology and coal resources of the Toledo-Castle Rock district, Cowlitz and Lewis Counties, Washington: U.S. Geological Survey Bulletin 1062, 71 p., 6 plates. [https://pubs.er.usgs.gov/publication/b1062]

Ross, G. M.; Parrish, R. R.; Winston, D., 1992, Provenance and U-Pb geochronology of the Mesoproterozoic Belt Supergroup (northwestern United States): implications for age of deposition and pre-Panthalassa plate reconstructions: Earth & Planetary Science Letters, v. 113, p. 55-57.

Sadowski, A. J.; Keller, W. E.; Polenz, Michael; Lau, T. R.; Cakir, Recep, Slaughter, S. L.; Nesbitt, E. A..; Tepper, J. H.; DuFrane, S. A.; Legorreta Paulín, Gabriel, 2018, Geologic map of the Centralia 7.5-minute quadrangle, Lewis County, Washington: Washington Geological Survey Map Series 2018-0X, 1 sheet, scale 1:24,000, XX p. text. [http://www.dnr.wa.gov/publications/ger_ms2018-0X_geol_map_centralia_24k.zip]

Satake, Kenji; Wang, Kelin; Atwater, B. F., 2003, Fault slip and seismic moment of the 1700 Cascadia earthquake inferred from Japanese tsunami description: Journal of Geophysical Research, v. 108, no. B11, 2535.

Schasse, H. W., 1987, Geologic map of the Centralia quadrangle, Washington: Washington Division of Geology and Earth Resources Open File Report 87-11, 28 p., 1 plate, scale 1:100,000. [http://www.dnr.wa.gov/Publications/ger_ofr87-11_geol_map_centralia_100k.zip]

Schasse, H. W., 2001, Washington's coal industry—2000: Washington Geology, v. 29, no. 1/2, p. 9. [http://www.dnr.wa.gov/Publications/ger_washington_geology_2001_v29_no1-2.pdf]

Schasse, H. W.; Logan, R. L., 1998, Geologic map of the Sequim 7.5-minute quadrangle, Clallam County, Washington: Washington Division of Geology and Earth Resources Open File Report 98-7, 22 p., 2 plates. [http://www.dnr.wa.gov/Publications/ger_ofr98-7_geol_map_sequim_24k.zip]

Schasse, H. W.; Logan, R. L.; Polenz, Michael; Walsh, T. J., 2003, Geologic map of the Shelton 7.5-minute quadrangle, Mason and Thurston Counties, Washington: Washington Division of Geology and Earth Resources Open File Report 2003-24, 1 sheet, scale 1:24,000. [http://www.dnr.wa.gov/Publications/ger_ofr2003-24_geol_map_shelton_24k.pdf]

Schasse, H. W.; Polenz, Michael, 2002, Geologic map of the Morse Creek 7.5-minute quadrangle, Clallam County, Washington: Washington Division of Geology and Earth Resources Open File Report 2002-8, 18 p., 2 plates, scale 1:24,000. [http://www.dnr.wa.gov/Publications/ger_ofr2002-8_geol_map_morsecreek_24k.zip]

Schasse, H. W.; Slaughter, S. L., 2005, Geologic map of the Port Townsend South and part of the Port Townsend North 7.5-minute quadrangles, Jefferson County, Washington: Washington Division of Geology and Earth Resources Geologic Map GM-57, 1 sheet, scale 1:24,000. [http://www.dnr.wa.gov/Publications/ger_gm57_geol_map_porttownsends_24k.pdf]

Schasse, H. W.; Wegmann, K. W., 2000, Geologic map of the Carlsborg 7.5-minute quadrangle, Clallam County, Washington: Washington Division of Geology and Earth Resources Open File Report 2000-7, 27 p., 2 plates, scale 1:24,000. [http://www.dnr.wa.gov/Publications/ger_ofr2000-7_geol_map_carlsborg_24k.zip]

Schasse, H. W.; Wegmann, K. W.; Polenz, Michael, 2004, Geologic map of the Port Angeles and Ediz Hook 7.5-minute quadrangles, Clallam County, Washington: Washington Division of Geology and Earth Resources Open File Report 2004-13, 1 sheet, scale 1:24,000. [http://www.dnr.wa.gov/Publications/ger_ofr2004-13_geol_map_portangeles_edizhook_24k.pdf]

Schmandt, Brandon; Humphreys, Eugene, 2011, Seismically imaged relict slab from the 55 Ma Siletzia accretion to the northwest United States: Geology, v. 39, no. 2, p. 175-178.

Sláma, Jiří; Košler, Jan; Condon, D. J.; Crowley, J. L.; Gerdes, Axel; Hanchar, J. M.; Horstwood, M. S.A.; Morris, G. A.; Nasdala, Lutz; Norberg, Nicholas; Schaltegger, Urs; Schoene, Blair; Tubrett, M. N.; Whitehouse, M. J., 2008, Plešovice zircon—A new natural reference material for U–Pb and Hf isotopic microanalysis: Chemical Geology, v. 249, n. 1-2, p. 1-35.

Snavely, P. D., Jr.; Brown, R. D., Jr.; Roberts, A. E.; Rau, W.W., 1958, Geology and coal resources of the Centralia-Chehalis district, Washington, with a section on Microscopical character of Centralia-Chehalis coal, by J. M. Schopf: U.S. Geological Survey Bulletin 1053, 159 p., 6 plates. [http://pubs.er.usgs.gov/usgspubs/b/b1053]

Snavely, P. D., Jr.; Rau, W. W.; Hoover, Linn, Jr.; Roberts, A. E., 1959, McIntosh Formation, Centralia-Chehalis coal district, Washington. *In* Washington Division of Mines and Geology, Tertiary stratigraphic papers, southwestern Washington: Washington Division of Mines and Geology Reprint 3, 10 p. [http://www.dnr.wa.gov/publications/ger_reprint3_strat_papers_sw_wa.pdf]

Snavely, P. D., Jr.; Roberts, A. E.; Hoover, Linn, Jr.; Pease, M. H., Jr., 1951, Geology of the eastern part of the Centralia-Chehalis coal district, Lewis and Thurston Counties, Washington: U.S. Geological Survey Coal Investigations Map, C-8, 2 sheets, scale 1:31,680. [https://pubs. er.usgs.gov/publication/b1053]

Stanley, W. D.; Johnson, S. Y.; Nuccio, V. F., 1994, Analysis of deep seismic reflection and other data from the southern Washington Cascades: U.S. Geological Survey Open-File Report 94-159, 180 p. [http://pubs.er.usgs.gov/publication/ofr94159]

Sun, S. S.; McDonough, W.F., 1989, Chemical and isotopic systematics of oceanic basalts: Implications for mantle composition and processes, *In* Saunders, A.D., and Norry, M.J., editors, Magmatism in the Ocean Basins: Geological Society of London Special Publication 42, p. 313-345.

Telford, W. M.; Geldart, L. P.; Sheriff, R. E., 1990, Applied geophysics; 2nd ed.: Cambridge University Press, 770 p.

Trehu, A. M.; Asudeh, Isa; Brocher, T. M.; Luetgert, J. H.; Mooney, W. D.; Nabelek, J. L.; Nakamura, Y., 1994, Crustal architecture of the Cascadia forearc: Science, v. 266, no. 5183, p. 237-243.

Triplehorn, D. M.; Turner, D. L.; Frizzell, V. A., Jr., 1980, Stratigraphic significance of radiometric ages for Eocene coals in western Washington [abstract]. *In* Carter, L. M., editor, Proceedings of the fourth symposium on the geology of Rocky Mountain coal—1980: Colorado Geological Survey Resource Series 10, p. 87.

Troost, K. G., 2016, Chronology, lithology and paleoenvironmental interpretations of the penultimate ice-sheet advance into the Puget Lowland, Washington State: University of Washington Doctor of Philosophy thesis, 239 p.

Troost, K. G.; Booth, D. B., 2008, Geology of Seattle and the Seattle area, Washington. *In* Baum, R. L.; Godt, J. W.; Highland, L. M., editors, Landslides and engineering geology of the Seattle, Washington, area: Geological Society of America Reviews in Engineering Geology XX, p. 1-35. [http://www.wou.edu/las/physci/taylor/g473/seismic_hazards/troost_booth_2008_geo_seattle.pdf]

U.S. Geological Survey Geologic Names Committee, 2010, Divisions of geologic time—Major chronostratigraphic and geochronologic units: U.S. Geological Survey Fact Sheet 2010-3059, 2 p. [http://pubs.usgs.gov/fs/2010/3059/]

Wagner, H. C., 1967, Preliminary geologic map of the Raymond quadrangle, Pacific County, Wash.: U.S. Geological Survey Open-File Report 67-265, 1 sheet, scale 1:62,500. [http://pubs.er.usgs.gov/usgspubs/ofr/ofr67265]

Walker, J. D.; Geissman, J. W., compilers, 2009, Geologic time scale: Geological Society of America, 1 p. [http://www.geosociety.org/science/timescale/timescl.pdf]

Walsh, T. J.; Korosec, M. A.; Phillips, W. M.; Logan, R. L.; Schasse, H. W., 1987, Geologic map of Washington—Southwest quadrant: Washington Division of Geology and Earth Resources Geologic Map GM-34, 2 sheets, scale 1:250,000, with 28 p. text. [http://www.dnr.wa.gov/publications/ger_gm34_geol_map_sw_wa_250k.pdf]

Walsh, T. J.; Logan, R. L., 2005, Geologic map of the East Olympia 7.5-minute quadrangle, Thurston County, Washington: Washington Division of Geology and Earth Resources Geologic Map GM-56, 1 sheet, scale 1:24,000. [http://www.dnr.wa.gov/Publications/ger_gm56_geol_map_eastolympia_24k.pdf]

Walsh, T. J.; Logan, R. L.; Schasse, H. W.; Polenz, Michael, 2003, Geologic map of the Tumwater 7.5-minute quadrangle, Thurston County, Washington: Washington Division of Geology and Earth Resources Open File Report 2003-25, 1 sheet, scale 1:24,000. [http://www.dnr.wa.gov/Publications/ger_ofr2003-25_geol_map_tumwater_24k.pdf]

Wang, Kelin, 1996, Simplified analysis of horizontal stresses in a buttressed fore arc sliver at an oblique subduction zone: Geophysical Research Letters, v.23, n. 16, p. 2021-2024.

Washburn, A. L., 1988, Mima mounds—An evaluation of proposed origins with special reference to the Puget Lowlands: Washington Division of Geology and Earth Resources Report of Investigations 29, 53 p. [http://www.dnr.wa.gov/publications/ger_ri29_mima_mounds.pdf]

Washington Division of Geology and Earth Resources, 2016, Surface geology, 1:100,000—GIS data, Nov. 2016: Washington Division of Geology and Earth Resources Digital Data Series 18, version 3.1, previously released June 2010. [https://www.dnr.wa.gov/publications/ger_portal_surface_geology_100k.zip]

Washington Geological Survey, 2017, Coal mine map inventory—GIS data, Nov. 2017: Washington Geological Survey Digital Data Series DS-20, version 1.0. [https://www.dnr.wa.gov/publications/ger_portal_coal_mine_maps.zip]

Weaver, C. E., 1912, A preliminary report on the Tertiary paleontology of western Washington: Washington Geological Survey Bulletin 15, 80 p. [http://www.dnr.wa.gov/publications/ger_b15_prelim_rep_teriary_paleo_western_wa.pdf]

Weaver, C. E., 1916, The Tertiary formations of western Washington: Washington Geological Survey Bulletin 13, 327 p., 6 plates. [http://www.dnr.wa.gov/publications/ger_b13_teriary_form_western_wa_1.pdf]

Weaver, C. E., 1937, Tertiary stratigraphy of western Washington and northwestern Oregon: University of Washington Publications in Geology, v. 4, 266 p.

Weaver, C. E., 1944, Grays Harbor County. *In* Weaver, C. E.; and others, Correlation of the marine Cenozoic formations of western North America: Geological Society of America Bulletin, v. 55, no. 5, p. 592.

Wells, Ray E., 1981, Geologic map of the eastern Willapa Hills, Cowlitz, Lewis, Pacific, and Wahkiakum Counties, Washington: U.S. Geological Survey Open-File Report 81-674, 1 sheet, scale 1:62,500. [http://pubs.er.usgs.gov/publication/ofr81674]

Wells, R. E., 1982, Paleomagnetism and geology of Eocene volcanic rocks in southwest Washington—Constraints on mechanisms of rotation and their regional tectonic significance: University of California at Santa Cruz Doctor of Philosophy thesis, 229 p., 1 plate, scale 1:62,500.

Wells, Ray E., 1989, Geologic map of the Cape Disappointment-Naselle River area, Pacific and Wahkiakum Counties, Washington: U.S. Geological Survey Miscellaneous Investigations Series Map I-1832, 1 sheet, scale 1:62,500. [http://pubs.er.usgs.gov/publication/i1832]

Wells, R. E.; McCaffrey, Robert, 2013, Steady rotation of the Cascade arc: Geology, v. 41, no. 9, p. 1027-1030.

Wells, R. E.; Sawlan, M. G., 2014, Preliminary geologic map of the eastern Willapa Hills, Cowlitz, Lewis, and Wahkiakum Counties, Washington: U.S. Geological Survey Open-File Report 2014-1063, 2 sheets, scale 1:50,000. [https://pubs.er.usgs.gov/publication/ofr20141063]

Wells, R. E.; Weaver, C. S.; Blakely, R. J., 1998, Cascadia forearc migration and its neotectonic significance [abstract]: Eos (American Geophysical Union Transactions), v. 79, no. 45, Supplement, p. F874.

Wells, R. E.; Bukry, David; Friedman, Richard; Pyle, Doug; Duncan, Robert; Haeussler, Peter; Wooden, Joe, 2014, Geologic history of Siletzia, a large igneous province in the Oregon and Washington Coast Range: Correlation to the geomagnetic polarity time scale and implications for a long-lived Yellowstone hotspot: Geosphere, v. 10, no. 4, 28 p.

Wells, R. E.; Blakely, R. J.; Wech, A. G.; McCrory, P. A.; Michael, Andrew, 2017, Cascadia subduction tremor muted by crustal faults: Geology, v. 45, no. 6, p. 551-518.

Appendix A. New Radiocarbon Age Estimates

Table A1. Radiocarbon ages from the map area. ^{14}C yr BP age estimates are in radiocarbon years before 1950 and uncertainty estimates are reported at 1σ (68% confidence). Ages in ka are calendar years before 1950 divided by 1,000 and have 2σ uncertainty ranges. An age range is preferred because uncertainties are unequally distributed as a result of the calibration curves used to convert between radiocarbon and calendar years. Uncertainty statements reflect random and lab errors; errors from unrecognized sample characteristics or flawed methodological assumptions (for example, ^{14}C sample contamination from younger carbon flux) are not known. Ages are adjusted for measured $^{13}C/^{12}C$ ratio (a 'conventional' age). Elevations were estimated using best lidar data available to the WGS, mosaicked as of spring 2017, projected to State Plane South, NAD 83 HARN, US Survey feet, supplemented by visual elevation estimates on bluffs. Lidar level 0 is theoretically 3.43 to 3.78 ft below base map level 0 [http://www.ngs.noaa.gov/cgi-bin/VERTCON/vert_con.prl]. Lidar elevation statements were not adjusted to account for systematic projection differences relative to the base map. Latitude and longitude coordinates are in WGS84.

^{14}C site ID (geologic unit)		Reference	Material	Method	$^{13}C/^{12}C$ (o/oo)	Age estimate
GD1 [VPM225] (Qa)		this study	wood	^{14}C	-22.1	130 ±30 ^{14}C yr BP (0.045-0.008 ka, 14.9% prob.; 0.152-0.056 ka, 42.4% prob.; 0.276-0.172 ka, 38.0% prob.)
Lab ID[a]	Beta-482031	Wood from a red, 1 ft-thick sand lens with abundant charcoal fragments and flat, detrital sticks, some of which include bark. The concentration of organic debris borders on peat; most sticks are flat and ~2 in. wide by 0.5–1 in. thick, and embedded flat in the host sand, which was deposited in a flood plain paleoenvironment. Exposed ~5 ft below the modern flood plain surface along a channel-left Skookumchuck River bank.				
TRS	sec 14, T15N R2W					
Lat/long. (degrees)	46.79218 -122.89477					
Elev. (ft)	225					
GD2 [VPM209] (Qa)		this study	wood	^{14}C	-27.6	480 ±30 14C yr BP (0.542–0.498 ka)
Lab ID[a]	Beta-482030	Wood from the roughly 60 outermost exposed growth rings of a 1.5–2 ft-thick log horizontally embedded in floodplain sediment 10 ft below the modern floodplain surface and exposed at summer water level along an eroding Skookumchuck River cutbank. Sampled from the top of the exposed log. No bark was recognized.				
TRS	sec. 28, T15N R2W					
Lat/long. (degrees)	46.75827 -122.93889					
Elev. (ft)	196					

Appendix B. New U-Pb Age Estimates

U-PB ANALYSIS METHODS

Each sample (~5 kg) was crushed to fine sand-sized particles. Heavy minerals were then concentrated using a Wilfley table. Between each sample great care was taken to clean crushing plates and the Wilfley table to reduce the risk of contamination. The zircon concentrate was then passed through a 220 µm sieve and the <220 µm fraction was sorted by magnetic separation using a Frantz LB1 to remove undesirable magnetic minerals. Zircons were then separated by density from the non-magnetic fraction using di-methylene iodide heavy liquid. From the zircon separate, 100 individual zircon grains were hand selected from each sample and mounted in epoxy. The grain mount was polished to expose the grain centers and regions suitable for analysis were identified from Cathodoluminescense imaging.

We obtained U-Pb zircon data using the laser ablation inductively coupled plasma mass spectrometry technique (LA-ICPMS) at the Canadian Center for Isotopic Micro-analysis (CCIM) at the University of Alberta. The analytical setup consists of a New Wave UP-213 laser ablation system interfaced with a Thermo Scientific ICAP-Q quadrupole ICPMS. We operated the laser at 5 Hz with a beam diameter of 30 um which yielded a fluence of ~3 J/cm^2. Ablations were conducted in a He atmosphere at a flow rate of 0.5 L/min through the ablation cell. Ar (0.55 l/min) makeup gas and N_2 (4 mls/min) join the output from the cell before entering the injector. We auto-tuned the instrument by ablating NIST 612 and then manually adjusted the Ar makeup gas to achieve a U/ Th of ~1.05. Data were collected in time resolved mode for each analysis, including a 25 sec blank, for a total analysis time of 70 sec, with a 45 sec washout between analyses. Dwell times were 50 ms for masses 238, 235, 232, 208 and 80 ms for masses 207, 206, 204, and 202, for an estimated sweep time of 550 ms. We analyzed zircon reference materials GJ1 (Jackson and others, 2004) and Plešovice (Sláma and others, 2008) before and after each set of 10-20 unknowns to monitor U-Pb fractionation, reproducibility, and instrument drift. All data were reduced offline using Iolite data reduction program and the visual-age data reduction scheme (Petrus and Kamber, 2012). Unknowns and secondary reference materials were normalized to GJ1 as the primary reference.

The uncertainties reported are a quadratic combination of the internal measurement precision (standard error) and the overall reproducibility of the standards during an analytical session (standard deviation). The 2 sec reproducibility for the standards is estimated to be ~2–3 % for $^{207}Pb/^{206}Pb$ and $^{206}Pb/^{238}U$. Data that contained significant amounts of common Pb were corrected using the method of Anderson (2002). All plots were generated using the Isoplot software of Ludwig (2003).

Table B1. U-Pb data . Analysis by S. Andrew DuFrane and staff at ICPMS Lab, Canadian Center for Isotopic Micro-analysis, Department of Earth & Atmospheric Sciences, University of Alberta, Edmonton, Alberta, Canada T6G 2E3. Uncertainty values are at the 2σ level. Systematic errors from unrecognized sample characteristics are not well understood, but likely amount to at least 2% (Marillo-Sialer and others, 2016, and references therein). Thus a realistic estimate of the total uncertainty for the youngest peak age is at minimum 2%, and conservatively up to 5%. *indicates common Pb correction by the method of Andersen (2002).

U-Pb site ID (sample no.) (geologic unit)		Age estimate	MSWD
GD3 (VPM179a) (Emm)		No older than ~47.23 ±0.80 Ma	0.33
TRS	sec. 24, T16N R2W	Analysis marks ages of 100 zircon grains from tuffaceous, micaceous marine sandstone with angular to subrounded medium sand grains in clayey, weathered matrix. The stated age is a maximum limiting age because the deposit cannot be older than the youngest zircons within it; the youngest single zircon (41 ±2 Ma) may more closely approximate the age of the deposit but is not by itself deemed to provide a limiting age because (1) unlike U-Pb age analysis by TIMS, the analytical technique we used is not designed to provide highly accurate, precise measurements of single grains, and (2) despite careful efforts to remove all particles possibly derived from younger deposits the possibility of post-depositional addition of a younger grain cannot be fully dismissed at the sample site in a forest road cut approximately 6–10 ft below the former land surface. For instance, a volcanic ash fall could have blanketed the surface with younger particles that could then have moved down to the sample via a fracture or a root hollow, both of which were present at the sample exposure. See Data Supplement for analytical results and age estimates from individual crystals. Outcrop color is pale gray to white with reddish brown and orange weathering, for an overall mottled exposure. The outcrop revealed no bedding, but relatively tuffaceous sedimentary rock could be horizontally traced more than 50 ft to the north-northwest; a lithologic contrast relative to less tuffaceous exposure at microfossil sample site GD37, 165 ft north-northwest and 8 ft below sample site GD3, suggests that bedding is close to horizontal, consistent with approximately flat-lying bedding in the historical Hercules 1 quarry 0.3 mi east-southeast of GD3. The weathered exposure at age site GD3 crumbles easily and is soft enough to be cut with a knife, as is typical of sedimentary rock exposures in the area. The sample from age site GD3 appears to be Tenino sandstone and therefore near the stratigraphic top of the McIntosh Formation, based on (1) geographic proximity to the Hercules 1 quarry, where Tenino sandstone was mined as building stone (microfossil sample GD37) and (2) elevation of age site GD3 200 ft above the quarry top. The likelihood of close to horizontal bedding and geographic proximity suggest approximate stratigraphic equivalence with microfossil sample from age site GD35, although bedding could not be traced between the two sites. Samples from sites GD35 and GD37 yielded no fossils; this is common in the typically barren Tenino sandstone. Thin section petrographic analysis shows quartz and feldspar as major minerals. Minor minerals include muscovite, trace quantities of opaque minerals, rutile, lithics, and (or) zircon. Most grains are angular to subangular. Age site GD3 was sampled in the Bucoda quadrangle 0.2 mi east of the Violet Prairie quadrangle.	
Lat/long. (degrees)	46.85467 -122.87166		
Elev. (ft)	597		
GD4 (VPM292b) (Ensk)		No older than ~41.4 ±1.4 Ma	0.67
TRS	sec. 12, T15N R3W	Analysis marks ages of 100 zircon grains from sandstone with subangular to subrounded medium sand grains and abundant, sand-sized glauconite pellets interpreted as invertebrate coprolites resembling those pictured in Carter (2017—cover photo). The stated age is a maximum limiting age because the deposit cannot be older than the youngest zircons within it; the youngest single zircon (38 ±2 Ma) may more closely approximate the age of the deposit but does not by itself provide a limiting age because, unlike U-Pb age analysis by TIMS, the analytical technique we used is not designed to provide highly accurate, precise measurements of single grains. See Data Supplement for analytical results and age estimates from all individual crystals. The outcrop is surficially stained (less than 1 ft-deep) to reddish-brown and is 10 ft above the base of a 90 ft-deep road cut excavated a few years prior to sampling. The exposure is weathered throughout and soft enough to be cut with a knife, as is typical of sedimentary rock exposures in the area, although in its position approximately 80 ft beneath the historic surface (Columnar Section 1), this rock is more competent than most exposures in the map area. The sample is lower (to middle?) Skookumchuck Formation from below the Mendota coal bed (Snavely and others, 1958, p. 112), based on elevation and geographic proximity to three U.S. Geological Survey drill holes (B6, 1.1 mi west of age site GD4; B1, 1.2 mi south-southeast of age site GD4; and boring B2, 1.2 mi northeast of age site GD4). Snavely and others (1958) presented these drill holes, respectively, as GS-CH2, GS-AA, and GS-BB, and asserted (in their plate 3) that all three are stratigraphically between 130 and 400 ft below the Mendota coal bed of the lower middle Skookumchuck Formation. Lidar suggests that the surface elevations of the three drill holes are all within 40 ft of sample GD4. Bedding dips gently southwest (215/08) 50 ft north of age site GD4 and is less well expressed but similarly oriented at age site GD4. Thin section petrographic analysis shows plagioclase and quartz as the only major minerals. Other observed minerals include glauconite (some banded), potassium feldspar, and microcline. Minerals observed in the matrix include chlorite (apparently altered from biotite), an unidentified yellow mineral with green spots (microfossil or altered glauconite), and polycrystalline quartz. Most grains are subangular to subrounded. GD3 was sampled in the Rochester quadrangle 0.4 mi west of the Violet Prairie quadrangle.	
Lat/long. (degrees)	46.79655 -123.01033		
Elev. (ft)	187		

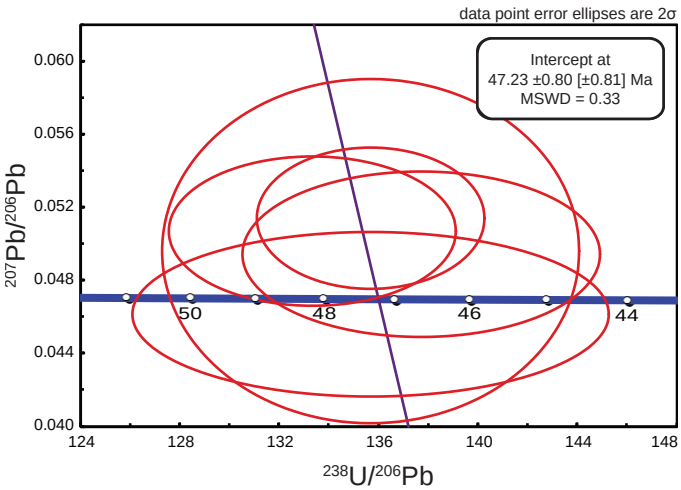

Figure B1A. Concordia plot for ages from five zircons at the young end of the age spectrum from age site GD3. The Concordia plot provides a mathematically more robust maximum constraining age statement than reliance on the single youngest zircon would, and it permits a confident assertion that the deposit is no older than the stated age. It does not dismiss the geologically reasonable possibility that the deposit is also younger than the single youngest grain (41 ±2 Ma).

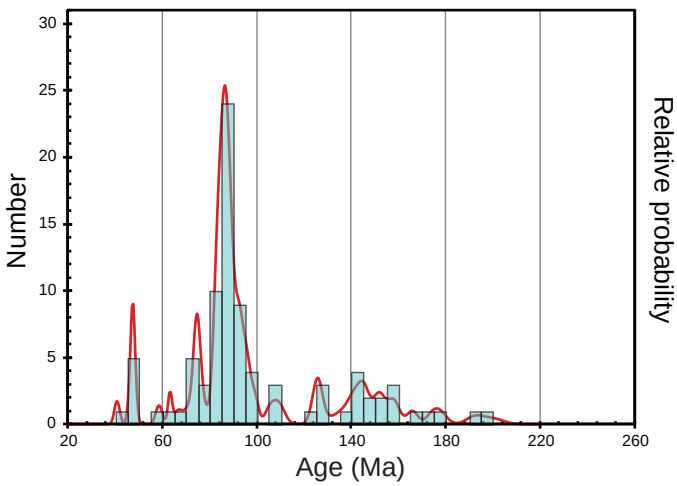

Figure B1B. Younger zircon age peaks for age site GD3.

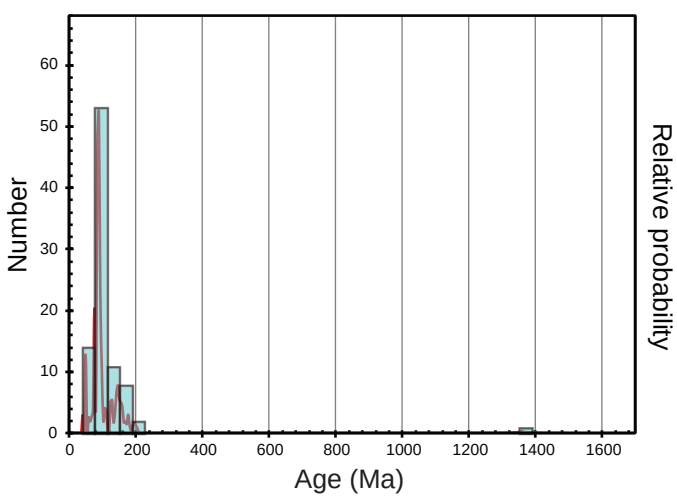

Figure B1C. Older zircon age peaks for age site GD3.

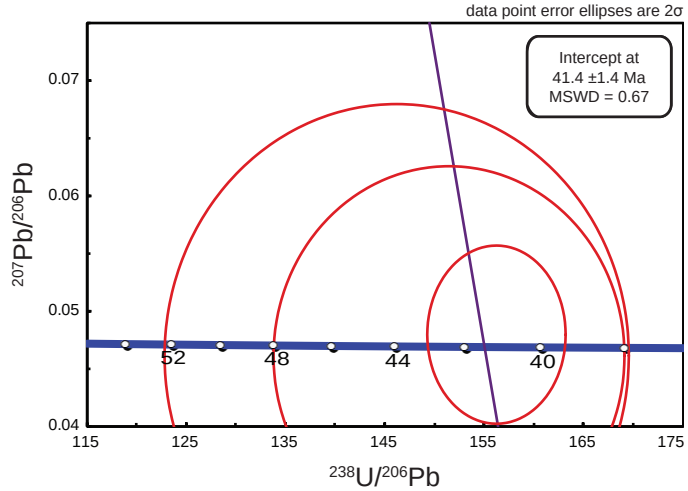

Figure B2A. Concordia plot for ages from the youngest three zircons at the young end of the age spectrum for age site GD4. The Concordia plot provides a mathematically more robust maximum constraining age statement than reliance on the single youngest zircon would, and it permits a confident assertion that the deposit is no older than the stated age. It does not dismiss the geologically reasonable possibility that the deposit is also younger than the single youngest grain (38 ±2 Ma).

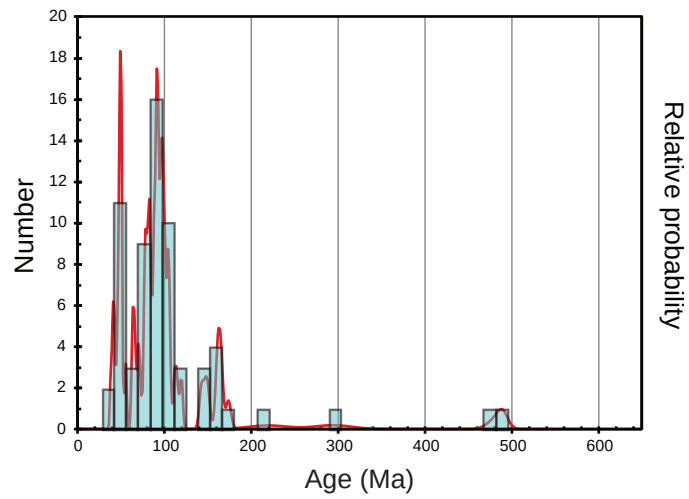

Figure B2B. Younger zircon age peaks for age site GD4.

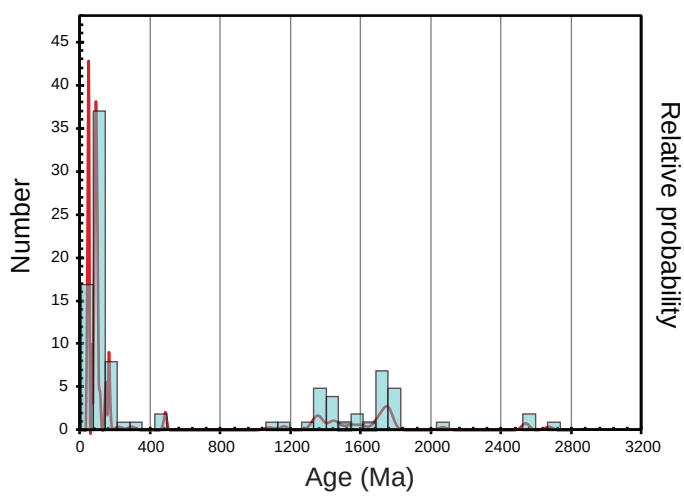

Figure B2C. Older zircon age peaks for age site GD4.